



### Cite as

Nano-Micro Lett.

(2025) 17:118

## Molecular Mechanism Behind the Capture of Fluorinated Gases by Metal–Organic Frameworks

Qian Wang<sup>1</sup>, Yong Hu<sup>2</sup>, Yifan Gu<sup>1,3,4</sup>

Received: 21 August 2024

Accepted: 1 November 2024

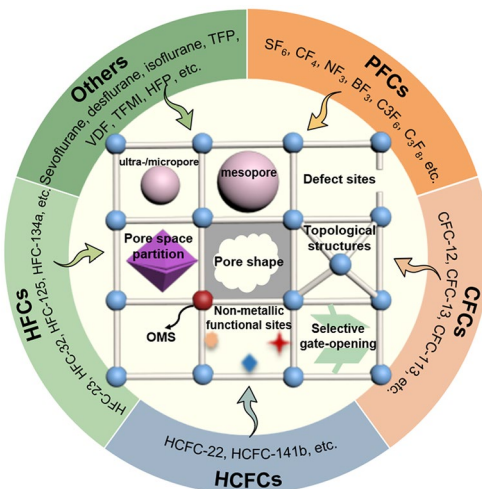
© The Author(s) 2024

### HIGHLIGHTS

- The progress of metal–organic frameworks (MOFs) in capturing and separating F-gases is highlighted.
- The molecular mechanisms of adsorption and separation are classified and analyzed.
- Toolboxes of MOFs structural design for fluorinated gases separation are provided.

**ABSTRACT** Fluorinated gases (F-gases) play a vital role in the chemical industry and in the fields of air conditioning, refrigeration, health care, and organic synthesis. However, the direct emission of waste gases containing F-gases into the atmosphere contributes to greenhouse effects and generates toxic substances. Developing porous materials for the energy-efficient capture, separation, and recovery of F-gases is highly desired. Recently, as a highly designable porous adsorbents, metal–organic frameworks (MOFs) exhibit excellent selective sorption performance toward F-gases, especially for the recognition and separation of different F-gases with highly similar properties, showing their great potential in F-gases control and recovery. In this review, we discuss the capture and separation of F-gases and their azeotropic, near-azeotropic, and isomeric mixtures in various application scenarios by MOFs, specifically classify and analyze molecular interaction between F-gases and MOFs, and interpret the mechanisms underlying their high performance regarding both adsorption capacity and selectivity, providing a repertoire for future materials design. Challenges faced in the transformation research roadmap of MOFs adsorbent separation technologies toward F-gases are also discussed, and areas for future research endeavors are highlighted.

**KEYWORDS** Fluorinated gas; Metal–organic framework; Adsorption; Separation; Molecular interaction



Yifan Gu, 159219yifan\_gu@tongji.edu.cn

<sup>1</sup> College of Environmental Science and Engineering, State Key Laboratory of Pollution Control and Resource Reuse, Tongji University, Siping Rd 1239, Shanghai 200092, People's Republic of China

<sup>2</sup> Department of Polymeric Materials, School of Materials Science and Engineering, Tongji University, Caoan Road 4800, Shanghai 201804, People's Republic of China

<sup>3</sup> Shanghai Institute of Pollution Control and Ecological Security, Shanghai 200092, People's Republic of China

<sup>4</sup> Key Laboratory of Cities' Mitigation and Adaptation to Climate Change, China Meteorological Administration (CMA), Tongji University, Shanghai 200092, People's Republic of China

## 1 Introduction

Fluorinated gases (F-gases), including perfluorocarbons (PFCs), hydrofluorocarbons (HFCs), chlorofluorocarbons (CFCs), hydrochlorofluorocarbons (HCFCs), inhaled volatile anesthetics (VAs), and other fluorine-containing gaseous compounds (Fig. 1), are widely used in air conditioning, refrigeration, medical, cable, semiconductor, and metal-processing industries [1–4]. The increasing use and emissions of F-gases have raised widespread environmental concerns. Most F-gases are typical greenhouse gases that exhibit much higher global warming potential (GWP) and longer atmospheric lifetime than carbon dioxide ( $\text{CO}_2$ ) and methane ( $\text{CH}_4$ ), and even lead to the depletion of the ozone layer [5–8]. In recent years, the greenhouse effect resulting

from F-gases and related substances (such as carbon tetrachloride) emitted annually by various industries is equivalent to emitting 870 million tonnes of  $\text{CO}_2$  equivalent, which is comparable to that of over 200 coal-fired power plants [9, 10]. In addition, the emissions and hydrolysis of F-gases are often accompanied by toxic or corrosive concomitants, such as HF, CO, and  $\text{NO}_x$ , which further adversely affect air quality and human health [11–16]. Therefore, achieving the effective capture, separation and recovery of F-gases to realize the climate goals, and the sustainable development of corresponding industries is top priority.

To date, cryogenic distillation is the main technology for separating F-gases for industrial applications [17–21]. However, some components of F-gases blends are similar in thermophysical properties, exhibiting azeotrope or

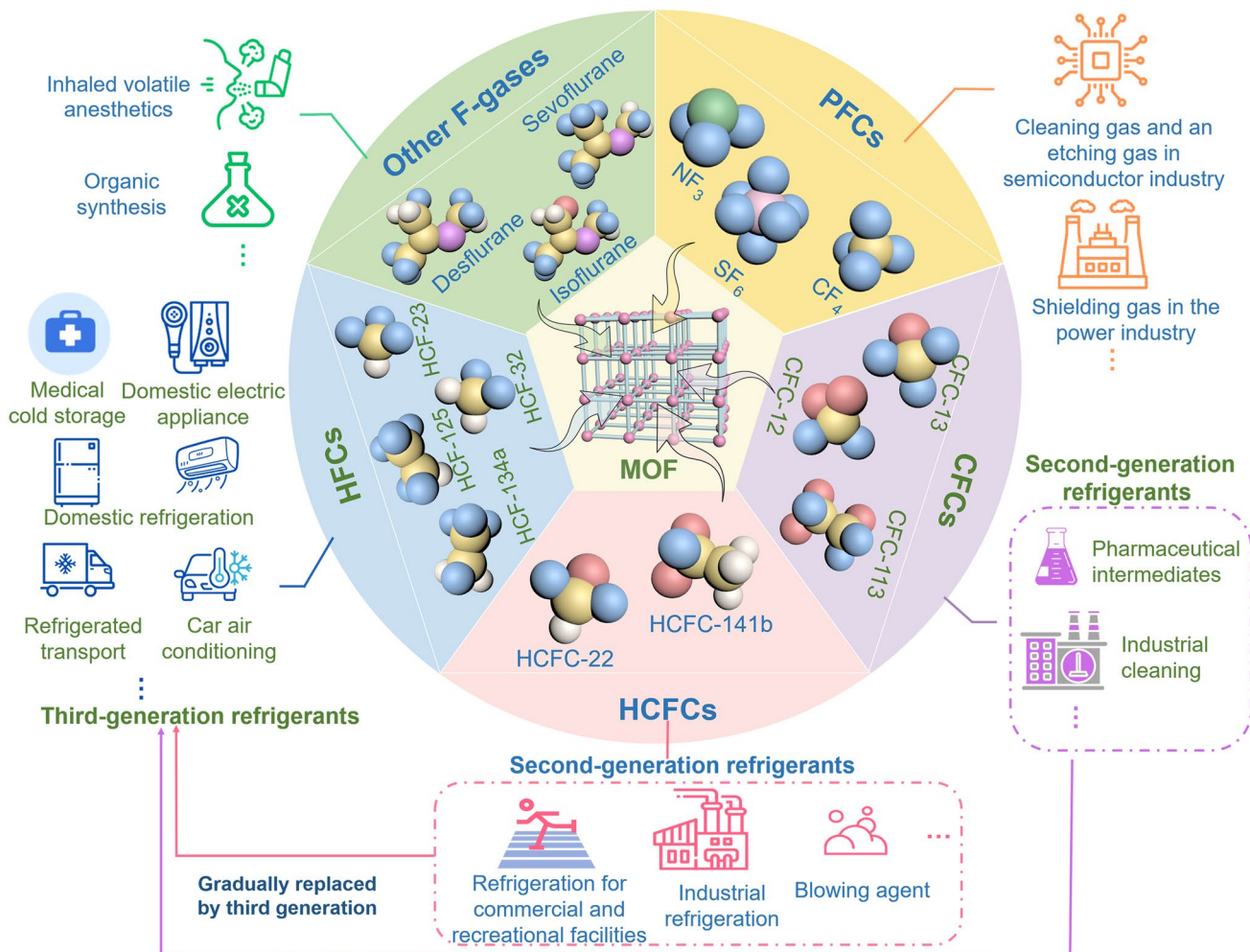


**Fig. 1** Schematic diagrams for trapping typical F-gases in a MOF platform

near-azeotrope. For example, the boiling points of  $\text{NF}_3$  and  $\text{CF}_4$  differ by approximately 1 K (143.35 K for  $\text{NF}_3$  and 144.95 K for  $\text{CF}_4$ ) and their relative volatility less than 1.05 at 193.15 K. Thus, cryogenic distillation is difficult to perform [22–25]. In addition, the huge energy consumption and anticorrosion equipment design of cryogenic distillation render it an infeasible choice [17, 23]. Membrane-based separation technologies are hampered by their low intrinsic permeability to F-gases and have low separation efficiency [23, 26–30]. Moreover, they have limited applications to large-scale membrane preparation and mass membrane production [31, 32]. Physical adsorptive separation based on porous materials has high selectivity, simple operation, and easy recovery, emerging as an energy-saving and environmentally friendly option for F-gases treatment [33–39]. However, traditional porous materials, such as zeolites and carbon materials, are highly stable but have poor separation selectivity toward F-gases [40–44]. Some F-gases (such as  $\text{CHClF}_2$ ) can react chemically with zeolites, and this feature is not conducive to desorption and sorbent recycling [45–47]. Moreover, in the separation of typical F-gases/ $\text{N}_2$  mixed gases, negatively charged oxides on zeolite surfaces and isolated cations on the front surfaces can enhance interactions with nitrogen molecules, which decrease selectivity to F-gases [40]. Therefore, designing efficient adsorbents for F-gases separation is highly desirable.

Metal–organic frameworks (MOFs) or porous coordination polymers are crystalline porous materials with periodic network structures formed by metal ions, clusters, and organic ligands through self-assembly [48–54]. As a highly designable porous material with multiple dimensions and customizable channels, MOFs have unique features for selectively adsorbing targets and have been widely used in olefin or alkane separation [55–58]; benzene, cyclohexane, and xylene separation [59–63]; carbon capture [64–69]; and natural gas purification [70–74]. Although research on MOFs for F-gases capture and purification is in the early stage, it has fully demonstrated its application potential in these fields and has begun to flourish. However, few studies have reviewed the application of MOFs in the management of fluorine-containing gases [75–80]. A comprehensive analysis of the adsorption mechanism at the molecular level is crucial for developing high-performance porous adsorbents [1, 40, 81].

In this review, we thoroughly reviewed the adsorption and separation of F-gases by MOFs in various application

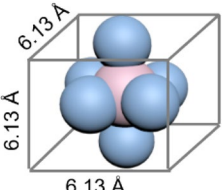
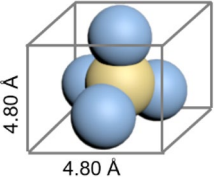
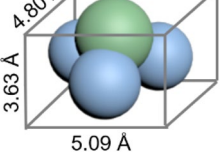
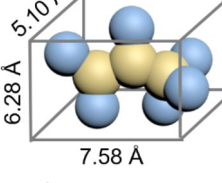
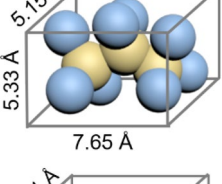
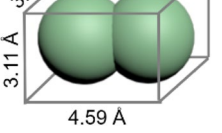
scenarios. The works on balancing the adsorption capacity and selectivity toward different F-gases by modifying the pore morphology, size, interacting sites, and framework flexibility of MOFs are summarized. Emphasis was placed on mechanisms for separating highly similar fluorine-containing gas components. We aimed to provide a reference for future MOFs design by classifying and analyzing molecular interaction between F-gases and MOFs and interpreting detailed mechanisms behind their high performance, instead of simply repeating existing work in chronological order or making a league table of the selectivity and adsorption capacities of the designs. In addition, we discussed challenges faced in the further development of MOF adsorbents for purifying F-gases for industrial applications and proposed future research opportunities and prospects.

## 2 Adsorption and Separation of PFCs

### 2.1 PFCs Capture from PFCs/ $\text{N}_2$ Mixtures

PFCs, mainly including  $\text{SF}_6$ ,  $\text{CF}_4$ ,  $\text{NF}_3$ , and  $\text{C}_3\text{F}_8$ , are irreplaceable gases in the semiconductor industry and often used as plasma-etching and plasma-cleaning gases. Most PFCs remain intact (60%–70% of the original component) in the manufacturing process. Given their high GWP and extremely long atmospheric lifetime (Table 1), used PFCs usually need to be removed through combustion and thermal plasma decomposition [1, 82]. However, these methods can not only recover F-gases but also produce inorganic fluorine waste, which needs further treatment [17, 43, 83]. An alternative solution to reduce PFCs consumption in the production process is to mix low-content PFCs with inert gases (typically  $\text{N}_2$ ). This approach is effective because a high-concentration  $\text{N}_2$  fluid mixture (with  $\text{SF}_6/\text{N}_2$  volume ratios often set to 0.1, 0.01, 0.002, or 0.0003) maintains a dielectric strength comparable to that of pure PFCs [84–91]. To meet the demand for high purity in power industry ( $\text{SF}_6 > 99\%$ ) and other industries, realize the recycling of expensive resources and reduce the environmental burden, the development of an effective physical adsorption process separating and recycling PFCs in PFCs/ $\text{N}_2$  mixtures is highly desired, which require sorbents with ideal adsorption selectivity and capacity for PFCs even at low concentrations. MOFs are potential sorbents for PFCs separation because of their highly designable pore chemistry. In this section, we will

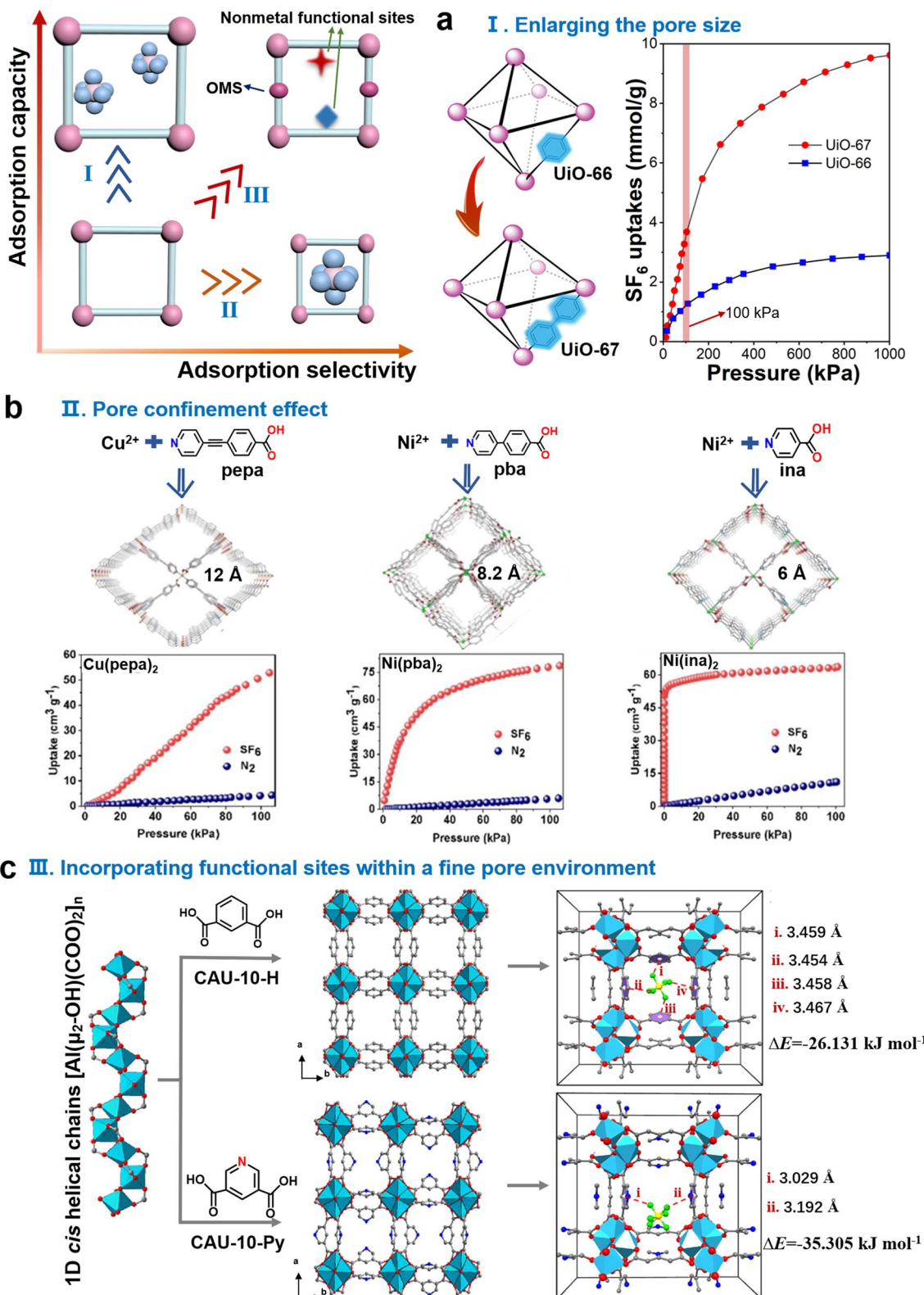
**Table 1** Properties of typical PFCs and N<sub>2</sub>

Gases [Refs.]	Molecular configurations and size	Kinetic diameter (Å)	Boiling points (K)	GWP (CO <sub>2</sub> =1)	Atmospheric lifetime (years)	Polarizability ( $\times 10^{-25}$ cm <sup>3</sup> )	Dipole moment ( $\times 10^{-18}$ esu·cm)
SF <sub>6</sub> [87, 92, 93]		5.2	209.25	22800	3200	65.4	0
CF <sub>4</sub> [86, 94]		4.8	145.11	7390	50,000	38.4	0
NF <sub>3</sub> [22, 23]		4.5	144.11	17,200	740	36.2	0.235
C <sub>3</sub> F <sub>6</sub> [95–97]		~6.0	236.3	100	10	63.5	–
C <sub>3</sub> F <sub>8</sub> [98–100]		~6.0	242	7000	> 2600	68.0	–
N <sub>2</sub> [88, 101]		3.8	77.35	–	–	17.4	0

discuss satisfactory performance of MOFs for capturing PFCs from PFCs/N<sub>2</sub> mixtures in terms of adsorption capacity, selectivity, and the trade-off between capacity and selectivity through pore environment and host–guest interaction regulation (Fig. 2). Current researches on PFCs adsorption by MOFs are at the initial stage and mostly focus on SF<sub>6</sub> capture (Table 2).

Void ratio and pore size are key factors for PFCs adsorption in porous materials, especially when capture capacity

is considered. An early study on SF<sub>6</sub> adsorption in UiO-66 (pore window size: 8, 11 Å) and MIL-100 (pore window size: 25 Å) demonstrated that MIL-100 with higher Brunauer–Emmett–Teller (BET) surface area (1947 m<sup>2</sup> g<sup>-1</sup> for MIL-100, 1333 m<sup>2</sup> g<sup>-1</sup> for UiO-66) adsorbed a higher amount of SF<sub>6</sub> (2.59 mmol g<sup>-1</sup>) than UiO-66 (1.45 mmol g<sup>-1</sup>) at 293 K and 1 bar, suggesting that PFCs adsorption capacity can be increased by using MOFs with large void ratios and pore size [102]. Compared with

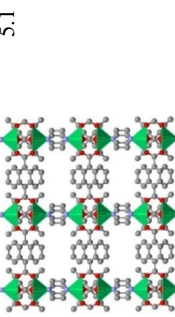
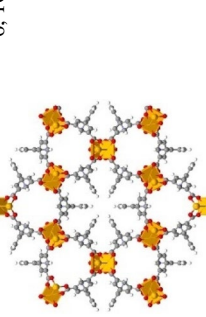
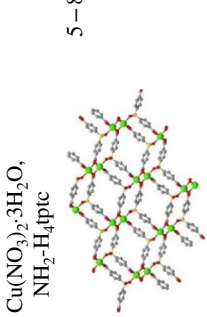
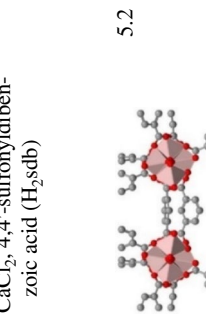


**Fig. 2** Three strategies for improving PFCs adsorption/separation by MOFs: (I) enlargement of pore size improves adsorption capacity for PFCs; (II) pore size constraint improves the adsorption selectivity of PFCs/ $\text{N}_2$ ; and (III) the introduction of metal or nonmetal sites breaks the trade-off between adsorption selectivity and adsorption capacity. **a** Adsorption isotherms of  $\text{SF}_6$  on  $\text{UiO-66}$  and  $\text{UiO-67}$  at 298 K. **b** Pore structure and adsorption isotherms of  $\text{Cu}(\text{pepa})_2$ ,  $\text{Ni}(\text{pba})_2$ , and  $\text{Ni}(\text{ina})_2$ . **c** Crystal structures of CAU-10-H and CAU-10-Py and binding sites with  $\text{SF}_6$

**Table 2** Properties, chemical compositions, and structures of various MOFs for adsorption and separation of PFCs mixtures (PFCs/N<sub>2</sub> and PFCs/PFCs)

F-gases	MOFs [Refs.]	Structures and Chemical compositions	Channel size (Å)	BET surface area (m <sup>2</sup> g <sup>-1</sup> )	IAST SF <sub>6</sub> /N <sub>2</sub> = 18.2 <sup>a</sup> (v/v=0.1)	Adsorption amount (mmol g <sup>-1</sup> )	Thermo-dynamic stability	Kinetic stability	Chemical stability	Main interactions
SF <sub>6</sub>	Cu(peba) <sub>2</sub> [92, 155]		12	814.3	SF <sub>6</sub> /N <sub>2</sub> = 18.2 <sup>a</sup> (v/v=0.1)	2.36 <sup>a</sup>	Stability up to 300 °C	Stable after 10 cycles		Pore confinement effect; vdW
Ni(peba) <sub>2</sub> [92, 156]			8.2	807.2	SF <sub>6</sub> /N <sub>2</sub> = 200.6 <sup>a</sup> (v/v=0.1)	3.50 <sup>a</sup>	Stability up to 400 °C	Stable after 10 cycles		Pore confinement effect; vdW
Ni(3-mpba) <sub>2</sub> [126]			11.93	835.1	SF <sub>6</sub> /N <sub>2</sub> = 221 <sup>a</sup> (v/v=0.1)	2.83 <sup>a</sup>	Stability up to 380 °C	Stable after 5 cycles		Functional group; vdW
Ni(infa) <sub>2</sub> [92, 157]			6	470	SF <sub>6</sub> /N <sub>2</sub> = 375.1 <sup>a</sup> (v/v=0.1)	2.84 <sup>a</sup> , 2.39 <sup>b</sup>	Framework decomposition occurs after 400 °C	Stable after 10 cycles		Pore confinement effect; vdW

**Table 2** (continued)

F-gases	MOFs [Refs.]	Structures and Chemical compositions	Channel size (Å)	BET surface area (m <sup>2</sup> g <sup>-1</sup> )	Adsorption amount (mmol g <sup>-1</sup> )	Thermo-dynamic stability	Kinetic stability	Chemical stability	Main interactions
Ni(adc) (dabco) <sub>0.5</sub> [112]		5.1	743.9	SF <sub>6</sub> /N <sub>2</sub> =948.2 <sup>a</sup> (v/v=0.1)	2.38 <sup>a</sup> , 2.23 <sup>b</sup>	Brilliant thermal stability	Stable after 10 cycles	Excellent resistance to water vapor	Pore confinement effect; vdW (F...π)
Cu-MOF-NH <sub>2</sub> [123]		6, 10, 13	2145	SF <sub>6</sub> /N <sub>2</sub> =266 <sup>a</sup> (v/v=0.1)	7.88 <sup>a</sup> , 3.39 <sup>b</sup>	Stability up to 270 °C	Stable after 10 cycles	Unstable in water environments	vdW (N-H...F)
SBMOF-I [106, 107]		5-8.5	169.33	SF <sub>6</sub> /N <sub>2</sub> =727 <sup>a</sup> (v/v=0.0003), 325 <sup>a</sup> (v/v=0.1)	1.02 <sup>a</sup>	Stable after 5 cycles	Good structural stability	Aromatic functionalized channels; noncovalent interaction enhance the pore confinement effect	Pore size; functional group
CAU-10-H [101]		5.2	684.4	SF <sub>6</sub> /N <sub>2</sub> =122.6 (v/v=0.1)	1.00 <sup>a</sup> ; 1.07 <sup>a</sup> (273 K); 0.66 <sup>b</sup>	Stability up to 400 °C			



**Table 2** (continued)

F-gases	MOFs [Refs.]	Structures and Chemical compositions	Channel size (Å)	BET surface area (m <sup>2</sup> g <sup>-1</sup> )	Adsorption amount (mmol g <sup>-1</sup> )	Thermo-dynamic stability	Kinetic stability	Chemical stability	Main interactions
CAU-10-Py [101]			5.2	935.9	SF <sub>6</sub> /N <sub>2</sub> =203.6 (v/v=0.1) 1.13 <sup>b</sup>	1.76 <sup>a</sup> ; 2.11 <sup>a</sup> (273 K); 1.13 <sup>b</sup>	Stability up to 420 °C Stable after 6 cycles		Pore size; functional group
AlCl <sub>3</sub> ·6H <sub>2</sub> O, 3,5-pyridinedicarboxylic acid (pydc)			5.5×5.5 Å <sup>2</sup>	930.08	SF <sub>6</sub> /N <sub>2</sub> =317.6 <sup>a</sup> (v/v=0.1), 133.63 <sup>a</sup> (v/v=0.01)	2.63 <sup>a</sup>	Stability up to 370 °C Stable after 5 cycles	Good water stability	Pore size; vDW
Co-MOF (GNU-3) [125]									
M-MOF-74 (M=Mg, Co, Zn) [118]		Co(NO <sub>3</sub> ) <sub>2</sub> ·6H <sub>2</sub> O, H <sub>2</sub> ipa	11	992–1631	SF <sub>6</sub> /N <sub>2</sub> =18.2 <sup>a</sup> –46 <sup>a</sup> (v/v=0.1)	3.71–6.42 <sup>a</sup>		OMS	
HBU-21 [116]		Metallic salt, benzenedicarboxylate (dobdc)	6.14	381.44	SF <sub>6</sub> /N <sub>2</sub> =184.05 <sup>a</sup> (v/v=0.1)	0.949 <sup>a</sup>	Stability up to 400 °C	Recyclable and reusable	Stable in acetone, but prone to collapse in distilled water and anhydrous methanol
		In(NO <sub>3</sub> ) <sub>3</sub> ·4H <sub>2</sub> O, 9-(4-carboxyphenyl)-9H-carbazole-3,6-dicarboxylic acid							

**Table 2** (continued)

F-gases	MOFs [Refs.]	Structures and Chemical compositions	Channel size (Å)	BET surface area ( $\text{m}^2 \text{ g}^{-1}$ )	Adsorption amount (mmol g <sup>-1</sup> )	Thermo-dynamic stability	Kinetic stability	Chemical stability	Main interactions
CTH-18 [158]		MnCl <sub>2</sub> ·4H <sub>2</sub> O, 1,2,3,4,5,6-Hexamis(4-carboxyphenyl)benzene (H <sub>6</sub> epb)	4.3, 5.1	354	SF <sub>6</sub> /N <sub>2</sub> =29 <sup>a</sup> (v/v=0.1)	~1.9 <sup>a</sup> , ~1.55 <sup>b</sup> before 425 °C	Stable in organic solvents	Pore confinement effect; vdW	
HKUST-1 (Cu-BTC or MOF-199) [1, 14, 109, 121, 131]		Cu(NO <sub>3</sub> ) <sub>2</sub> ·3H <sub>2</sub> O, 1,3,5-benzenetricarboxylic acid (H <sub>3</sub> btc)	7~12	1428~1880	SF <sub>6</sub> /N <sub>2</sub> =127 <sup>a</sup> (v/v=0.1)	6.71 <sup>a</sup> before 370 °C	Stable before 370 °C	Minor decrease after 7 cycles	Structural decomposition occurs in water or humid air
Im% @ HKUST-1 [21]		Cu(NO <sub>3</sub> ) <sub>2</sub> ·3H <sub>2</sub> O, H <sub>3</sub> btc, imidazole	6.4	1211.0	SF <sub>6</sub> /N <sub>2</sub> =93 <sup>a</sup> (v/v=0.1)	5.98 <sup>a</sup> before 370 °C	Stable before 370 °C	Minor decrease after 7 cycles	Functional groups; OMS
MIL-100 [93, 159, 160]		FeCl <sub>3</sub> solutions, H3btc	25, 29	1772	SF <sub>6</sub> /N <sub>2</sub> =24.4 <sup>a</sup> (v/v=0.1)	2.95 <sup>a</sup> before 270 °C	Stable before 270 °C	Great water stability	OMS
MIL-100 granule [161]		Fe(NO <sub>3</sub> ) <sub>3</sub> ·9H <sub>2</sub> O, H3btc	-	1619	SF <sub>6</sub> /N <sub>2</sub> =24.4 <sup>a</sup> (v/v=0.1)	1.658 <sup>a</sup>	Stable after 5 cycles	Great water stability	OMS



**Table 2** (continued)

F-gases	MOFs [Refs.]	Structures and Chemical compositions	Channel size (Å)	BET surface area (m <sup>2</sup> g <sup>-1</sup> )	Adsorption amount (mmol g <sup>-1</sup> )	Thermo-dynamic stability	Kinetic stability	Chemical stability	Main interactions
MIL-101 [93, 119, 162]		Cr(NO <sub>3</sub> ) <sub>3</sub> ·9H <sub>2</sub> O, terephthalic acid	29, 34	2162.01	SF <sub>6</sub> /N <sub>2</sub> ~24 <sup>a</sup>	2.01 <sup>a</sup>	Stable before 500 °C	3.39 <sup>a</sup>	Pore size; OMS
Co <sub>2</sub> (1,4-bdc) <sub>2</sub> (dabco) [93, 163]		7.6	1600						Framework flexibility
MOFF-5 [111]		Co(NO <sub>3</sub> ) <sub>2</sub> ·6H <sub>2</sub> O, bdc, dabco	22	2445		1.74	Framework decomposition occurs at approximately 220 °C		Poor stability in water and under humid conditions
UiO-66 [102, 127, 142]		Cu(NO <sub>3</sub> ) <sub>2</sub> ·2.5H <sub>2</sub> O, fluorinated tetrazole	8.11	1074	SF <sub>6</sub> /N <sub>2</sub> =74 <sup>a</sup> ( $\text{v}/\text{v}=0.1$ ), 130 <sup>a</sup> ( $\text{v}/\text{v}=0.002$ )	1.45 <sup>a</sup> (293 K)	Good thermal stability	1.45 <sup>a</sup> (293 K)	Fluorine functional groups
		ZrCl <sub>4</sub> , bdc							vdW
									Good chemical, mechanical stability

Table 2 (continued)

**Table 2** (continued)

F-gases	MOFs [Refs.]	Structures and Chemical compositions	Channel size (Å)	BET surface area (m <sup>2</sup> g <sup>-1</sup> )	Adsorption amount (mmol g <sup>-1</sup> )	Thermo-dynamic stability	Kinetic stability	Chemical stability	Main interactions
Tm-TBAPy [164]		Tm(C <sub>2</sub> H <sub>3</sub> O <sub>2</sub> ) <sub>3</sub> ·xH <sub>2</sub> O, H <sub>4</sub> TBAPy	6.4–6.9	716	SF <sub>6</sub> /N <sub>2</sub> =48 <sup>a</sup> (v/v=0.1, 293 K)	1.83 <sup>a</sup> (293 K)	Stability up to 400 °C	Stable under conditions other than acidic (1 M HCl, pH=1) and alkaline (1 M NaOH, pH=14)	Pore confinement effect; vdW
M <sub>3</sub> (HC <sub>2</sub> O <sub>4</sub> ) <sub>6</sub> (M=Co, Ni, Mn) [83]		Co(NO <sub>3</sub> ) <sub>2</sub> ·6H <sub>2</sub> O, formic acid	5–6	330.1	SF <sub>6</sub> /N <sub>2</sub> =120 <sup>a</sup> (v/v=0.01)	2.17 <sup>a</sup> (Co)	2.17 <sup>a</sup> (Co)	Polar functional groups (charge exchange between the F atom in F <sub>2</sub> gases and the H atom in HC <sub>2</sub> O <sub>4</sub> <sup>-</sup> ); pore confinement effect	
BUT-53 [124]		Co(OAc) <sub>2</sub> ·4H <sub>2</sub> O, H <sub>2</sub> dpb	4–8	866	SF <sub>6</sub> /N <sub>2</sub> =248 <sup>a</sup> (v/v=0.1)	3.55 <sup>a</sup> , 2.82 <sup>b</sup>	Stability up to 550 °C	Superior water stability	F...H interaction

**Table 2** (continued)

F-gases	MOFs [Refs.]	Structures and Chemical compositions	Channel size (Å)	BET surface area (m <sup>2</sup> g <sup>-1</sup> )	Adsorption amount (mmol g <sup>-1</sup> )	Thermo-dynamic stability	Kinetic stability	Chemical stability	Main interactions
CF <sub>4</sub>	Ni(adc) (dabco) <sub>0.5</sub> [86, 112]		5.1	743.9	CF <sub>4</sub> /N <sub>2</sub> =23 <sup>a</sup> (v/v=0.1) 1.76 <sup>a</sup> , 0.52 <sup>b</sup>	Brilliant thermal stability	Stable after 5 cycles	Excellent resistance to water vapor	Pore confinement effect; vdW (F...π)
	Ni(inma) <sub>2</sub> [23]		6	434	CF <sub>4</sub> /N <sub>2</sub> =34.7 <sup>a</sup> (v/v=0.1)	2.92 <sup>a</sup> , 1.15 <sup>b</sup>	Stable before 400 °C	vdW	
	NiCl <sub>2</sub> ·6H <sub>2</sub> O, H <sub>2</sub> adc, dabco								
	Ni(CH <sub>3</sub> COO) <sub>2</sub> ·4H <sub>2</sub> O, Isonicotinic acid		5	872	CF <sub>4</sub> /N <sub>2</sub> =46.3 <sup>a</sup> (v/v=0.1)	2.69 <sup>a</sup> , 1.25 <sup>b</sup>	Stable before 400 °C	Amino functional groups	Pore confinement effect; vdW; electrostatic interaction
	NH <sub>2</sub> -Ni-MOF (Ni(3-ain) <sub>2</sub> ) [23]								
	JUCXEK [22]		6.26	1253.1	CF <sub>4</sub> /NF <sub>3</sub> =50.15 <sup>a</sup> (v/v=0.05)	0.8 (20 bar, v/v=0.05)	Stable after 12 cycles		
	Zn(fba) [113]		5	345	CF <sub>4</sub> /NF <sub>3</sub> =29 <sup>a</sup> (v/v=0.76)	~1.05 <sup>a</sup>	Stable before 500 °C	Good water stability	vdW; close match with the arene-lined pores
	C <sub>4</sub> H <sub>10</sub> O <sub>6</sub> Zn, benzoic acid								



**Table 2** (continued)

F-gases	MOFs [Refs.]	Structures and Chemical compositions	Channel size (Å)	BET surface area (m <sup>2</sup> g <sup>-1</sup> )	IAST CF <sub>4</sub> /CH <sub>4</sub> =4.6	Adsorption amount (mmol g <sup>-1</sup> )	Thermo-dynamic stability	Kinetic stability	Chemical stability	Main interactions
LiFM-90 [138]	ZnCl <sub>4</sub> , bpdc	Co <sub>2</sub> (1,4-bdc) <sub>2</sub> (dabco) [93, 163]	6.96–7.97	2933.4	CF <sub>4</sub> /CH <sub>4</sub> =4.6	2.0	0.714 <sup>a</sup>	Stable before 500 °C	0.714 <sup>a</sup>	OMS; pore size
MIL-100 [93, 159, 160]	FeCl <sub>3</sub> solutions, bic	Cr(NO <sub>3</sub> ) <sub>3</sub> ·9H <sub>2</sub> O, terephthalic acid	7.6	1600	25, 29	1772	0.53 <sup>a</sup>	Stable before 270 °C	0.53 <sup>a</sup>	Pore size; OMS
MIL-101 [93, 119, 162]										

**Table 2** (continued)

F-gases	MOFs [Ref.]	Structures and Chemical compositions	Channel size (Å)	BET surface area (m <sup>2</sup> g <sup>-1</sup> )	Adsorption amount (mmol g <sup>-1</sup> )	Thermo-dynamic stability	Kinetic stability	Chemical stability	Main interactions
	MOFF-5 [111]		22	2445	0.09	Framework decomposition occurs at approximately 220 °C	Poor stability in water and under humid conditions	Fluorine functional groups	
	Cu(NO <sub>3</sub> ) <sub>2</sub> ·2.5H <sub>2</sub> O, fluorinated tetrazole		8, 11	1074	~0.75 <sup>a</sup>	Good thermal stability	Good chemical and mechanical stability	vdW	
	UiO-66 [102, 127, 142]								
	ZrCl <sub>4</sub> , bdc		9	616	~0.68 <sup>a</sup>	Good thermal stability	Stable after 20 cycles	Good chemical and mechanical stability	Pore confinement effect; polar functional groups enhance vdW effect
	UiO-66-Br <sub>2</sub> [127]								
	ZrCl <sub>4</sub> , bdc-Br								
	SBMOF-1 [107]		5–8.5	169.33	CF <sub>4</sub> /N <sub>2</sub> =18.21(v/v=0.01, P/P <sub>0</sub> =1))	1.01 (P/P <sub>0</sub> =1)	Good structural stability	Aromatic functionalized channels; noncovalent interaction enhance the pore confinement effect	
	CaCl <sub>2</sub> , sdb								

**Table 2** (continued)

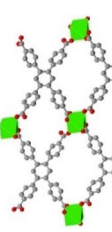
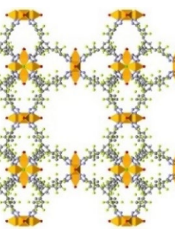
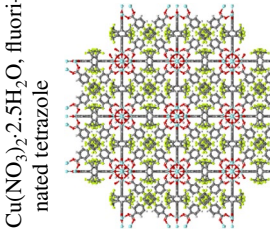
F-gases	MOFs [Refs.]	Structures and Chemical compositions	Channel size (Å)	BET surface area (m <sup>2</sup> g <sup>-1</sup> )	Adsorption amount (mmol g <sup>-1</sup> )	Thermo-dynamic stability	Kinetic stability	Chemical stability	Main interactions
M <sub>3</sub> (HCOO) <sub>6</sub> (M=Co, Ni, Mn) [83]		5–6	330.1	CF <sub>4</sub> /N <sub>2</sub> =11.6 <sup>a</sup> (v/v=0.01)	1.42 <sup>a</sup>			Polar functional groups (charge exchange between the F atom in F-gases and the H atom in HCOO <sup>-</sup> ); pore confinement effect vDW	
Co(NO <sub>3</sub> ) <sub>2</sub> ·6H <sub>2</sub> O, formic acid	Ni(ina) <sub>2</sub> [23]	6	434	NF <sub>3</sub> /N <sub>2</sub> =35.8 <sup>a</sup> (v/v=0.1)	2.69 <sup>a</sup>	Stable before 400 °C			
Ni(CH <sub>3</sub> COO) <sub>2</sub> ·4H <sub>2</sub> O, isonicotinic acid		5	872	NF <sub>3</sub> /N <sub>2</sub> =32.4 <sup>a</sup> (v/v=0.1)	2.62 <sup>a</sup>	Stable before 400 °C		Amino functional groups	
NH <sub>2</sub> -Ni-MOF (Ni(3-ain) <sub>2</sub> ) [23]		5–8.5	169.33		1.17 (P/P <sub>0</sub> =1)		Good structural stability	Aromatic functionalized channels; noncovalent interaction enhance the pore confinement effect	
SBMOF-I [107]									
CaCl <sub>2</sub> , sdb									

**Table 2** (continued)

F-gases	MOFs [Refs.]	Structures and Chemical compositions	Channel size (Å)	BET surface area (m <sup>2</sup> g <sup>-1</sup> )	IAST (w/v=0.01)	Adsorption amount (mmol g <sup>-1</sup> )	Thermo-dynamic stability	Kinetic stability	Chemical stability	Main interactions
M <sub>3</sub> (HCOO) <sub>6</sub> (M=Co, Ni, Mn) [83]		5–6	330.1	NF <sub>3</sub> /N <sub>2</sub> =19.2 <sup>a</sup> (w/v=0.01)	1.46 <sup>a</sup>					Polar functional groups (charge exchange between the F atom in F-gases and the H atom in HCOO <sup>-</sup> ); pore confinement effect OMS
BF <sub>3</sub>	M-MOF-74 (M=Mg, Co, Zn) [14]		11	992–1631		0.9 bar: 7.3 (Co-MOF-74), 3.5 (Mn-MOF-74), 2.1 (Mg-MOF-74)	Stable after 10 cycles			
C <sub>3</sub> F <sub>8</sub>	Co <sub>x</sub> Cr-MIL-101 [119]	Metallic salt, dobdc	14–20, 22–30	2162.01– 2518.14	C <sub>3</sub> F <sub>8</sub> /N <sub>2</sub> =146.7 <sup>a</sup>	0.078 (180 Pa)	Good thermal stability	Good cyclic stability	Good cyclic stability	OMS; unique layered porous structure
		Cr(NO <sub>3</sub> ) <sub>3</sub> ·9H <sub>2</sub> O, Co(NO <sub>3</sub> ) <sub>2</sub> ·6H <sub>2</sub> O, terephthalic acid								



**Table 2** (continued)

F-gases	MOFs [Ref.]	Structures and Chemical compositions	Channel size (Å)	BET surface area (m <sup>2</sup> g <sup>-1</sup> )	Adsorption amount (mmol g <sup>-1</sup> )	Thermo-dynamic stability	Kinetic stability	Chemical stability	Main interactions
C <sub>3</sub> F <sub>6</sub>	Ca-tcpb [142]		260.65	C <sub>3</sub> F <sub>6</sub> /C <sub>3</sub> F <sub>8</sub> >10000 <sup>a</sup> (w/v=0.01)	2.0 <sup>a</sup>	Stable up to approximately 400 °C	Stable after 5 cycles		Kinetic sieving; vdW
C <sub>6</sub> F <sub>14</sub>	MOFF-5 [111]		22	2445	6.65	Framework decomposition occurs at approximately 220 °C		Poor stability in water and under humid conditions	Fluorine functional groups
Compound 2 [128]	Cu(NO <sub>3</sub> ) <sub>2</sub> ·2.5H <sub>2</sub> O, fluorinated tetrazole ZrCl <sub>4</sub> , tpdc-(CF <sub>3</sub> ) <sub>2</sub>		11, 16	2819	142 wt% (50 Torr)	Stable up to approximately 200 °C	Stable after 10 cycles	Great water stability	Fluorine functional groups

298 K. <sup>a</sup> At 1 bar. <sup>b</sup> At 0.1 bar

traditional porous materials, such as activated carbon, highly porous MOFs have well-developed reticular chemistry and are thus easy to design [84, 103, 104]. For example, when a long linker (biphenyl-4,4'-dicarboxylate) was replaced with benzene-1,4-dicarboxylic acid in UiO-66 for the preparation of UiO-67 (Fig. 2a), the larger pore size (12 and 23 Å) and higher BET surface area ( $2411 \text{ m}^2 \text{ g}^{-1}$ ) in UiO-67 led to a higher  $\text{SF}_6$  adsorption capacity ( $3.7 \text{ mmol g}^{-1}$ ) [105]. However, UiO-66 (~37) had higher  $\text{SF}_6/\text{N}_2$  selectivity predicted by ideal adsorption solution theory (IAST) at 298 K and 1 bar than UiO-67 (~21). These results suggest that only increasing the pore size of MOFs may lead to a trade-off between adsorption capacity and selectivity.

Strong interactions between PFCs and MOFs are conducive to adsorption selectivity for PFCs/ $\text{N}_2$  separation. Regulating the pore size of MOFs to be close to that of PFCs can enhance host–guest van der Waals (vdW) interaction through the pore confinement effect and enhance adsorption affinity. For example, SBMOF-1 has a similar pore size ( $6.703 \times 7.840 \text{ \AA}$ ) to  $\text{SF}_6$  ( $6.13 \times 6.13 \times 6.13 \text{ \AA}$ ), which can achieve an IAST selectivity of up to 325 for  $\text{SF}_6/\text{N}_2$  ( $v/v=0.1$ ) at 298 K and 1 bar [106, 107]. The appropriate pore size in SBMOF-1 contributes to the strong hydrogen bonding interactions between hydrogen atoms on the benzene ring, and the fluorine atoms of  $\text{SF}_6$ .  $\text{Ni}(\text{ina})_2$  (pore size: 6 Å),  $\text{Ni}(\text{pba})_2$  (8.2 Å), and  $\text{Cu}(\text{peba})_2$  (12 Å) with similar diamond networks were synthesized using pyridine carboxylic acid ligands with different length [92].  $\text{Ni}(\text{ina})_2$  with the closest kinetic diameter to  $\text{SF}_6$  (5.2 Å) has a selectivity of as high as 375.1 ( $\text{SF}_6/\text{N}_2$ ,  $v/v=0.1$  at 298 K and 1 bar) (Fig. 2b), and its high isosteric heat of adsorption (the  $Q_{\text{st}}$  for  $\text{Ni}(\text{ina})_2$ ,  $\text{Ni}(\text{pba})_2$ , and  $\text{Cu}(\text{peba})_2$  are 33.4, 24.0 and 14.4  $\text{kJ mol}^{-1}$ , respectively) further confirms affinity (Fig. 2c). Density functional theory (DFT) calculation and Grand canonical Monte Carlo (GCMC) simulation reveals the reason from the molecular point of view, calculated using the forcite module with a universal force field (UFF) for the geometrically optimized single-crystal frameworks of these three MOFs, and also employing a  $Q_{\text{qe}}$  fitted charges [108]. The pore structure of  $\text{Ni}(\text{ina})_2$  is perfectly matched with  $\text{SF}_6$ , resulting in a significantly shorter interaction distance (2.74–3.18 Å) between the fluorine atom of  $\text{SF}_6$  and the H atom on the pyridine ring of MOF than that of  $\text{Ni}(\text{pba})_2$  (3.06–4.26 Å) and  $\text{Cu}(\text{peba})_2$  (3.11–3.27 Å). The  $\text{SF}_6$  interaction sites are highly consistent with the results revealed by single-crystal X-ray diffraction (SCXRD). And the molecular simulation shows that

the binding energies ( $\Delta E$ ) of  $\text{SF}_6$  with  $\text{Ni}(\text{ina})_2$ ,  $\text{Ni}(\text{pba})_2$ , and  $\text{Cu}(\text{peba})_2$  are 59.08, 38.21, and 30.18  $\text{kJ mol}^{-1}$ , respectively, which also aligns with the trend of  $Q_{\text{st}}$  values obtained from experiments. In addition, the adsorption capacity of  $\text{Ni}(\text{ina})_2$  for  $\text{SF}_6$  at 0.1 bar ( $2.39 \text{ mmol g}^{-1}$ ) is higher than that of most reported MOFs (Table 2), such as HKUST-1 (1.37  $\text{mmol g}^{-1}$ ) [109], HKUST-1c (1.32  $\text{mmol g}^{-1}$ ) [91], UU-200 (0.99  $\text{mmol g}^{-1}$ ) [110], DUT-9 (0.80  $\text{mmol g}^{-1}$ ) [93],  $\text{Zn}_4\text{O}(\text{dmcpz})_3$  (1.12  $\text{mmol g}^{-1}$ ) [93], and MOFF-5 (0.09  $\text{mmol g}^{-1}$ ) [111], further demonstrating its potential to capture  $\text{SF}_6$  at a low partial pressure. Both  $\text{Ni}(\text{ina})_2$  (IAST = 34.7, 298 K, 1 bar) and  $\text{Ni}(\text{adc})(\text{dabco})_{0.5}$  (IAST = 23, 298 K, 1 bar) exhibit good selectivity for  $\text{CF}_4/\text{N}_2$ , but achieving industrial application requires good water stability [23, 86, 112]. The MOF structure  $\text{Zn}(\text{fba})$  synthesized from fluorine-containing aromatic ligands not only possesses the water stability inherent in Zn-MOFs, but also shows excellent equilibrium selectivity for  $\text{CF}_4$  (the IAST of  $\text{CF}_4/\text{N}_2$  is 29 at 298 K and 1 bar) due to the close matching of small spherical pores (5 Å) within its corrugated channel, which is the highest selectivity reported for  $\text{CF}_4$  in a water-stabilized MOFs [113]. However, MOFs with pore size comparable to that of PFCs often do not exhibit remarkable adsorption capacities due to the limited pore volume.

Both adsorption capacity and selectivity are crucial to PFCs capture and separation performance. Introducing interaction sites into MOF's apertures allow for extraordinary host–guest interactions for PFCs sorption might be the key to balancing selectivity and adsorption capacity. MOFs with open metal sites (OMS) usually have strong electrostatic interactions between metal sites and F-gases with certain polarity or charge distribution [114–117]. The OMS-containing series of isostructured M-MOF-74 ( $M=\text{Co, Mg, Zn}$ ) exhibit remarkable adsorption capacities for  $\text{SF}_6$  at 298 K and 1 bar, and Mg-MOF-74 (BET surface area =  $1631 \text{ m}^2 \text{ g}^{-1}$ ) and Co-MOF-74 (BET surface area =  $1219 \text{ m}^2 \text{ g}^{-1}$ ) reach as high as 6.42 and 5.34  $\text{mmol g}^{-1}$ , respectively [118]. The adsorption capacity of Zn-MOF-74 (BET surface area =  $992 \text{ m}^2 \text{ g}^{-1}$ ) under the same conditions is relatively lower (3.79  $\text{mmol g}^{-1}$ ) but still higher than the adsorption capacities of MOFs with comparable specific surface area but no OMS (such as 2.36  $\text{mmol g}^{-1}$  for  $\text{Cu}(\text{peba})_2$ ; Table 2), and the selective adsorption capacity of  $\text{SF}_6/\text{N}_2$  is as high as 46. The introduction of accessible cobalt ions into MIL-101's framework enriches its active sites and simultaneously improves the adsorption capacity of  $\text{Co}_{0.2}\text{Cr-MIL-101}$  for  $\text{C}_3\text{F}_8$  (0.078  $\text{mmol g}^{-1}$  at 298 K and

1.8 bar) and the selectivity of  $C_3F_8/N_2$  (IAST = 146.7 at 298 K and 1 bar), which are 3.03 and 14.3 times the adsorption capacity and selectivity of the original MIL-101, respectively [119]. However, OMS in MOFs usually preferentially coordinate with water, causing the competitive adsorption of  $H_2O$  and low water stability of MOFs when moisture is present in the gas mixture. For example, the OMS-containing HKUST-1 has an excellent adsorption capacity for  $SF_6$  ( $6.71 \text{ mmol g}^{-1}$ , 298 K, and 1 bar), but its structure irreversibly decomposes once exposed to water or humid air, which significantly limits its application [120]. However, after the introduction of imidazole (Im) ligand into HKUST-1, water stability was significantly enhanced due to the pre-attached of Im to the unsaturated Cu sites [121, 122]. There was also no significant decrease in Im-HKUST-1 performance after several adsorption/desorption cycles. Doping MOFs with hybridized ligands is an effective strategy to enhance their adsorption and water stability properties.

Given that PFCs have multiple fluorine atoms in their molecular structures, introducing hydrogen bonding receptors into a pore surface might enhance the affinity of MOFs with PFCs. The hydrogen atom on the  $-NH_2$  group introduced into Cu-MOF- $NH_2$  can simultaneously form hydrogen bonds with the three fluorine atoms ( $N-H \dots F$ ) of  $SF_6$ , and cooperates with vdW interactions and pore confinement effect afforded to the framework by the calix[3]zrene-analogous nanospace, enabling the selective adsorption of  $SF_6$  from mixtures with  $N_2$  [123]. At 298 K and 1 bar, the benchmark adsorption of  $SF_6$  reaches  $7.88 \text{ mmol g}^{-1}$ , with an IAST selectivity of 266 ( $v/v = 0.1$ ). The Co(II)-pyrazolate MOF (BUT-53) exhibits excellent  $SF_6$  adsorption capacity ( $3.55 \text{ mmol g}^{-1}$ ) and unprecedented  $SF_6/N_2$  selective adsorption (IAST = 2485,  $v/v = 0.1$ ) at 1 bar and 298 K, and can efficiently recover high-purity (>99.9%)  $SF_6$  from low-concentration (10%) mixtures through breakthrough experiments [124]. These features are due to  $F \dots H$  interactions between the benzene and pyrazole groups of dipyrazolate (dpb) ligands on BUT-53 and  $SF_6$ , and dpb ligands afford MOFs dynamic molecular traps that can accommodate guest molecules of different sizes. The charge exchange between H atoms from formic acid and F atoms from PFCs ( $SF_6$ ,  $CF_4$  and  $NF_3$ ) in  $M_3(HCOO)_6$  ( $M=Co$ ,  $Ni$ ,  $Mn$ ) channel results in PFC adsorption performance exceeding that of  $N_2$ , and the restriction of appropriate pore size on gas molecules further enhances the affinity between host and guest [83]. At 298 K and 1 bar, the adsorption capacities of  $Co_3(HCOO)_6$  are  $2.17 \text{ mmol g}^{-1}$  for  $SF_6$  and only

$0.16 \text{ mmol g}^{-1}$  for  $N_2$ , which exhibits outstanding  $SF_6/N_2$  selective adsorption ( $v/v = 0.01$  for  $SF_6/N_2$ , IAST = 120). A Co-MOF (GNU-3) containing a  $H_2ipa$  ligand has a localized nanomolecular trap, which offsets the trade-off effect of  $SF_6$  using functional pore surface modification and suitable pore size [125]. The adsorption position of  $SF_6$  in GNU-3 was visualized by GCMC simulation (the frame and gases used the  $Q_{eq}$  method for atomic partial charges and the UFF adopted by Lennard-Jones parameters) and combined with DFT calculations to reveal the adsorption behavior within the MOFs. Through strong hydrogen bonding interactions with the benzene ring of the framework and the hydrogen atoms of the  $ipa^{2-}$  in the pore,  $SF_6$  is trapped in the polyaromatic ring-functionalized channel centers and nanomolecular traps in the pore walls. At 298 K and 1 bar experimental conditions, activated GNU-3a exhibits an  $SF_6$  selectivity of 317.6 ( $SF_6/N_2$ ,  $v/v = 0.1$ ) with an adsorption capacity of  $2.63 \text{ mmol g}^{-1}$ , which closely aligns with the adsorption trends and capacities (about  $2.75 \text{ mmol g}^{-1}$ ) obtained from theoretical calculations. In addition, GNU-3 has excellent thermal/chemical stability and kinetic stability, and its cost-effective raw materials and environmentally friendly synthesis method highlight its potential for industrial applications.

Compared with  $Ni(pba)_2$ ,  $Ni(3-mpba)_2$  obtained by introducing methyl into pores has more binding sites with  $SF_6$  and smaller pores, which enhances affinity with  $SF_6$ , and thus shows improved adsorption selectivity for  $SF_6/N_2$  (IAST = 221 at 298 K and 1 bar,  $v/v = 0.1$ ) and adsorption capacity ( $2.83 \text{ mmol g}^{-1}$ ) [126]. As shown in Fig. 2c, CAU-10-Py obtained by replacing the benzene ring (CAU-10-H) with a pyridine ring not only increases the adsorption selectivity from 122.6 to 203.6 (298 K, 1 bar,  $v/v = 0.1$ ) but also doubles the adsorption capacity under low- (0.1 bar) and high-pressure (1 bar) conditions [101]. The reasons for the improved were deeply analyzed from a molecular perspective by using GCMC simulations (DREIDING force field for nonmetallic atoms, UFF force field for Al) to understand the interactions between  $SF_6$  (S and F, with characteristic energies ( $\mathcal{E}$ ) of 165.14 and 27.02 K, collision diameters ( $\delta$ ) of 3.228 and 2.947 Å, and charges ( $q$ ) of 0.660 and  $-0.110 e$ , respectively) and MOFs, NVT-Monte Carlo (NVT-MC) simulations to determine the preferential adsorption sites of the adsorbates within the MOFs frameworks, and DFT calculations to ascertain the optimal adsorption configurations and bonding energies. The introduction of nitrogen atoms alters the electrostatic potential distribution in the pore, which

leads to the adsorption site of SF<sub>6</sub> moving to the edge of the channel. The interaction between the pyridine ring and SF<sub>6</sub> (the distance is 3.029–3.192 Å, ΔE = −35.305 kJ mol<sup>−1</sup>) is stronger than the S–F...π interaction in CAU-10-H (the distance is 3.454–3.467 Å, ΔE = −26.131 kJ mol<sup>−1</sup>), and the pore diameter is enlarged by the substitution of the benzene ring by pyridine (CAU-10-Py is 5.9 Å and CAU-10-H is 5.7 Å), which enables pores to accommodate SF<sub>6</sub>. The overall trend of adsorption behavior between simulation and experiment is consistent. Given that the polarizability of absorbing atoms is closely related to vdW force, introducing highly polarizable functional groups into MOFs can enhance vdW interactions with PFCs and thus improves the selective adsorption of PFCs/N<sub>2</sub>. The adsorption of SF<sub>6</sub> and CF<sub>4</sub> was investigated after the introduction of different polar functional groups (−NH<sub>2</sub>, −NO<sub>2</sub>, −Cl, −Br, −Br<sub>2</sub>, −I) into UiO-66 [127]. The results show that UiO-66-Br<sub>2</sub>, characterized by high polarization, considerably enhances the uptake of SF<sub>6</sub> and CF<sub>4</sub> under industrially relevant low-pressure conditions (298 K, <0.05 bar). Moreover, UiO-66-Br<sub>2</sub> has high SF<sub>6</sub>/N<sub>2</sub> selectivity at low (IAST = 560–580, v/v = 0.0003) and high concentrations (v/v = 0.1, IAST = 200) and can exhibit superior performance in separating SF<sub>6</sub>/N<sub>2</sub> to UiO-66 under dynamic mixed flow conditions. Under the guidance of reticular chemistry, three isostructural MOFs with varying linker lengths and fluorine contents were synthesized from Zr-MOFs, utilizing fluorinated phenyl or biphenyl linkers [128]. Among them, compounds 2 and 3 not only exhibit high water stability and thermal stability, but can also absorb over 140 wt% of C<sub>6</sub>F<sub>14</sub> within a few minutes at 300 °C and a partial pressure of 50 Torr. This indicates that the functionalization of the framework structure with trifluoromethyl groups contributes to enhancing the hydrophobicity of the MOFs, thereby further improving its adsorption capacity.

Both adsorption capacity and selectivity are crucial indicators for the adsorption and separation of PFCs by MOFs, and are the primary considerations for the development of new MOFs adsorbents. At present, the research subject of adsorptive separation of PFCs/N<sub>2</sub> is still robust MOFs. The adsorption capacity for PFCs can be effectively enhanced by modulating the void ratio and pore size of MOFs, but the results suggest that increasing the pore size alone may lead to a trade-off between adsorption capacity and selectivity. Controlling the pore size to be close to the diameter of the PFCs can enhance the adsorption selectivity through pore confinement effect, but the limited pore size tends not to exhibit excellent adsorption capacity. To overcome this

trade-off, researchers have combined the introduction of metal/nonmetal sites to further regulate the pore environment, which is currently an important method to achieve efficient adsorption and separation of PFCs/N<sub>2</sub> by MOFs.

## 2.2 Separation of Gas Mixtures of Different PFCs Species

Apart from separating PFCs/N<sub>2</sub> mixtures, separating different species of PFCs gas mixtures is of great importance to the electronic industry. The physical and chemical properties of PFCs and N<sub>2</sub> are quite different, especially in polarity, facilitating separation. However, the separation of different PFCs species is extremely difficult due to the highly similar physicochemical properties, requiring MOFs with high molecular recognition capability. To date, few studies have explored the separation of different PFCs species by MOFs.

In a synthetic route, CF<sub>4</sub> is the impurity with the highest content in NF<sub>3</sub> products, seriously affecting the etching of NF<sub>3</sub> in semiconductor chip production [24, 129–131]. For the identification of suitable MOF candidates for CF<sub>4</sub>/NF<sub>3</sub> separation, JUCXEK (JUCXEK is a structured crystalline substance combining actinide Np with the organic ligand oxalic acid [132, 133]) was screened from 796 kinds of MOFs in the CoRe MOF database through high-throughput GCMC calculations (metal elements used the UFF force field [134], while nonmetal elements used the DREIDING force field [135]) with a selectivity of up to 50.15 (298 K, 1 bar, v/v = 0.05/0.95) for CF<sub>4</sub>/NF<sub>3</sub> [22]. To better understand the relationship between properties and guest structures, unlike previous studies that considered the NF<sub>3</sub> and CF<sub>4</sub> models are only single spheres with zero charge and zero natural electrostatic interaction energy, the four- and five-site models of NF<sub>3</sub> (N: δ = 4.28 Å, ε = 173.86 K, q = 0.084 e) and CF<sub>4</sub> (C: δ = 4.66 Å, ε = 134 K, q = 0.76 e) were established by adding virtual atoms F\_N (q = −0.028 e) and F\_C (q = −0.19 e), respectively [136, 137]. The performance is attributed to the relative enhancement of vdW interactions because the pore-limiting diameter (6.26 Å) of JUCXEK is close to the CF<sub>4</sub> molecule (4.66 Å), and the charge of each atom of CF<sub>4</sub> is higher than that of NF<sub>3</sub> leading to enhances electrostatic interactions between CF<sub>4</sub> and JUCXEK. When the metal position is optimized, Zr-JUCXEK shows industrial value in simulated pressure swing adsorption (298 K, 1 bar, v/v = 0.05/0.95), with both

$\text{CF}_4$  outlet concentration (< 20 ppm) and  $\text{NF}_3$  recovery (88.9%). This work demonstrates the potential application of computational chemistry in the separation of fluorine compounds [89, 90, 138–140].

The formation of  $\text{C}_2\text{F}_6$  in an industrial process is mainly catalyzed by fluoroethanes, such as  $\text{CF}_3\text{CH}_2\text{F}$  and  $\text{CF}_3\text{CHF}_2$  with metal fluoride or fluorine gas, at high temperatures, resulting in a mixture of residual  $\text{CF}_3\text{CH}_2\text{F}$  or  $\text{CF}_3\text{CHF}_2$  in  $\text{C}_2\text{F}_6$ .  $\text{Ni}(\text{pba})_2$  with fourfold intermingled structure exhibits high selectivity to  $\text{CF}_3\text{CH}_2\text{F}/\text{C}_2\text{F}_6$  ( $v/v = 5/95$ , IAST = 38.8) and  $\text{CF}_3\text{CHF}_2/\text{C}_2\text{F}_6$  ( $v/v = 5/95$ , IAST = 19.8) at 298 K and 1 bar [141]. The breakthrough experiment shows that this approach can directly obtain high-purity  $\text{C}_2\text{F}_6$  from the ternary mixture of  $\text{CF}_3\text{CH}_2\text{F}/\text{CF}_3\text{CHF}_2/\text{C}_2\text{F}_6$  ( $v/v/v = 5/5/90$ ) with a yield of  $7.1 \text{ mol kg}^{-1}$ . In addition to the C–H...F interactions between three F-gases and  $\text{Ni}(\text{pba})_2$ , the C–H bond in  $\text{CF}_3\text{CH}_2\text{F}$  and  $\text{CF}_3\text{CHF}_2$  can enhance the interaction with pore surface through additional C–H... $\pi$  interactions, thus allowing for the one-step purification of  $\text{C}_2\text{F}_6$  in  $\text{CF}_3\text{CH}_2\text{F}/\text{CF}_3\text{CHF}_2/\text{C}_2\text{F}_6$  mixtures.

A typical method for producing  $\text{C}_3\text{F}_8$  involves the direct fluorination of  $\text{C}_3\text{F}_6$  but leads to 1%–10% residual  $\text{C}_3\text{F}_6$  in products, whereas high-purity  $\text{C}_3\text{F}_8$  (more than 99.999%) is usually used in various industries [98, 143]. Thus, further purifying  $\text{C}_3\text{F}_8/\text{C}_3\text{F}_6$  with similar physical and chemical properties is important. The adsorption separation of  $\text{C}_3\text{F}_8/\text{C}_3\text{F}_6$  is considered to be one of the most difficult challenges in the field of adsorbents, because the subtle physicochemical differences between  $\text{C}_3\text{F}_8$  and  $\text{C}_3\text{F}_6$  (Table 1) need to be realized through the ultraprecise modulation of adsorbents [144]. At present, the researches mainly based on robust MOFs for F-gases capture and separation, but the adsorption–desorption kinetics and absorption in confined space are usually low, limiting the pore editing of rigid frames at the sub-angstrom level [145–147]. Flexible MOFs refer to a novel type of porous materials, which can undergo dynamic structural changes (“breathing” or “swelling” behavior) in response to external stimuli (temperature, pressure, light, or molecular exchanges of the object), which is theoretically useful for the separation of gas mixtures [54, 148–151]. However, flexible MOFs often exhibit low thermal and chemical stability, and will co-adsorb other gases with the “gate-open” process caused by a certain gas, which are not suitable for gas separation [152]. Flexibility–rigidity can keep its whole structure under low pressure and show its significant plateau. At the same time, the flexible-robust

MOFs structure usually show an adsorbate-dependent gas sorption isotherm, which can be used for the separation of different gas mixtures [153, 154]. An adsorbent with flexible–robust microporous was reported, Ca-tcpb, which used the influence of temperature on the varying degrees of the local twisting and vibrational motion of benzene ring ligands (R1, R2, R3, R4) to adjust the gating effect, thus reducing the co-adsorption of the  $\text{C}_3\text{F}_6/\text{C}_3\text{F}_8$  mixture (Fig. 3a, b). At different temperatures, Ca-tcpb remains porous for small  $\text{C}_3\text{F}_6$ , but its gating pressure increases with temperature for the larger  $\text{C}_3\text{F}_8$ , enabling the efficient sieving of  $\text{C}_3\text{F}_6/\text{C}_3\text{F}_8$  at ambient pressure (1 bar) by simply modulating the temperatures. (The IAST reaches 10,000 at 298 K.) And its adsorption performance on  $\text{C}_3\text{F}_6$  was almost unchanged after 20 adsorption/desorption cycles. The dynamic penetration experiment (Fig. 3c) of  $\text{C}_3\text{F}_6/\text{C}_3\text{F}_8$  ( $v/v = 0.1$ ) shows that Ca-tcpb can preferentially adsorb  $\text{C}_3\text{F}_6$  at  $106.5 \text{ min g}^{-1}$  (298 K), resulting in a high-purity  $\text{C}_3\text{F}_8$  (99.999%) [142, 145–147]. This work demonstrates the unique advantages of flexible–robust MOFs in separating highly similar PFCs.

For the adsorptive separation of PFCs/PFCs with highly similar structures, editing the pores of robust MOFs at the sub-angstrom level becomes exceedingly challenging. Flexible–robust MOFs, with unique flexible structure, enable precise tuning of the pore environment while overcoming the problems of poor structural stability and co-adsorption of flexible MOFs. They can maintain structural integrity at low pressure and exhibit adsorbate-dependent gas sorption isotherms, making them more suitable for the molecular screening of complex separation systems. Flexible–robust MOFs have shown great potential in the emerging field of F-gases adsorption and separation, warranting further study.

### 3 Adsorption and Separation of CFCs, HCFCs, and HFCs

In the 1930s, Thomas Midgely, Albert L. Henne, and Robert R. McNary discovered fluorocarbon refrigerants. CFCs and HCFCs refrigerants were widely used as second-generation refrigerants [143, 165]. Due to the serious consumption of ozone layer by CFCs, the Montreal Protocol in 1987 signed a restriction order about the production of ozone-depleting substances, such as CFCs. The Copenhagen Amendment in 1992 called for the gradual phaseout of HCFCs by 2030 [166, 167]. Over the past few decades, the market has been

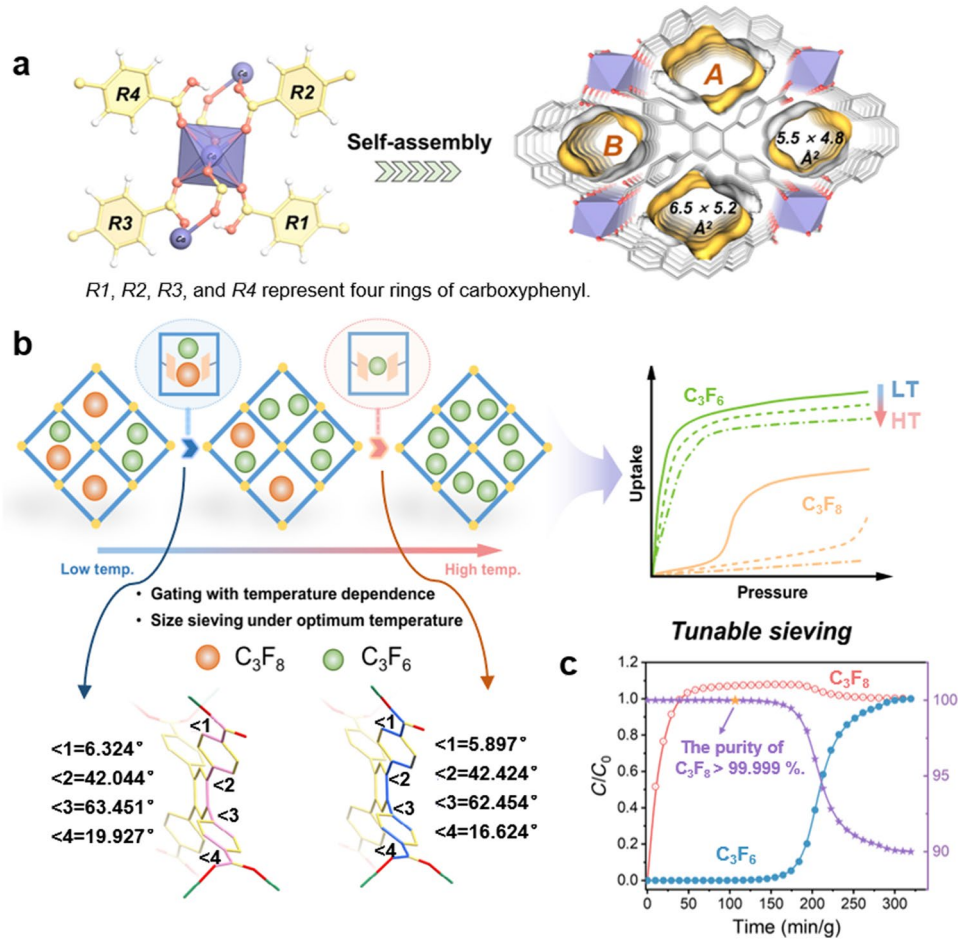


**Fig. 3** **a** Local coordination environment of  $\text{H}_2\text{tcpb}^{2+}$  with Ca (Ca is purple, C is yellow, O is rose red, and H is white) and the single-crystal structure of Ca-tcpb (A and B represent two types of one-dimensional channels). **b** Schematic of adjustable molecular sieve for promoting  $\text{C}_3\text{F}_8/\text{C}_3\text{F}_6$  mixture by a thermal regulation–gating effect, difference before and after  $\text{H}_2\text{tcpb}^{2+}$  adsorption frame  $\text{C}_3\text{F}_6$ , and the adsorption isotherms of  $\text{C}_3\text{F}_8$  and  $\text{C}_3\text{F}_6$  at different temperatures. **c** Breakthrough curve of Ca-tcpb on the packed column bed of a mixture of  $\text{C}_3\text{F}_6/\text{C}_3\text{F}_8$  (v/v = 0.1) at 298 K and 1 bar

dominated by third-generation refrigerants, called HFCs, but some of them have been banned or are being phased out due to their high GPW characteristics [40]. Table 3 lists the physical properties of several typical common fluorocarbon

refrigerants. To control the emission of these gases, MOFs have been developed to capture fluorocarbon refrigerants that have azeotropic or near-azeotropic characteristics and are difficult to separate through conventional low-temperature

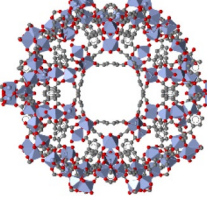
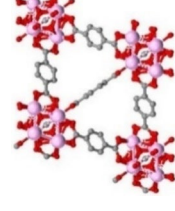
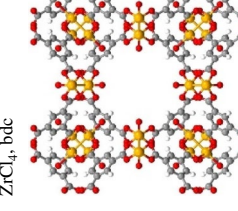
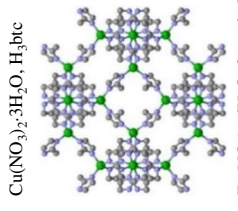
**Table 3** Physical properties of common fluorocarbon refrigerants

Species (R-number) [Refs.]	Chemical formula	Kinetic Diameter ( $\text{\AA}$ )	Molecular Weight	Boiling Point (K)	Dipole Moment (D)	Polarizability ( $\times 10^{-25} \text{ cm}^3$ )	GWP ( $\text{CO}_2 = 1$ )
CFC-12 [81, 111, 168]	$\text{CCl}_2\text{F}_2$	4.4	120.91	243.5	0.51	63.7	10,890
HCFC-22 [169–173]	$\text{CHClF}_2$	4.2	86.46	232.1	1.46	44.7	5280
HFC-32 [168, 174, 175]	$\text{CH}_2\text{F}_2$	3.9	50.02	221.5	1.98	26.5	675
HFC-125 [16, 176, 177]	$\text{CHF}_2\text{CF}_3$	4.4	120.02	224.9	1.56	43.6	3500
HFC-134a [77, 178–180]	$\text{CH}_2\text{FCF}_3$	—	102.03	246.9	2.06	43.2	1430
HFC-143a [40, 80, 169]	$\text{CH}_3\text{CF}_3$	—	84.04	225.8	2.34	40.4	4470

**Table 4** Properties, structures and compositions of various MOFs for adsorption/separation of fluorocarbon refrigerants

F-gases	MOFs [Refs.]	Structures and Chemical compositions	Channel size (Å)	BET surface area ( $\text{m}^2 \text{g}^{-1}$ )	LAST	Absorption amount (mmol g $^{-1}$ )	Thermodynamic stability	Kinetic stability	Chemical stability	Main interactions
R12	M-MOF-74 (M = Ni, Co) [168, 196]		11	940–1135	—	4.58 ( $P/P_0=0.01$ )	OMS	OMS	—	—
	Ni(NO <sub>3</sub> ) <sub>2</sub> ·6H <sub>2</sub> O or Co(NO <sub>3</sub> ) <sub>2</sub> ·6H <sub>2</sub> O, dodecane		5–8, 24–30	~2000	—	6.7 (4 bar)	OMS	—	—	—
	FeCl <sub>3</sub> solutions, bic or trimetic acid		11.7, 16, 25–29	4230	—	15 (4 bar), <2 ( $P/P_0=0.01$ )	OMS (C–F <sub>R12</sub> ... Cr <sup>3+</sup> )	—	—	—
	FeCl <sub>3</sub> ·6H <sub>2</sub> O, bdc		22	2445	—	6.6	Framework decomposition occurs at approximately 220 °C	Poor stability in water and under humid conditions	Fluorine functional groups, vdW	Cu(NO <sub>3</sub> ) <sub>2</sub> ·2.5H <sub>2</sub> O, fluorinated tetrazole

**Table 4** (continued)

F-gases	MOFs [Refs.]	Structures and Chemical compositions	Channel size (Å)	BET surface area ( $\text{m}^2 \text{g}^{-1}$ )	IAST	Adsorption amount (mmol g <sup>-1</sup> )	Thermodynamic stability	kinetic stability	chemical stability	Main interactions
R32	MIL-101(Fe) [168]		11.7, 16, 25–29	4230	—	8 (2 bar)	—	—	—	OMS
UiO-66 [172]	FeCl <sub>3</sub> ·6H <sub>2</sub> O, bdc		8, 11	1383	—	2.9 <sup>a</sup>	Good thermal stability	Over 15 adsorption-regeneration cycles still stable	—	Defect sites; vdW
ZrCl <sub>4</sub> , bdc	HKUST-1 (Cu-BTC or MOF-199) [174, 197]		7–12	1172	303.15 K, R32/R125 (v/v = 7/30 = 0.09) <sup>b</sup> , 1.91 (6 bar), 4.29 (10 bar)	303.15 K: 0.921 (0.09 bar), 8.58 <sup>a</sup> , 13.1 (13.13 bar) (10 bar)	Stability up to 350 °C	—	The host backbone will be damaged in humid air	OMS
Cu(NO <sub>3</sub> ) <sub>2</sub> ·3H <sub>2</sub> O, H <sub>4</sub> bic	ZIF-8 [174, 198]		12–17	1302	303.15 K, R32/R125 (v/v = 7/30 = 0.238) <sup>b</sup> , 0.652 (6 bar), 0.897 (1 bar), 8.17 (10 bar)	303.15 K: 0.0856 (0.09 bar), 1.53 (1 bar), 8.17 (13.13 bar)	High thermal stability	Great water stability	vdW; ligand rotation	—
Zn(NO <sub>3</sub> ) <sub>2</sub> ·6H <sub>2</sub> O, 2-methylimidazole	—	—	—	—	—	—	—	—	—	—

**Table 4** (continued)

F-gases	MOFs [Ref.s.]	Structures and Chemical compositions	Channel size (Å)	BET surface area ( $\text{m}^2 \text{g}^{-1}$ )	IAST	Adsorption amount (mmol g <sup>-1</sup> )	Thermodynamic stability	kinetic stability	chemical stability	Main interactions
CO <sub>2</sub>	MOF-177 [174, 199]	Zn(NO <sub>3</sub> ) <sub>2</sub> ·6H <sub>2</sub> O, benzene-1,3,5-tribenzoic acid (H <sub>3</sub> bba)	17–20, 20–25	4190	303.15 K, R32/R125 (v/v = 7/0/30) = 0.355 <sup>b</sup> , 0.557 (6 bar), 0.741 (10 bar)	303.15 K: 0.295 (0.23 bar), 1.64 (1.21 bar), 30 (12.99 bar)				vW
N <sub>2</sub>	MIL-53 [174, 200]		8–10	1043	303.15 K, R32/R125 (v/v = 7/0/30) = 0.113 <sup>b</sup> , 0.801 (6 bar), 1.15 (10 bar)	303.15 K: 0.437 (0.07 bar), 3.12 (1.14 bar), 6.71 (11.57 bar)				vW
CH <sub>4</sub>	DUT-67 [169, 201]	Al(NO <sub>3</sub> ) <sub>3</sub> ·9H <sub>2</sub> O, bdc ZrCl <sub>4</sub> , 2,5-thiophenedicarboxylate (tcic)	5.8, 11.2	1300	R22/CO <sub>2</sub> =51.4–33.3 <sup>b</sup> (v/v=10/90, 50/50, 90/10)	5.54 <sup>a</sup> , 6.21 (6.23 bar)	Stability up to 220 °C	The performance of the six adsorption/desorption cycles is stable	Having good water stability and stability in extreme environments such as NaOH (1 M), HCl (6 and 12 M) and boiling water	Cl/F...H–O and O...H–C hydrogen bonds

**Table 4** (continued)

F-gases	MOFs [Ref.s.]	Structures and Chemical compositions	Channel size (Å)	BET surface area ( $\text{m}^2 \text{g}^{-1}$ )	IAST	Adsorption amount (mmol g <sup>-1</sup> )	Thermodynamic stability	Kinetic stability	Chemical stability	Main interactions
ZrCl <sub>4</sub> ·H <sub>3</sub> bhb, 4',4'',4''',4''''''-(ethene- 1,1,2,2-tetrayl)biskis ([1,1'-biphenyl]- -4-carboxylate) (H <sub>4</sub> ettc)	LJFM-66 [170]		16.2	3631	R22/N <sub>2</sub> =186 <sup>a</sup> (v/v=1/99)	9.8 <sup>a</sup>	Stability up to 450 °C	Great stability in water and harsh chemical environments (pH=2–10)	Strong O...H-C <sub>FC</sub> and O-H...F <sub>FC</sub> interactions, weak vdW forces	
ZrCl <sub>4</sub> =5'-(4- carboxyphenyl)-2',4',6'- trimethyl-[1,1',3,1"-terphenyl]-4,4"-dicarboxylic acid (H <sub>3</sub> ettc), H <sub>4</sub> ettc	LJFM-67 [170]		15.5	2904	R22/N <sub>2</sub> =154 <sup>a</sup> (v/v=1/99)	11.2 <sup>a</sup>	Stability up to 450 °C	Great stability in water and harsh chemical environments (pH=2–10)	Methyl functional group (strong O...H-C <sub>FC</sub> interactions, weak C-H...F <sub>FC</sub> and C-H...Cl <sub>FC</sub> van der Waals forces)	
Cu(NO <sub>3</sub> ) <sub>2</sub> ·2.5HO, 2,2'-bis(trifluoromethyl) [1,1'-biphenyl]-4,4'- dicarboxylate acid	LJFM-100 [194]		14.3	663	R22/N <sub>2</sub> =399.1 1.6 (1 atm)	3.1 (273 K, 1 atm), 1.6 (1 atm)	Stability up to 250 °C	High chemical stability	vdW (interaction between fluorine atoms and R22)	



**Table 4** (continued)

F-gases	MOFs [Ref.s.]	Structures and Chemical compositions	Channel size (Å)	BET surface area ( $\text{m}^2 \text{g}^{-1}$ )	IAST	Adsorption amount (mmol g <sup>-1</sup> )	Thermodynamic stability	kinetic stability	chemical stability	Main interactions
LIFM-26 [171]		$\text{Fe}_3\text{O}(\text{H}_2\text{O})_3$ , 2,3,5,6-tetra-chloride terephthalic acid ( $\text{H}_2\text{tdc}$ )	12.6	1513	R22/N <sub>2</sub> =202 (1 atm, v/v = 10/90)	6.5 <sup>a</sup>	Stability up to 200 °C	Great water and chemical (pH = 1, 7, 11.5) stability	OMS; functional polar groups	
LIFM-28 [192]		$\text{ZrCl}_4$ , 2,2'-bis(trifluoromethyl)-4,4'-biphenyldicarboxylate	11–13	940	R22/N <sub>2</sub> =42 (v/v = 10/90, 273 K)	~2.29 <sup>a</sup>	Good thermal stability	Stable in boiling water and harsh environments (pH = 1, 12)	Functional group; pore space partition	
UiO-66 [172]		$\text{ZrCl}_4$ , bdc	8,11	1383		5 <sup>a</sup>	Good thermal stability	Over 15 adsorption-regeneration cycles still stable	Defect sites; vdW	
PCN-700 [173, 202]		$\text{ZrCl}_4$ , 2,2'-dimethylbiphenyl-4,4'-dicarboxylic acid ( $\text{H}_2\text{Me}_2\text{bpdc}$ )	14.3	879	R22/N <sub>2</sub> ~123 <sup>a</sup> (v/v = 10/90, 273 K)	~2.9 <sup>a</sup>	Stability up to 450 °C	vdW		

**Table 4** (continued)

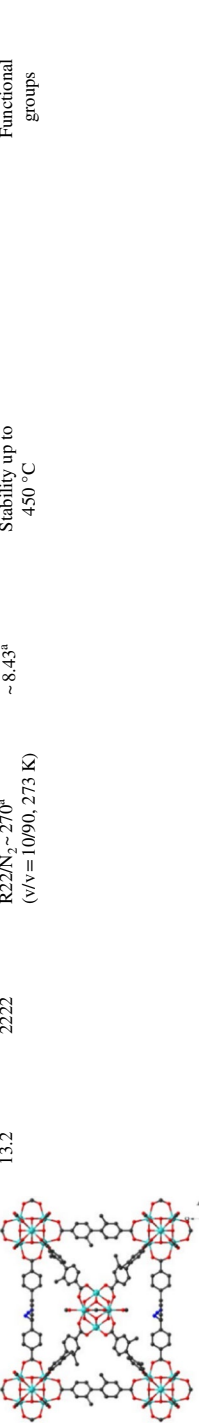
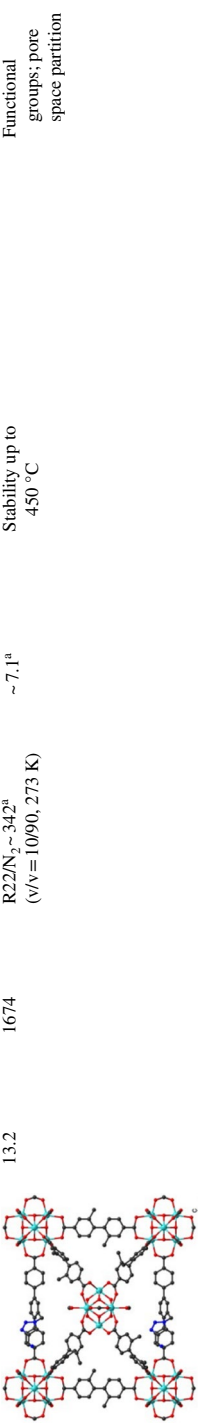
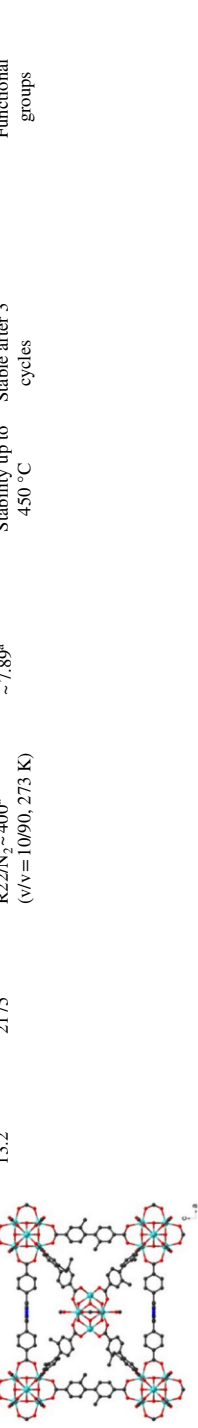
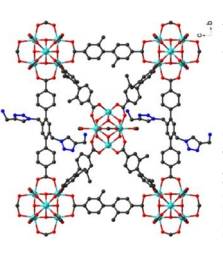
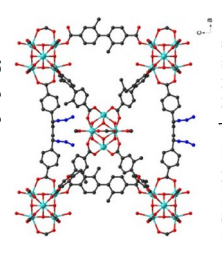
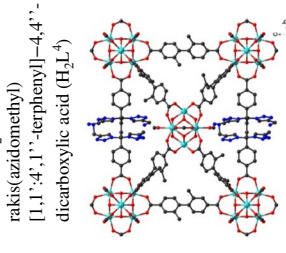
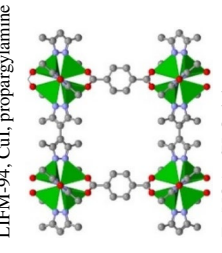
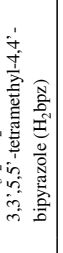
F-gases	MOFs [Ref.s.]	Structures and Chemical compositions	Channel size (Å)	BET surface area ( $\text{m}^2 \text{g}^{-1}$ )	IAST	Adsorption amount (mmol g <sup>-1</sup> )	Thermodynamic stability	Kinetic stability	Chemical stability	Main interactions
LIFM-90 [173]		$\text{C}_{101}\text{H}_{73}\text{N}_3\text{O}_{32}\text{Zn}_6$ PCN-700, 2,2'-dimethylbibiphenyl-4,4'-dicarboxylic acid ( $\text{H}_2\text{L}'$ ), 2'- <i>azidomethyl</i> -[1,1':4',1''-terphenyl]-4,4''-dicarboxylic acid ( $\text{H}_2\text{L}''$ )	13.2	2222 ( $\text{v/v}=10/90, 273 \text{ K}$ )	R22/N <sub>2</sub> ~270 <sup>a</sup> ( $\text{v/v}=10/90, 273 \text{ K}$ )	~8.43 <sup>a</sup>	Stability up to 450 °C			Functional groups
LIFM-91 [173]		LIFM-90, CuII propargylamine	13.2	1674 ( $\text{v/v}=10/90, 273 \text{ K}$ )	R22/N <sub>2</sub> ~342 <sup>a</sup> ( $\text{v/v}=10/90, 273 \text{ K}$ )	~7.1 <sup>a</sup>	Stability up to 450 °C			Functional groups; pore space partition
LIFM-92 [173]		PCN-700, $\text{H}_2\text{L}'$ , 2',5'-bisazidomethyl-[1,1':4',1''-terphenyl]-4,4''-dicarboxylic acid ( $\text{H}_2\text{L}''$ )	13.2	2175 ( $\text{v/v}=10/90, 273 \text{ K}$ )	R22/N <sub>2</sub> ~400 <sup>a</sup> ( $\text{v/v}=10/90, 273 \text{ K}$ )	~7.89 <sup>a</sup>	Stability up to 450 °C	Stable after 3 cycles		Functional groups

Table 4 (continued)

F-gases	MOFs [Refs.]	Structures and Chemical compositions	Channel size (Å)	BET surface area ( $\text{m}^2 \text{g}^{-1}$ )	IAST (v/v=10/90, 273 K)	Adsorption amount (mmol g <sup>-1</sup> )	Thermodynamic stability	kinetic stability	chemical stability	Main interactions
LIFM-93 [173]		12.7	1577	R22/N <sub>2</sub> ~223 <sup>a</sup> (v/v=10/90, 273 K)	~5.94 <sup>a</sup>	Stability up to 450 °C	Stable after 3 cycles			Functional groups; pore space partition
LIFM-92, CuI, propargylamine		13.2	1057	R22/N <sub>2</sub> ~308 <sup>a</sup> (v/v=10/90, 273 K)	~6.31 <sup>a</sup>	Stability up to 450 °C				Functional groups
PCN-700, H <sub>2</sub> L <sup>1</sup> , 2',3',5',6'-tetraakis(azidomethyl)[1,1':4',1"-terphenyl]-4,4'-dicarboxylic acid (H <sub>2</sub> L <sup>2</sup> )		12.7	1496	R22/N <sub>2</sub> ~231 <sup>a</sup> (v/v=10/90, 273 K)	~6.50 <sup>a</sup>	Stability up to 450 °C				Functional groups; pore space partition
LIFM-95 [173]		12.7	1577	R22/N <sub>2</sub> ~223 <sup>a</sup> (v/v=10/90, 273 K)	~5.94 <sup>a</sup>	Stability up to 450 °C				Pore size and shape; C <sub>K22</sub> ...N, C <sub>K22</sub> ...O
MAF-X10 [181]		9.4×9.9×13.2	2032	9.4 Å <sup>3</sup>	~9.48 <sup>a</sup>	Stability up to 550 °C	The adsorption-desorption at 313 K can reach equilibrium within 50 s			

**Table 4** (continued)

F-gases	MOFs [Ref.s.]	Structures and Chemical compositions	Channel size (Å)	BET surface area ( $\text{m}^2 \text{g}^{-1}$ )	IAST	Adsorption amount (mmol g <sup>-1</sup> )	Thermodynamic stability	kinetic stability	chemical stability	Main interactions
MAF-X12 [181]		Zn(NO <sub>3</sub> ) <sub>2</sub> ·6H <sub>2</sub> O, H <sub>2</sub> bpyz, 1,4-dicarboxylic acid (H <sub>2</sub> ndc)	9.4×9.9×13.2	1787	9.4 <sup>a</sup>	~8.1 <sup>a</sup>	Stability up to 450 °C	The adsorption–desorption at 313 K can reach equilibrium within 50 s	Pore size and shape; C <sub>R22</sub> ...N, C <sub>R22</sub> ...O	
MAF-X13 [181]		Zn(NO <sub>3</sub> ) <sub>2</sub> ·6H <sub>2</sub> O, H <sub>2</sub> bpyz, biphenyl-4,4'-dicarboxylic acid (H <sub>2</sub> ndc)	9.4×9.9×15.9	2742	9.4 <sup>a</sup>	11.22 <sup>a</sup>	Stability up to 450 °C	The adsorption–desorption at 313 K can reach equilibrium within 50 s	Pore size and shape; C <sub>R22</sub> ...N, C <sub>R22</sub> ...O	
MIL-101(Fe) [168]		FeCl <sub>3</sub> ·6H <sub>2</sub> O, bdc	11.7, 16, 25–29	4230	—	9.83 <sup>a</sup> , 11 (2 bar)	OMS; C–H...π/ C–H...O			
R125	UiO-66 [172, 176, 177]	ZrCl <sub>4</sub> , bdc	8, 11	1383	4.6 <sup>a</sup>	Good thermal stability	Over 15 adsorption–regeneration cycles still stable		Defect sites; vdW	



**Table 4** (continued)

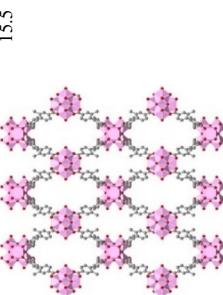
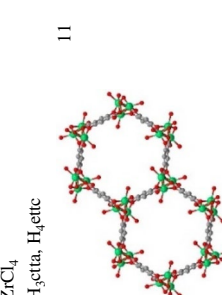
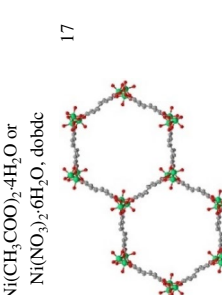
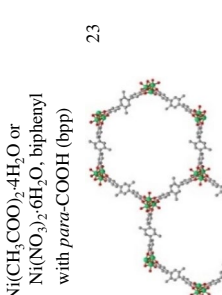
F-gases	MOFs [Refs.]	Structures and Chemical compositions	Channel size (Å)	BET surface area ( $\text{m}^2 \text{g}^{-1}$ )	IAST	Adsorption amount (mmol g <sup>-1</sup> )	Thermodynamic stability	kinetic stability	chemical stability	Main interactions
HKUST-1 [174, 176, 197]			7–12	1172	303.15 K, R32/ R125/R134a (v/v/v = 47/21/32); R125/R32 = 9.05 <sup>b</sup> , 0.644 (4 bar), 0.422 (6 bar)	303.15 K: 2.39 (0.05 bar), 5.74 <sup>b</sup> , 6.85 (11.14 bar)	Stability up to 350 °C	The host backbone will be damaged in humid air	OMS	
ZIF-8 [174, 176, 198]			12–17	1302	303.15 K, R32/R125/R134a (v/v/v = 47/21/32); R125/R32 = 4.18 <sup>b</sup> , 1.58 (4 bar), 1.28 (6 bar)	303.15 K: 0.307 (0.05 bar), 3.23 <sup>a</sup> , 4.51 (11.14 bar)	High thermal stability	High water stability	vdW; ligand rotation	
Zn(NO <sub>3</sub> ) <sub>2</sub> ·6H <sub>2</sub> O, 2-methylimidazole			17–20, 20–25	4190	303.15 K, R32/ R125/R134a (v/v/v = 47/21/32); R125/R32 = 2.9 <sup>b</sup> , 1.79 (4 bar), 1.46 (6 bar)	303.15 K: 0.437 (0.13 bar), 4.11 (0.99 bar), 17.8 (11.16 bar)	vdW			
MOF-177 [174, 199]			8–10	1043	303.15 K, R32/ R125/R134a (v/v/v = 47/21/32); R125/R32 = 6.91 <sup>b</sup> , 1.46 (4 bar), 1.18 (6 bar)	303.15 K: 0.757 (0.04 bar), 2.54 (1.10 bar), 3.75 (9.61 bar)	vdW			
MIL-53 [174, 200]										

**Table 4** (continued)

F-gases	MOFs [Ref.s.]	Structures and Chemical compositions	Channel size (Å)	BET surface area ( $\text{m}^2 \text{g}^{-1}$ )	IAST	Adsorption amount (mmol g <sup>-1</sup> )	Thermodynamic stability	kinetic stability	chemical stability	Main interactions
R 134a	DUT-67 [169, 201]		5.8, 11.2	1300	R134a/CO <sub>2</sub> =31.1–25.8 (0.01 bar, v/v=10/90, 50/50, 90/10)	5.18 <sup>a</sup> , 6.12 (6.23 bar)	Stability up to 220 °C	The performance of the 6 adsorption/desorption cycles is stable	Having good water stability and stability in extreme environments such as NaOH (1 M), HCl (6 and 12 M) and boiling water	Cl/F...H–O and O...H–C hydrogen bonds
ZrCl <sub>4</sub> , tdc	MOFF-5 [111]		22	2445	5.4	Framework decomposition occurs at approximately 220 °C	Poor stability in water and under humid conditions	Poor stability in water and under humid conditions	Fluorine functional groups	
Cu(NO <sub>3</sub> ) <sub>2</sub> ·2.5H <sub>2</sub> O, fluorinated tetrazole	LIFM-66 [170]		16.2	3631	R134a/N <sub>2</sub> =232 <sup>a</sup> (v/v=1/99)	10.6 <sup>a</sup>	Stability up to 450 °C	Great stability in water and harsh chemical environments (pH = 2–10)	Strong C–H...F/cf interactions and weak vdw forces	



**Table 4** (continued)

F-gases	MOFs [Ref.s]	Structures and Chemical compositions	Channel size (Å)	BET surface area ( $\text{m}^2 \text{g}^{-1}$ )	IAST	Adsorption amount (mmol g <sup>-1</sup> )	Thermodynamic stability (mmol g <sup>-1</sup> )	kinetic stability	chemical stability	Main interactions
ZrCl <sub>4</sub>	LIFM-67 [170]		15.5	2904	R134a/N <sub>2</sub> =154 <sup>a</sup> (v/v=1/99)	11.1 <sup>a</sup>	Stability up to 450 °C	Great stability in water and harsh chemical environments (pH = 2 ~ 10)	Methyl functional group (strong C—H...F <sub>FCF</sub> interactions, weak O...H—C <sub>FCF</sub> and C—H...F <sub>FCF</sub> vdW forces)	
Ni-MOF-74 [178, 182]		H <sub>3</sub> cpta, H <sub>3</sub> etcic	11	1150	—	4.7 (0.12 bar), about 4.98 (6 bar)	Framework decomposition occurs after 400 °C	CH <sub>3</sub> F moiety of R134a interacts with the Ni <sup>2+</sup>		
Ni(CH <sub>3</sub> COO) <sub>2</sub> ·4H <sub>2</sub> O or Ni(NO <sub>3</sub> ) <sub>2</sub> ·6H <sub>2</sub> O, dobdc	Ni-MOF-74-BPP [178, 182]		17	2040	—	3.63 (0.12 bar), about 7.37 (6 bar)	Framework decomposition occurs after 400 °C	Pore size: OMS		
Ni(CH <sub>3</sub> COO) <sub>2</sub> ·4H <sub>2</sub> O or Ni(NO <sub>3</sub> ) <sub>2</sub> ·6H <sub>2</sub> O, biphenyl with <i>para</i> -COOH (bpp)	Ni-MOF-74-TPP [178, 179, 182]		23	1980	—	2.74 (0.12 bar), ~7.63 (6 bar)	Framework decomposition occurs after 400 °C	Pore size: OMS		

**Table 4** (continued)

F-gases	MOFs [Refs.]	Structures and Chemical compositions	Channel size (Å)	BET surface area ( $\text{m}^2 \text{g}^{-1}$ )	IAST	Adsorption amount (mmol g <sup>-1</sup> )	Thermodynamic stability	Kinetic stability	Chemical stability	Main interactions
NU-1000 [179, 203]			12, 30	2259	-	17 (~6 bar)	Framework decomposition occurs after 400 °C	The performance of the 20 adsorption/desorption cycles is stable	vW	
ZrOCl <sub>2</sub> ·8H <sub>2</sub> O benzoic acid, H <sub>4</sub> TBAPy	PCN-222 [179, 204]		11, 30	1869	-	13 (~6 bar)	Stability up to 500 °C		vW	
ZrOCl <sub>2</sub> ·8H <sub>2</sub> O, benzoic acid, FeTCPP	MIL-101(Cr) [179, 205]		11, 16, 23–29	2642	-	~14.3 (~6 bar)	Stability can reach about 380 °C		vW; OMS	
Cr(NO <sub>3</sub> ) <sub>3</sub> ·9H <sub>2</sub> O, H <sub>2</sub> bdc	Ni <sub>3</sub> (C <sub>2</sub> O <sub>4</sub> ) <sub>3</sub> (tpd) <sub>2</sub> (MCF-61) [180]		20	2096	-	11.2 (5.34 bar), 10.78 (4.88 bar)	Stability up to 300 °C		Pore size	
NiCl <sub>2</sub> , dimethyl oxalate, 2,4,6-tris(4-pyridyl)-1,3,5-triazine (tp)										

**Table 4** (continued)

F-gases	MOFs [Refs.]	Structures and Chemical compositions	Channel size (Å)	BET surface area ( $\text{m}^2 \text{g}^{-1}$ )	IAST	Adsorption amount (mmol g <sup>-1</sup> )	Thermodynamic stability	Kinetic stability	Chemical stability	Main interactions
N <sub>2</sub>	Ni <sub>3</sub> (C <sub>2</sub> O <sub>4</sub> ) <sub>3</sub> (tpda) <sub>2</sub> (MCF-62) [180]		33	2630	—	17.03 (5.28 bar), 16.6 (4.88 bar)	Stability up to 300 °C	Stability up to 300 °C	Stability up to 300 °C	Pore size
CO <sub>2</sub>	Ni <sub>3</sub> (C <sub>2</sub> O <sub>4</sub> ) <sub>3</sub> (tpd) <sub>2</sub> (MCF-63) [180]		37	2749	—	20.29 (5.72 bar), 18.6 (4.88 bar)	Stability up to 300 °C	Stability up to 300 °C	Stability up to 300 °C	Pore size
CH <sub>4</sub>	HKUST-1 [174, 197]		7–12	1172	303.15 K, R32/ R125/R134a (v/v/v = 47/21/32); R134a/R32 = 8.71 <sup>b</sup> , 1.76 (4 bar), 1.33 (6 bar); R134a/R125 = 0.962 <sup>b</sup> , 2.73 (4 bar), 3.15 (6 bar)	303.15 K: 2.91 (0.04 bar), 6.62 (0.98 bar), 7.35 (5.27 bar)	Stability up to 350 °C	The host backbone will be damaged in humid air	OMS	
H <sub>2</sub>	Cu(NO <sub>3</sub> ) <sub>2</sub> ·3H <sub>2</sub> O, H <sub>3</sub> bfc									

**Table 4** (continued)

F-gases	MOFs [Ref.s.]	Structures and Chemical compositions	Channel size (Å)	BET surface area (m <sup>2</sup> g <sup>-1</sup> )	IAST	Adsorption amount (mmol g <sup>-1</sup> )	Thermodynamic stability (nmol g <sup>-1</sup> )	kinetic stability	chemical stability	Main interactions
ZIF-8 [174, 198]		12–17	1302	303.15 K, R32/ R125/R134a (v/v/v = 47/21/32); R134a/R32 = 7.63 <sup>b</sup> , 2.96 (4 bar), 2.47 (6 bar); R134a/ R125 = 1.83 <sup>b</sup> , 1.87 (4 bar), 1.93 (6 bar)	303.15 K: 0.194 (0.04 bar), 3.87 (0.98 bar), 4.85 (5.27 bar)	303.15 K: 0.194 (0.04 bar), 3.87 (0.98 bar), 4.85 (5.27 bar)	High thermal stability	High water stability	vW; ligand rotation	
Zn(NO <sub>3</sub> ) <sub>2</sub> ·6H <sub>2</sub> O, 2-methylimidazole	MOF-177 [174, 199]		17–20, 20–25	4190	303.15 K, R32/ R125/R134a (v/v/v = 47/21/32); R134a/R32 = 1.88 <sup>b</sup> , 3.48 (4 bar), 2.98 (6 bar); R134a/R125 = 1.34 <sup>b</sup> , 1.94 (4 bar), 2.04 (6 bar)	303.15 K: 0.534 (0.11 bar), 13.5 (0.92 bar), 19.3 (4.7 bar)	303.15 K: 0.534 (0.11 bar), 13.5 (0.92 bar), 19.3 (4.7 bar)	303.15 K: 0.534 (0.11 bar), 13.5 (0.92 bar), 19.3 (4.7 bar)	vW	
Zn(NO <sub>3</sub> ) <sub>2</sub> ·6H <sub>2</sub> O, H <sub>3</sub> bttb	MIL-53 [174, 200]		8–10	1043	303.15 K, R32/ R125/R134a (v/v/v = 47/21/32); R134a/R32 = 12.0 <sup>b</sup> , 1.96 (4 bar), 1.50 (6 bar); R134a/R125 = 1.73 <sup>b</sup> , 1.35 (4 bar), 1.27 (6 bar)	303.15 K: 0.40 (0.01 bar), 2.49 (1.11 bar), 3.34 (4.71 bar)	303.15 K: 0.40 (0.01 bar), 2.49 (1.11 bar), 3.34 (4.71 bar)	303.15 K: 0.40 (0.01 bar), 2.49 (1.11 bar), 3.34 (4.71 bar)	vW	
Al(NO <sub>3</sub> ) <sub>3</sub> ·9H <sub>2</sub> O, bdc	R13 (CFC-13, CFCl <sub>3</sub> )		11.7, 16, 25–29	4230	—	—	4 (2 bar)	—	OMS	
FeCl <sub>3</sub> ·6H <sub>2</sub> O, bdc	MIL-101(Fe) [168]		—	—	—	—	—	—	—	



**Table 4** (continued)

F-gases	MOFs [Refs.]	Structures and Chemical compositions	Channel size (Å)	BET surface area (m <sup>2</sup> g <sup>-1</sup> )	IAST	Adsorption amount (mmol g <sup>-1</sup> )	Thermodynamic stability	kinetic stability	chemical stability	Main interactions
R113	MOFF-5 [111] (CFC-113, CFCl <sub>2</sub> CF <sub>2</sub> Cl)		22	2445	10.09 <sup>a</sup>	Framework decomposition occurs at approximately 220 °C	Poor stability in water and under humid conditions	Fluorine functional groups		

298 K.<sup>a</sup> At 1 bar. <sup>b</sup> At 0.1 bar. The single-crystal structure of PCN-700 and LiFM-90–95 are derived from Ref. [173]. Copyright 2017, Royal Society of Chemistry

distillation (Table 4). Their recovery through MOFs can be performed for the production of fourth-generation refrigerant and can prevent the direct release of refrigerants to the atmosphere.

### 3.1 Adsorption of Fluorocarbon Refrigerants

The diverse topological structures arising from different metal nodes and coordination can directly alter the pore structure of MOFs, thereby affecting the accessibility of fluorocarbon refrigerants (Fig. 4). By exploring a series of mesoporous MOFs with different topological structures but the same chemical properties, it was found that two MOFs with similar pore size show excellent adsorption capacities for R134a, namely, NU-1000 composed of mesoporous hexagonal (~30 Å) and microporous triangular channels (~12 Å) and MIL-101 connected by microporous pentagonal (~11 Å) and hexagonal windows (~16 Å; Fig. 4a) [179]. However, NU-1000 shows an S-shaped isotherm because of its two-dimensional extended Kagome network structure, which enhances saturation capacity by approximately 170 wt%. Meanwhile, MIL-101 only produces 60% working capacity with I-shaped isotherm. This analysis reveals that a structure with micropore and mesopore combinations has higher absorption performance than an ordered adsorbent with one shape and uniform pore size. This unique composition of micropores and macropores permits the stepwise adsorption isotherm showing strong host–guest interaction as well as sorbate–sorbate interactions with sufficient pore volume. These properties may be the reason that the micro- and mesoporous MOF-177 is superior to other microporous MOFs (Cu-BTC, MIL-53(Al), and ZIF-8) for HFCs (R134a, R32, and R125) adsorption [174]. MOF-177 has adsorption rates more than twofold those of the other three microporous materials. Therefore, MOFs with hierarchical micro/mesoporous structure may be suitable for the capture of fluorocarbon refrigerants in terms of adsorption capacity.

Without changing the topological structure, finely adjusting pore size and shape by changing ligands or introducing pore defects directly affects the gas adsorption performance of MOFs. A study on the adsorption behavior of R22 in the presence of isoreticular MOFs (MAF-X10, MAF-X12, and MAF-X13) showed that the subtle modification of the pore size and shape of sorbents induced by the length and side groups of ligands can dramatically improve adsorption

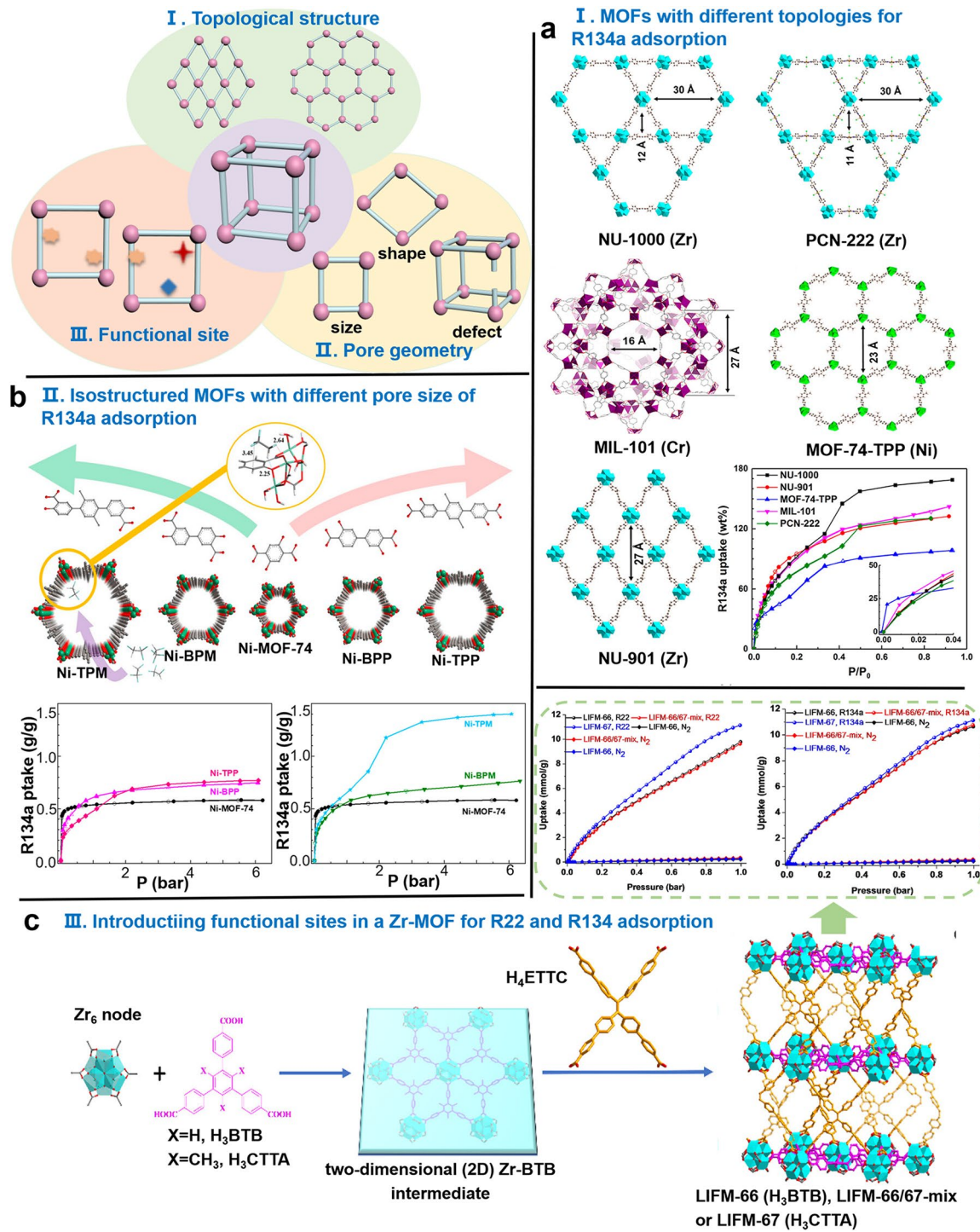


**Fig. 4** Topological structure (I), pore geometry (II), and functional sites (III) that affect the adsorption of fluorocarbon refrigerants by MOFs. **a** Single-crystal structure of five representative MOFs with different topological structures and isothermal adsorption curve of R134a at 298 K. **b** Structural features of pore-engineered Ni-MOF-74 members and the isothermal adsorption curve of R134a at 298 K. **c** Synthesis procedure, single-crystal structure, and the isothermal adsorption (298 K) of R22 and R134a of LIFM-66, LIFM-66/67-mix, and LIFM-67

performance [181]. MAF-X13 with the largest pore size allows for the saturable uptake of R22 ( $11.22 \text{ mmol g}^{-1}$ ) at 293 K and 1 bar and is higher than that of MAF-X10 and MAF-X12. Ni-MOF-74 members, Ni-MOF-74 (11 Å), Ni-BPP (17 Å), Ni-BPM (19 Å), Ni-TPP (23 Å), and Ni-TPM (27 Å) are constructed by adjusting the relative locations of hydroxyl and carboxyl groups in dihydroxyterephthalic acid ligand phenyl ring analogs (Fig. 4b), with the largest pore sizes of Ni-TPM showing a considerably high saturation capacity for R134a, especially under high-pressure conditions, exhibiting a 300% increase in saturation capacity compared with Ni-MOF-74 (the saturation absorption of Ni-TPM is higher than  $13.7 \text{ mmol g}^{-1}$ ) [178, 182]. The initial adsorption of R134a occurs near nickel nodes, and it interacts with the inorganic nodes and organic linkers of Ni-TPM to form a monolayer as pressure increases. Pore filling occurs at high pressure. By contrast, pore filling in Ni-MOF-74 and Ni-BPP with small pore size usually occurs at low pressure. The adsorption of R12 by microporous M-MOF-74 ( $M = \text{Ni, Co}$ ) and mesoporous MIL-101 shows the same trend, and the adsorption capacity of M-MOF-74 ( $4.58 \text{ mmol g}^{-1}$ ) is more than twice that of MIL-101 ( $< 2 \text{ mmol g}^{-1}$ ) under low-pressure conditions ( $P/P_0 = 0.01$ ) and saturates at  $P/P_0 = 0.05$ , while the saturation capacity of MIL-101 ( $15 \text{ mmol g}^{-1}$ ) is twice that of M-MOF-74 at 4 bar ( $P/P_0 = 0.6$ ) [168]. Under the condition of the same ligand bridging length, the effective pore size of isotactic mesoporous MOFs (MCF-61, MCF-62, and MCF-63) with unique honeycomb-like structure is fourfold the ligand bridging length (5.5, 8.8, and 9.9 Å). Thus, pore size can be easily increased and fine-tuned, and resulting changes directly affect the adsorption performance of R134a [180]. The saturated adsorption of MCF-63 for R134a ( $20.29 \text{ mmol g}^{-1}$ ) with the highest pore volume ( $2.36 \text{ cm}^3 \text{ g}^{-1}$ ) and BET surface area ( $2749 \text{ m}^2 \text{ g}^{-1}$ ) is almost the same as that of activated carbon Maxsorb III, which has a surface area of over  $3000 \text{ m}^2 \text{ g}^{-1}$ . Its isotherm shape is related to its pore size and exhibits excellent adsorption thermal conversion performance. Introducing defect sites into MOFs is also an effective method for generating additional voids or pores and adjusting gas adsorption isotherms [183, 184]. In the capture experiments of R125 by UiO-66 (6–7 Å), Cu-BTC (5.5, 10, and 12 Å), and ZIF-8 (11 Å), UiO-66, which has low pore size and surface area, shows the exceptional adsorption capacity ( $7 \text{ mmol g}^{-1}$ ) because of the presence of defects in its structure, which

facilitate the formation of additional pores and accessible adsorption sites [16, 174, 176, 177, 185].

Introducing nonmetallic/metallic functional sites for the regulation of the pore environment can enhance the affinity of MOFs for fluorocarbon refrigerants. Isostructural MOFs (LIFM-66, LIFM-66/67-mix, and LIFM-67) can be prepared by introducing methyl groups that modulate the adsorption performance of R22 and R134a (Fig. 4c), and LIFM-67 with numerous methyl groups can exhibit high adsorption capacity for R22 ( $11.2 \text{ mmol g}^{-1}$ ) and R134a ( $11.1 \text{ mmol g}^{-1}$ ) at 298 K and 1 bar despite possessing a small pore size (LIFM-66 is 16.2 Å, LIFM-66/67-mix is 15.6 Å, and LIFM-67 is 15.5 Å) and pore volume (LIFM-66 is  $1.42 \text{ cm}^3 \text{ g}^{-1}$ , LIFM-66/67-mix is  $1.30 \text{ cm}^3 \text{ g}^{-1}$ , and LIFM-67 is  $1.27 \text{ cm}^3 \text{ g}^{-1}$ ) [170]. In LIFM-66, R134a located in a pocket consisting of a  $\text{Zr}_6$ -cluster, one ettc linker and two btb ligands, with the presence of strong C–H...F<sub>FCF</sub> (2.76, 2.88, and 3.1 Å) interactions and weak vdW forces (3.28–3.92 Å). In LIFM-67, R134a located in a pocket surrounded by a  $\text{Zr}_6$ -cluster and two cta connectors, and there are strong C–H...F<sub>FCF</sub> (2.52, 2.69, 2.77, 3.14, and 3.16 Å) and weak vdW forces (3.31–3.49 Å). These results further confirm that the introduction of methyl group enhances the interaction between the gas and the framework. The fluorine-functionalized MOFF-5 greatly enhances performance for adsorbing fluorocarbon/CFC gases, such as R12 ( $6.6 \text{ mmol g}^{-1}$ ), R134a ( $5.4 \text{ mmol g}^{-1}$ ), and CFC-113 ( $\text{Cl}_2\text{FC}-\text{CClF}_2$ , approximately  $9.7 \text{ mmol g}^{-1}$ ) [111, 186]. This feature is related to the high-polarity environment inside fluorinated cavities and the size of gas molecules. OMS-containing MOFs can adsorb fluorocarbon refrigerants at low pressure irrespective of pore geometry [77, 178, 187]. A study of R134a adsorption by mesoporous MOFs (Ni-MOF-74 members) with similar chemical properties, it demonstrated that the enthalpy of adsorption exceeded that reported for non-OMS MOFs ( $< 35 \text{ kJ mol}^{-1}$ ) even though the increase in pore size resulted in the saturation of the open  $\text{Ni}^{2+}$  sites in Ni-MOF-74 with R134a (Ni-MOF-74 about  $50 \text{ kJ mol}^{-1}$ ; Ni-TPM, approximately  $45 \text{ kJ mol}^{-1}$ ) [179]. The ionic radii of metal sites on MOFs directly affect affinity with gas molecules. Adsorption studies of M-MOF-74 ( $M = \text{Zn, Ni, Mg, Co}$ ) on refrigerants showed that  $\text{Mg}^{2+}$ , which has small ionic radius, has strong C–F...M<sup>+</sup> interactions that considerably increase the adsorption capacity of Mg-MOF-74 [175, 188].

MOFs with the highly tunable structure can obtain diverse topologies through the coordination of different metal nodes and ligands. Compared to structures with single and uniform

pore size, MOFs with layered micro/mesoporous exhibit greater advantages in gas capture. Additionally, adjusting the pore size/shape, introducing defect sites to create additional pores, and introducing metal/nonmetal sites are all effective strategies for modulating gas adsorption isotherms.

### 3.2 Separation of Fluorocarbon Refrigerants

Fluorocarbon refrigerants have different molecule size and configurations, polarity, and electronic structures, and separation based on a customized pore size or functional sites can be achieved using MOFs. UiO-66 is highly effective for separating and recovering binary (R22/R32, R32/R125) and ternary (R32/R125/R134a) fluorocarbon azeotropic mixtures [172]. These mixtures in decreasing order of adsorption strength are R134a, R125, R22, and R32 because highly polar gases usually have strong interactions with adsorbents. The large molecular size, molar mass, and high boiling points of the gases also promote vdW interactions ( $C-H \dots \pi$  and  $C-H \dots O$  interactions with phenyl in UiO-66) and gas–gas interactions. In the separation and recovery of R-401A (R32/R125 blend) and R-407F (R32/R25/R134a blend) by MOF-177, Cu-BTC, MIL-53, and ZIF-8, R125 and R134 can be preferentially adsorbed by all adsorbents at low pressure (<3 bar) because of the enthalpy factor from a high degree of interaction between gases and MOFs. At high pressure (>4 bar), gas adsorption may involve entropy factors, and thus, a selective shift to R32 with small molar volume or no selectivity occurs [174].

Zr-MOF (DUT-67) composed of  $Zr_6$ -nodes and 2,5-thiophenedicarboxylate linker has good separation ability for R22/R134a/ $CO_2$  [169]. The adsorption mechanism was analyzed by SCXRD and found that the  $Zr_6$ -nodes with rich  $OH^-/H_2O$  group can selectively adsorb FC/CFCs through interactions between  $O-H \dots F$  or  $O-H \dots Cl$  and  $F/Cl$  atoms, which explained the corresponding high  $Q_{st}$  values of R22 (42.3  $kJ mol^{-1}$ ) and R134a (49.3  $kJ mol^{-1}$ ,  $Q_{st}$  of  $CO_2$  is 29.2  $kJ mol^{-1}$ ). This is consistent with the adsorption position and adsorption energy trend ( $\Delta E_{R134a}=34.31 kJ mol^{-1}$ ,  $\Delta E_{R22}=26.31 kJ mol^{-1}$ ) obtained by GCMC simulation (the charges of R22/R134a and DUT were calculated using ESP and  $Q_{eq}$  methods, respectively [189, 190]; the force field parameters for Zr were obtained from the UFF, while others from the Dreiding force field [135, 191]) and DFT calculation (UFF). The pore space of PCN-700 as the

prototype was divided by inserting azide groups as spacers after synthesis (LIFM-90/92/94), and interactions with guest molecules were enhanced by introducing 1,2,3-triazole functional groups (TAZ) through a click reaction with propylamine (LIFM-91/93/95), which effectively changes the pore environment and increases the performance of MOFs in separating R22/ $N_2$  (Fig. 5a) [173]. The initial selectivity (Fig. 5b) of LIFM-91/93/95 (the IAST of LIFM-91 reaches 996) bearing TAZ groups for R22/ $N_2$  is sixfold that of PCN-700-c (IAST, ~163). The introduction of polar functional groups in MOFs can enhance the interactions of MOFs with gas molecules through larger dipole or quadrupole moments or carbon–carbon double bonds, thus guiding the selective adsorption separation of gases [192]. The bifunctional (functional polar groups and OMS) LIFM-26 synthesized by connecting triangular prism  $Fe_3(\mu_3-O)$  units with four chlorine atoms exhibits good separation performance for R22/ $N_2$  (IAST = 202) at 298 K and 1 atm, which is realized by its cooperation with the highly electronegative open  $Fe^{II/III}$  site and polar chlorine atoms [171]. However, the introduction of metal sites can produce strong electrostatic interactions with fluorocarbon refrigerants, which usually reduce adsorption selectivity and are not conducive to gas separation, especially when high product purity is required [77, 172, 193]. The flexible MOFs structure LIFM-28 with modified trifluoromethyl group was used as a prototype, and the reversible transition from narrow-pore to large-pore crystalline form was achieved by the precise installation of variable spacers with different functional groups after the synthesis, and the precise fine-tuning of the pore properties improved its adsorption selectivity for R22/ $N_2$  [192]. Compared to LIFM-28-lp (lp means large pore), the selectivity of LIFM-28-33 obtained by installing the spacer was improved by 4–7 times (IAST = 170–279, v/v = 10/90, 273 K). The abundance of fluorine atoms in the pores of the flexible–rigid MOFs (LIFM-100) promotes preferential adsorption of R22, and its selectivity up to 399.1 (298 K, v(R22)/v( $N_2$ ) = 10/90) is higher than that of many reported MOFs structures (Table 4) [194]. It is worth mentioning that due to the existence of fluorine-containing functional groups, these MOFs structures have shown excellent thermal stability and chemical stability. Therefore, the combination of polar functional groups and the structural flexibility of MOFs will make the separation of complex fluorocarbon gas mixtures more controllable [195].

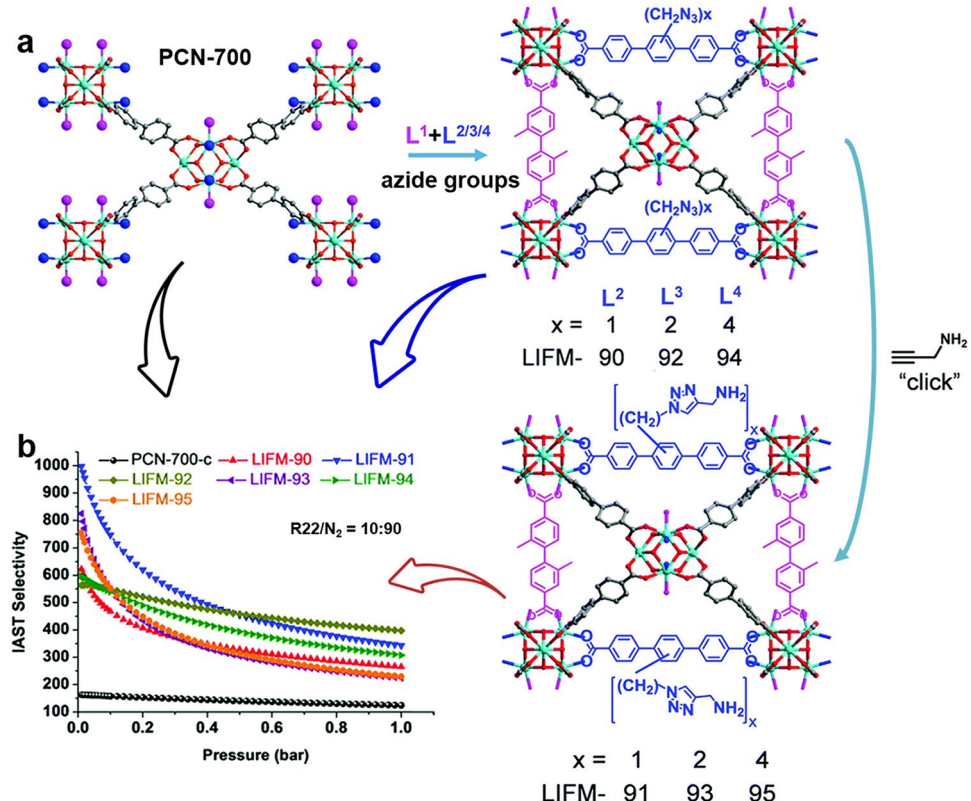


**Fig. 5** **a** Stepwise synthesis of LIFM-90–95 through the introduction of azide groups and click reaction using PCN-700 as a prototype. **b** IAST selectivity of LIFM-90–95 to R22/N<sub>2</sub> at 273 K

Fully understanding the behavior of MOFs and the different interactions and mechanisms involved in fluorocarbon refrigerants adsorption is the basis for developing new MOFs materials. Combining the differences of fluorocarbon refrigerant properties and the unique advantages of MOFs structure, the efficient separation of fluorocarbon refrigerant mixtures is within reach.

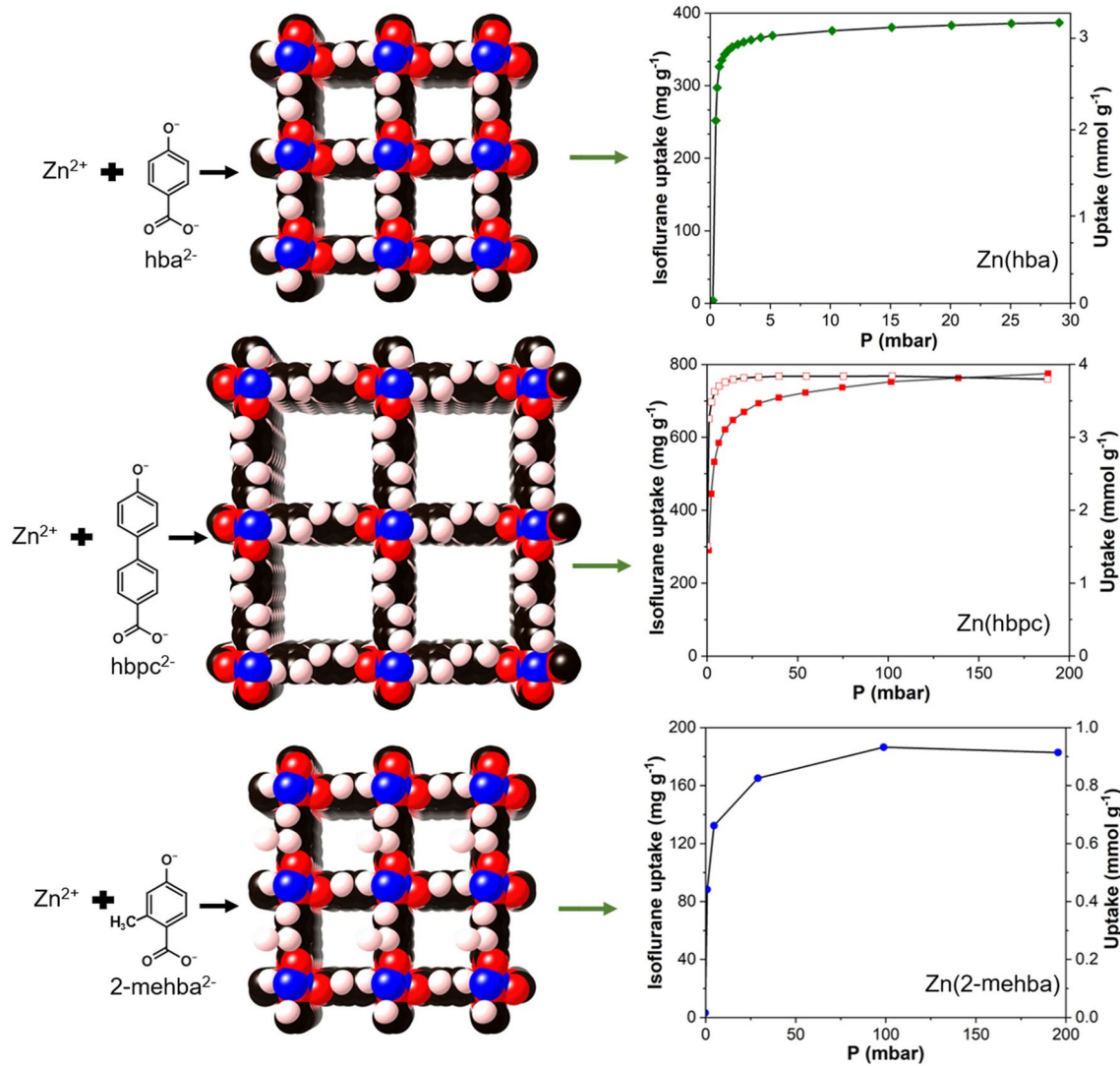
#### 4 Adsorption of VAs

Inhaled VAs, which are commonly used to induce and maintain general anesthesia in surgery, are fluorocarbons, and common VAs include sevoflurane, desflurane, and isoflurane [206–210]. The chemical structure and properties of VAs are similar to those of CFCs and HFCs which are potent greenhouse gases (Table 5) [211–214]. Unlike other F-gases, such as PFCs and CFCs, VAs are not restricted by legislation and international treaties due to “medical necessity” [215, 216].

Zn(hba), Zn(hbpc), and Zn(2-mehba) have the same topological structure, and Zn(hbpc) ( $10 \text{ \AA} \times 10 \text{ \AA}$ ) obtained by using a long ligand has a larger pore size than Zn(hba) ( $6 \text{ \AA} \times 6 \text{ \AA}$ ), and saturated adsorption ( $4.2 \text{ mmol g}^{-1}$ ) of isoflurane is twice that of Zn(hba) at 298 K (Fig. 6) [217, 219]. Zn(2-mehba) can be obtained by introducing methyl groups into the framework of Zn(hba), which has a small pore size due to the arrangement of methyl groups on its pore surface. Thus, it has low saturated adsorption performance for isoflurane ( $1.013 \text{ mmol g}^{-1}$ ) but promotes the interactions of isoflurane with pore surfaces, which is favorable for storage. Chen et al. synthesized a porous fluorinated ( $1159 \text{ m}^2 \text{ g}^{-1}$ ) MOFF-5 with a high surface area and good adsorption capacity (up to  $73.4 \pm 0.2\%$  by weight) for common inhalational anesthetics, such as sevoflurane, enflurane, halothane, isoflurane, and methoxyflurane; the uptake of the anesthetics was quite fast, and saturated adsorption was reached within 130 s [211, 218]. However, the poor stability of MOFF-5 in water and under humid conditions limits its performance in capturing fluorocompounds. Mixed gases discharged by the

**Table 5** Physical properties of common VAs

Species [Refs.]	Chemical formula	Molecular weight	Boiling Point (K)	GWP (100 years)
Sevoflurane [206]	C <sub>4</sub> H <sub>3</sub> F <sub>7</sub> O	200.055	331.6	130
Isoflurane [217]	C <sub>3</sub> H <sub>2</sub> ClF <sub>5</sub> O	184.49	321.5	510
Desflurane [218]	C <sub>3</sub> H <sub>2</sub> F <sub>6</sub> O	168.04	296.65	2540

**Fig. 6** Network structure of ZnL ( $L = hba^{2-}$ ,  $hbpc^{2-}$ , and  $2\text{-mehba}^{2-}$ ), and the adsorption isotherms of isoflurane by Zn(hba), Zn(hbpc), and Zn(2-mehba) at 298 K

anesthesia gas machine are usually accompanied by water vapor, and thus, enduring high moisture environments is the basis of capturing VAs by MOFs. MIL-101 shows excellent adsorption capacity ( $4.5 \text{ mmol g}^{-1}$ ) for sevoflurane due to its high surface area ( $2041 \text{ m}^2 \text{ g}^{-1}$ ) and abundant pore structure,

and the adsorption capacity ( $3.9 \text{ mmol g}^{-1}$ ) at 50% relative humidity only slightly decreases during single-component absorption [220, 221].

The promising application of MOFs in VAs capture provides new development possibilities for the healthcare

industry. Placing small equipment using MOFs in medical settings or medical gas recovery systems can effectively reduce the risk to patients and medical staff exposed to VAs. Alternatively, an intelligent monitoring and control system can be developed by combining sensor technologies and artificial intelligence for the real-time monitoring and control of VAs emission, and automatic activation of MOFs device to capture VAs at concentrations exceeding the safety threshold, ensuring the safety of the medical environment.

## 5 Adsorption of Other F-Gases

F-gases have potential applications in other important fields. The selective and late-stage introduction of fluoroethenyl and fluoroalkyl groups into drug-like molecules is the frontier in the field of organic synthesis, and common gaseous fluorinated commodities, such as trifluoropropene, vinylidene fluoride, trifluoromethyl iodide, and hexafluoropropene, are inexpensive and potential cornerstones for installing fluoroethenyl and fluoroalkyl groups [2, 222, 223]. They provide an entry point for fluorinated olefins, which are the important biological isomers of carbonyl groups, thus streamlining the synthesis of complex fluorinated molecules [224]. However, these gaseous fluorinated commodities are toxic, flammable, and environmentally unfriendly [225]. Therefore, the safe use of F-gases is critical for the synthesis of fluorinated molecules related to medicinal chemistry, agriculture, and biomedical imaging. The reversible adsorption of F-gases by porous solid materials allows for the treatment of F-gases as recyclable solid reagents, and MOFs can optimize the storage capacities and adsorption enthalpy ( $-\Delta H_{\text{ads}}$ ) of guest molecules because MOFs are distinctively modular [226, 227]. MOFs containing OMS can reversibly bind synthetically relevant F-gases through strong metal–fluorine interactions [178, 228]. However, available data about the adsorption of gaseous fluorinated commodity by MOFs are few. The adsorption of F-gases, such as vinylidene fluoride, by 12 representative open metal-site MOFs is reversible, and  $\text{M}_2(\text{dobdc})$  containing high Lewis acidic  $\text{Mg}^{2+}$  sites exhibit high gravimetric capacities (7.95 mmol g<sup>-1</sup>, 34 wt%) and adsorption ( $-\Delta H_{\text{ads}} = 41 \text{ kJ mol}^{-1}$ ) on vinylidene fluoride, demonstrating potential as an agent for transporting and storing controlled F-gases and enabling the development of high-throughput reactions for these gases [229].

## 6 Technological Readiness Level

MOFs adsorbents exhibit great potential in the field of trapping and separation of F-gases, but still face many unsolved challenges, and there also exist many directions worth exploring and trying to break through these bottlenecks (Fig. 7).

1. Breaking the trade-off between the selectivity and capacities of MOFs for F-gases is the key to designing novel MOFs. The preparation of MOFs with hierarchical porous structure provides opportunities for structural diversity and performance improvement of MOFs [230–232]. For example, a corrugated channel having small pores and large cavities can be designed, in which the small pores connect the large cavities and enhance adsorption selectivity, while the large cavities improve adsorption capacity. In addition, the structural flexibility of MOFs should be fully utilized, and dynamic structural changes induced by external stimuli not only are suitable for the separation of complex systems but also have high adsorption capacity in specific pressure regions.
2. The separation of F-gases by MOFs is based on differences in physical and chemical properties between different gas types. The typical example is the separation of  $\text{SF}_6/\text{N}_2$ , which is relatively easy due to the considerable difference in molecular size and polarity. However, when

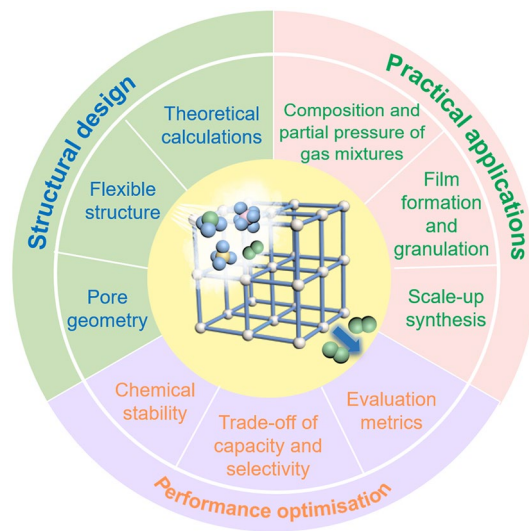


**Fig. 7** Key elements in the design of MOFs for the adsorption and separation of F-gases

separating mixed gases of different PFCs species or fluorocarbon refrigerants, their highly similar physicochemical properties reduce the precision of identification when only the pore size of MOFs is considered. The ideal selectivity may be achieved by combining the dynamic diffusion regulation, thermodynamic equilibrium, and structural flexibility of MOFs, which requires a deliberate manipulation at the molecular or even atomic level of structural geometry, flexibility, and various intermolecular interactions.

3. In designing MOF structures, considering that most F-gases are inherently corrosive to MOFs is essential, which accelerate the oxidation or the other chemical reactions of metals and organic ligands, leading to structural collapse or performance degradation. Moreover, F-gases in practical production often contain water vapor and toxic or corrosive components (such as HF, CO, and NO<sub>x</sub>). Therefore, the high stability of MOFs is crucial to their separation performance, and the competitive adsorption of moisture and other gases should be considered.
4. In constructing design guidelines for MOFs that effectively separate F-gases mixtures, understanding of structure–activity relationships is crucial. The entire adsorption and separation processes should be monitored with the assistance of additional *in situ* characterization techniques. Mature characterization techniques, such as *in situ* single-crystal X-ray diffraction, powder X-ray diffraction, and neutron powder diffraction techniques, are used to detect the spatial binding sites of guest molecules. *In situ* infrared ray and *in situ* nuclear magnetic resonance techniques are employed to monitor structural changes in MOFs during adsorption. Different from the *in situ* characterization, the proposed *operando* enables the characterization of reactions under real working/operating conditions, offering opportunities for elucidating actual reaction mechanisms through real-time *in situ* characterization [233]. Three-dimensional electron diffraction and environmental transmission electron microscopy can allow for the direct observation of guests adsorbed by MOFs. Furthermore, interactions between MOFs and target gas molecules can be studied in depth with methods, such as computational chemistry and molecular dynamics simulations, for the accurate identification of adsorption mechanisms.
5. The composition and partial pressure of F-gases mixtures are crucial for evaluating the performance of MOFs. For example, SF<sub>6</sub>/N<sub>2</sub> volume ratios of 0.1, 0.01, 0.002, and 0.0003 are common, and MOFs (such as SBMOF-1, Ni(ina)<sub>2</sub>) with high adsorption capacities in low-pressure regions are typically effective in separating SF<sub>6</sub> from a mixture. IAST selectivity is often used as a reference metrics in evaluating separation performance, but it is calculated from a single-component adsorption isotherm and cannot fully represent selectivity in gas separation scenarios. In addition, the current gas flow rate for laboratory-scale breakthrough experiments is far below the industrial demand for time efficiency. Therefore, precise measurements are needed to refine and clarify the evaluation metrics and methods for MOFs separation performance in academic research.
6. In addition to high adsorption capacity and selectivity for F-gases, the realization of industrial applications also requires economic feasibility, excellent chemical stability, and ease of scalability in production [234, 235]. As can be seen from the compositions of MOFs listed in Tables 2 and 4, the raw materials for most MOFs are costly and not easily available. And the high-temperature and high-pressure equipment commonly used in its synthesis further increases both production costs and expenses related to safety precautions. Therefore, stable MOFs structures that can be obtained at room temperature using inexpensive raw materials can be selected as a foundation, and combine with the regulation of pore environment to make it have industrialization potential. MOFs such as ZJU-75a [235], MOF-303 [236], and Al-PyDC [237], which can realize industrial production in the field of olefin gas separation, provide reference for this. In addition, the formation of MOFs is also a crucial yet often overlooked step that affects industrialization [238–241]. Powdered MOFs will cause considerable drop in pressure and heat transfer problems in practical adsorption systems, which is unsuitable for direct integration into a commercial application [242]. Many traditional molding methods reported cannot be widely used in the synthesis of MOFs, and the optimization of its key parameters needs researchers to continue to strengthen their understanding of the characteristics of MOFs.

## 7 Conclusion and Outlook

For controlling the emissions of F-gases, using MOFs for direct capture is one of the effective strategies for achieving climate objectives and fostering sustainable development in various industries. However, this strategy imposes specific demands on the adsorption capacities of MOFs. Consciously modulating energy and stereochemistry in the molecular structure of MOFs provides a unique platform for this purpose. Under the guidance of reticular chemistry, the adsorption capacities of MOFs for F-gases can be improved by using diverse topologies, ligand length, and by introducing defects. However, in practical applications, F-gases are often utilized as mixed gases to reduce energy consumption or meet the requirements of gas synthesis processes. Therefore, selectivity is another key indicator for separating and recovering target gases. Typically, to improve the adsorption selectivity of F-gases mixtures, the pore size of MOFs is often controlled to be close to the diameter of guest molecules. This approach strengthens vdW interactions between a host and guest. However, a narrow pore size usually results in a trade-off between adsorption capacity and selectivity. Metal or nonmetal functional sites that provide specific host–guest interactions for F-gases are crucial to offsetting this trade-off. Inhibiting the adsorption of other components by introducing sites of action is an ideal strategy for improving the separation performance of MOFs, and increasing the sites of action can further improve affinity for F-gases. However, this approach is not entirely satisfactory for the selective adsorption of PFCs/PFCs and fluorocarbon refrigerant blends with highly similar physicochemical properties. Flexible-robust MOFs can edit pores at the sub-angstrom level to realize precise regulation of pore environment, thus enabling the separation of F-gases with highly similar structures. At the same time, it overcomes the shortcomings of co-adsorption and low thermal/chemical stability of flexible MOFs. Flexible-robust MOFs can maintain its structural integrity at low pressure and show its significant plateau. More importantly, it has an adsorbate-dependent gas sorption isotherm, which is more suitable for molecular sieve components of complex systems. Numerous studies demonstrated the unique advantages of MOFs over other materials in the adsorption and separation of F-gases, but this emerging research field still faces many unresolved challenges, as well as a number of proposed directions

worth exploring to address these bottlenecks. We encourage research on the adsorption and reuse of MOFs in other F-gases applications, which will reduce the negative impacts on the environment while promoting the effective utilization of potential resources for MOFs.

MOFs have great application potential for the actual adsorption and separation of F-gases and will be further developed through experiments and calculation research. The adsorption and separation strategies of F-gases in this review provide effective guidance for the design of other porous materials, such as organic frameworks and hydrogen-bonded organic frameworks. These materials have clear pore size and crystal structure, and thus, capturing gas mixtures by adjusting pore size geometry or introducing functional effective sites on the basis of reticular chemistry and advanced crystal engineering is feasible. In addition, the methods summarized and proposed in this review can be applied not only to MOFs but also to other systems, such as MOFs membrane, which provides a new solution for the design of the next-generation separation materials for F-gases.

**Acknowledgements** This research was funded by the National Key Research and Development Program of China (2022YFE0110500), National Natural Science Foundation of China (22376161, 52373154, 52103181), the Fundamental Research Funds for the Central Universities of China, and the Interdisciplinary Project in Environmental Science and Engineering of Tongji University (2023-3-YB-02). Y.H. is the recipient of National Science Fund for Excellent Young Scientists Fund Program.

**Author Contributions** Qian Wang contributed to data curation (lead), investigation (lead), and writing—original draft (lead). Yong Hu was involved in funding acquisition (supporting), supervision (supporting), and writing—reviewing and editing (supporting). Yifan Gu contributed to conceptualization (lead), funding acquisition (lead), supervision (lead), and writing—reviewing and editing (lead).

### Declarations

**Conflict of Interest** The authors declare no interest conflict. They have no known competing financial interests or personal relationships that could have appeared to influence the work reported in this paper.

**Open Access** This article is licensed under a Creative Commons Attribution 4.0 International License, which permits use, sharing, adaptation, distribution and reproduction in any medium or format, as long as you give appropriate credit to the original author(s) and the source, provide a link to the Creative Commons licence, and indicate if changes were made. The images or other third party material in this article are included in the article's Creative

Commons licence, unless indicated otherwise in a credit line to the material. If material is not included in the article's Creative Commons licence and your intended use is not permitted by statutory regulation or exceeds the permitted use, you will need to obtain permission directly from the copyright holder. To view a copy of this licence, visit <http://creativecommons.org/licenses/by/4.0/>.

## References

- D.K.J.A. Wanigarathna, J. Gao, B. Liu, Metal organic frameworks for adsorption-based separation of fluorocompounds: a review. *Mater. Adv.* **1**, 310–320 (2020). <https://doi.org/10.1039/d0ma00083c>
- W.C. Fu, P.M. MacQueen, T.F. Jamison, Continuous flow strategies for using fluorinated greenhouse gases in fluoroalkylations. *Chem. Soc. Rev.* **50**, 7378–7394 (2021). <https://doi.org/10.1039/D0CS00670J>
- B.K. Sovacool, S. Griffiths, J. Kim, M. Bazilian, Climate change and industrial F-gases: a critical and systematic review of developments, sociotechnical systems and policy options for reducing synthetic greenhouse gas emissions. *Renew. Sustain. Energy Rev.* **141**, 110759 (2021). <https://doi.org/10.1016/j.rser.2021.110759>
- Y. Heredia-Aricapa, J.M. Belman-Flores, A. Mota-Babiloni, J. Serrano-Arellano, J.J. García-Pabón, Overview of low GWP mixtures for the replacement of HFC refrigerants: R134a, R404A and R410A. *Int. J. Refrig.* **111**, 113–123 (2020). <https://doi.org/10.1016/j.ijrefrig.2019.11.012>
- D.J. Sheldon, M.R. Crimmin, Repurposing of F-gases: challenges and opportunities in fluorine chemistry. *Chem. Soc. Rev.* **51**, 4977–4995 (2022). <https://doi.org/10.1039/d1cs01072g>
- L. Guo, Y. Yang, P.J. Fraser, G.J.M. Velders, Z. Liu et al., Projected increases in emissions of high global warming potential fluorinated gases in China. *Commun. Earth Environ.* **4**, 205 (2023). <https://doi.org/10.1038/s43247-023-00859-6>
- W.-T. Tsai, C.-H. Tsai, A survey on fluorinated greenhouse gases in Taiwan: emission trends, regulatory strategies, and abatement technologies. *Environments* **10**, 113 (2023). <https://doi.org/10.3390/environments10070113>
- J.E. Sosa, R.P.P.L. Ribeiro, I. Matos, M. Bernardo, I.M. Fonseca et al., Exploring the potential of biomass-derived carbons for the separation of fluorinated gases with high global warming potential. *Biomass Bioenergy* **188**, 107323 (2024). <https://doi.org/10.1016/j.biombioe.2024.107323>
- M. Ghandehari, F-gases at the fenceline: exposing the fluorochemical production sector's undisclosed emissions. EIA (2023). [https://eia-international.org/wp-content/uploads/2023-EIA-F-Gases-at-the-Fenceline\\_SINGLES.pdf](https://eia-international.org/wp-content/uploads/2023-EIA-F-Gases-at-the-Fenceline_SINGLES.pdf)
- Z. Rošková, J. Schneider, M. Štengel, Predicted hydrofluorocarbon (HFC) and perfluorocarbon (PFC) emissions for the years 2010–2050 in the Czech republic. *Atmosphere* **14**, 111 (2023). <https://doi.org/10.3390/atmos14010111>
- S.M.W. Wilson, F. Handan, Tezel Adsorption separation of  $\text{CF}_4$ ,  $\text{O}_2$ ,  $\text{CO}_2$ , and  $\text{COF}_2$  from an excimer gas mixture. *Sep. Purif. Technol.* **258**, 117659 (2021). <https://doi.org/10.1016/j.seppur.2020.117659>
- J.L. Boot, Overview of alternatives to CFCs for domestic refrigerators and freezers. *Int. J. Refrig.* **13**, 100–105 (1990). [https://doi.org/10.1016/0140-7007\(90\)90008-K](https://doi.org/10.1016/0140-7007(90)90008-K)
- A.J. Howarth, Y. Liu, P. Li, Z. Li, T.C. Wang et al., Chemical, thermal and mechanical stabilities of metal–organic frameworks. *Nat. Rev. Mater.* **1**, 15018 (2016). <https://doi.org/10.1038/natrevmats.2015.18>
- P.W. Siu, J.P. Siegfried, M.H. Weston, P.E. Fuller, W. Morris et al., Boron trifluoride gas adsorption in metal–organic frameworks. *Inorg. Chem.* **55**, 12110–12113 (2016). <https://doi.org/10.1021/acs.inorgchem.6b02273>
- M.J. Molina, F.S. Rowland, Stratospheric sink for chlorofluoromethanes: chlorine atom-catalysed destruction of ozone. *Nature* **249**, 810–812 (1974). <https://doi.org/10.1038/249810a0>
- T. Chokbunpiam, S. Fritzsche, T. Ploymerusmee, R. Chanajaree, S. Thompno et al., Separation of the chlorofluorocarbon (CFC)  $\text{CCl}_2\text{F}_2$  from  $\text{N}_2$  in NaY zeolite, in MIL-127(Fe) and in the two carbon nanotubes CNT (9, 9) and CNT (11, 11). *J. Mol. Graph. Model.* **125**, 108597 (2023). <https://doi.org/10.1016/j.jmgm.2023.108597>
- C.Y. Chuah, Y. Lee, T.-H. Bae, Potential of adsorbents and membranes for  $\text{SF}_6$  capture and recovery: a review. *Chem. Eng. J.* **404**, 126577 (2021). <https://doi.org/10.1016/j.cej.2020.126577>
- K. Kim, K.S. Kim, J.E. Lee, S. Park, C.-K. Ahn et al., Status of  $\text{SF}_6$  separation/refining technology development for electric industry in Korea. *Sep. Purif. Technol.* **200**, 29–35 (2018). <https://doi.org/10.1016/j.seppur.2018.02.016>
- K. Lee, W.C. Isley, A.L. Dzubak, P. Verma, S.J. Stoneburner et al., Design of a metal–organic framework with enhanced back bonding for separation of  $\text{N}_2$  and  $\text{CH}_4$ . *J. Am. Chem. Soc.* **136**, 698–704 (2014). <https://doi.org/10.1021/ja4102979>
- F. Pardo, S.V. Gutiérrez-Hernández, C. Hermida-Merino, J.M.M. Araújo, M.M. Piñeiro et al., Integration of stable ionic liquid-based nanofluids into polymer membranes. Part II: gas separation properties toward fluorinated greenhouse gases. *Nanomater. (Basel)* **11**, 582 (2021). <https://doi.org/10.3390/nano11030582>
- F. Pardo, S.V. Gutiérrez-Hernández, G. Zarca, A. Urtiaga, Toward the recycling of low-GWP hydrofluorocarbon/hydrofluoroolefin refrigerant mixtures using composite ionic liquid–polymer membranes. *ACS Sustain. Chem. Eng.* **9**, 7012–7021 (2021). <https://doi.org/10.1021/acssuschemeng.1c00668>
- M. Zhang, L. Liu, Q. Li, H. Gong, Y. Chen, Theoretical design of MOFs and PSA process for efficient separation of  $\text{CF}_4/\text{NF}_3$ . *Ind. Eng. Chem. Res.* **62**, 7103–7113 (2023). <https://doi.org/10.1021/acs.iecr.2c04592>
- S.-M. Wang, H.-L. Lan, G.-W. Guan, Q.-Y. Yang, Amino-functionalized microporous MOFs for capturing greenhouse gases  $\text{CF}_4$  and  $\text{NF}_3$  with record selectivity. *ACS Appl. Mater. Interfaces* **14**, 40072–40081 (2022). <https://doi.org/10.1021/acsami.2c12164>

24. R. Hassanalizadeh, W.M. Nelson, B.K. Naidoo, M. Ebrahimnejadhasanabadi, P. Naidoo et al., Purification of nitrogen trifluoride by physical separation. *Fluid Phase Equilib.* **560**, 113405 (2022). <https://doi.org/10.1016/j.fluid.2022.113405>
25. D.J. Branken, H.M. Krieg, J.P. le Roux, G. Lachmann, Separation of NF<sub>3</sub> and CF<sub>4</sub> using amorphous glassy perfluoropolymer Teflon AF and Hyflon AD60 membranes. *J. Membr. Sci.* **462**, 75–87 (2014). <https://doi.org/10.1016/j.memsci.2014.03.033>
26. R. Srinivasan, S.R. Auvil, P.M. Burban, Elucidating the mechanism(s) of gas transport in poly[1-(trimethylsilyl)-1-propyne](PTMSP) membranes. *J. Membr. Sci.* **86**, 67–86 (1994). [https://doi.org/10.1016/0376-7388\(93\)E0128-7](https://doi.org/10.1016/0376-7388(93)E0128-7)
27. K. Ishii, A. Shibata, T. Takeuchi, J. Yoshiura, T. Urabe et al., Development of silica membranes to improve dehydration reactions. *J. Jpn. Petrol. Inst.* **62**, 211–219 (2019). <https://doi.org/10.1627/jpi.62.211>
28. Y. Sun, J. Yan, Y. Gao, T. Ji, S. Chen et al., Fabrication of highly oriented ultrathin zirconium metal-organic framework membrane from nanosheets towards unprecedented gas separation. *Angew. Chem. Int. Ed.* **62**, e202216697 (2023). <https://doi.org/10.1002/anie.202216697>
29. D.-Y. Kang, J.S. Lee, Challenges in developing MOF-based membranes for gas separation. *Langmuir* **39**, 2871–2880 (2023). <https://doi.org/10.1021/acs.langmuir.2c03458>
30. S. Li, W. Han, Q.-F. An, K.-T. Yong, M.-J. Yin, Defect engineering of MOF-based membrane for gas separation. *Adv. Funct. Mater.* **33**, 2303447 (2023). <https://doi.org/10.1002/adfm.202303447>
31. K. Shiojiri, Y. Yanagisawa, A. Yamasaki, F. Kiyono, Separation of F-gases (HFC-134a and SF<sub>6</sub>) from gaseous mixtures with nitrogen by surface diffusion through a porous Vycor glass membrane. *J. Membr. Sci.* **282**, 442–449 (2006). <https://doi.org/10.1016/j.memsci.2006.06.003>
32. J.-W. Choi, S. Lee, B. An, S.-B. Kim, S.-H. Lee, Separation of sulfur hexafluoride from a nitrogen/sulfur hexafluoride mixture using a polymer hollow fiber membrane. *Water Air Soil Pollut.* **225**, 1807 (2014). <https://doi.org/10.1007/s11270-013-1807-7>
33. L. Wang, N. Xu, Y. Hu, W. Sun, R. Krishna et al., Efficient capture of C<sub>2</sub>H<sub>2</sub> from CO<sub>2</sub> and CnH<sub>4</sub> by a novel fluorinated anion pillared MOF with flexible molecular sieving effect. *Nano Res.* **16**, 3536–3541 (2023). <https://doi.org/10.1007/s12274-022-4996-9>
34. O.T. Qazvini, R. Babarao, S.G. Telfer, Selective capture of carbon dioxide from hydrocarbons using a metal-organic framework. *Nat. Commun.* **12**, 197 (2021). <https://doi.org/10.1038/s41467-020-20489-2>
35. Z. Di, C. Liu, J. Pang, C. Chen, F. Hu et al., Cage-like porous materials with simultaneous high C<sub>2</sub>H<sub>2</sub> storage and excellent C<sub>2</sub>H<sub>2</sub>/CO<sub>2</sub> separation performance. *Angew. Chem. Int. Ed.* **60**, 10828–10832 (2021). <https://doi.org/10.1002/anie.202101907>
36. M. Kang, D.W. Kang, J.H. Choe, H. Kim, D.W. Kim et al., A robust hydrogen-bonded metal-organic framework with enhanced ethane uptake and selectivity. *Chem. Mater.* **33**, 6193–6199 (2021). <https://doi.org/10.1021/acs.chemmater.1c01892>
37. Y. Zhang, L. Yang, L. Wang, S. Duttwyler, H. Xing, A microporous metal-organic framework supramolecularly assembled from a Cu<sup>II</sup> dodecaborate cluster complex for selective gas separation. *Angew. Chem. Int. Ed.* **58**, 8145–8150 (2019). <https://doi.org/10.1002/anie.201903600>
38. L. Wang, W. Sun, Y. Zhang, N. Xu, R. Krishna et al., Interpenetration symmetry control within ultramicroporous robust boron cluster hybrid MOFs for benchmark purification of acetylene from carbon dioxide. *Angew. Chem. Int. Ed.* **60**, 22865–22870 (2021). <https://doi.org/10.1002/anie.202107963>
39. P. Pullumbi, F. Brandani, S. Brandani, Gas separation by adsorption: technological drivers and opportunities for improvement. *Curr. Opin. Chem. Eng.* **24**, 131–142 (2019). <https://doi.org/10.1016/j.coche.2019.04.008>
40. A.D. Yancey, S.J. Terian, B.J. Shaw, T.M. Bish, D.R. Corbin et al., A review of fluorocarbon sorption on porous materials. *Microporous Mesoporous Mater.* **331**, 111654 (2022). <https://doi.org/10.1016/j.micromeso.2021.111654>
41. W. Zhang, Y. Li, Y. Wu, Y. Fu, S. Chen et al., Fluorinated porous organic polymers for efficient recovery perfluorinated electronic specialty gas from exhaust gas of plasma etching. *Sep. Purif. Technol.* **287**, 120561 (2022). <https://doi.org/10.1016/j.seppur.2022.120561>
42. X. Yuan, M.K. Cho, J.G. Lee, S.W. Choi, K.B. Lee, Upcycling of waste polyethylene terephthalate plastic bottles into porous carbon for CF<sub>4</sub> adsorption. *Environ. Pollut.* **265**, 114868 (2020). <https://doi.org/10.1016/j.envpol.2020.114868>
43. S.W. Choi, H.J. Yoon, H.J. Lee, E.-S. Lee, D.-S. Lim et al., CF<sub>4</sub> adsorption on porous carbon derived from silicon carbide. *Microporous Mesoporous Mater.* **306**, 110373 (2020). <https://doi.org/10.1016/j.micromeso.2020.110373>
44. W. Zhang, Y. Wu, Y. Li, S. Chen, Y. Fu et al., Fluorine-functionalized porous organic polymers for durable F-gas capture from semiconductor etching exhaust. *Macromolecules* **55**, 1435–1444 (2022). <https://doi.org/10.1021/acs.macromol.1c02413>
45. P. Cannon, C.P. Rutkowski, The sorptive properties of a zeolite containing a preadsorbed phase. *J. Phys. Chem.* **63**, 1292–1296 (1959). <https://doi.org/10.1021/j150578a018>
46. H. Kodama, S. Okazaki, Alkylation of benzene, alkylbenzenes, and halobenzenes catalyzed by protonated mordenite pretreated with chlorofluorocarbons. *J. Catal.* **132**, 512–523 (1991). [https://doi.org/10.1016/0021-9517\(91\)90167-3](https://doi.org/10.1016/0021-9517(91)90167-3)
47. M. Sugimoto, H. Katsuno, T. Murakawa, Improvement of platinum-supported zeolite catalysts for n-hexane aromatization by halocarbon treatment and alkaline soaking. *Appl. Catal. A Gen.* **96**, 201–216 (1993). [https://doi.org/10.1016/0926-860X\(90\)80010-C](https://doi.org/10.1016/0926-860X(90)80010-C)
48. O.M. Yaghi, M. O’Keeffe, N.W. Ockwig, H.K. Chae, M. Eddaoudi et al., Reticular synthesis and the design of new materials. *Nature* **423**, 705–714 (2003). <https://doi.org/10.1038/nature01650>

49. S. Kitagawa, R. Kitaura, S.-I. Noro, Functional porous coordination polymers. *Angew. Chem. Int. Ed.* **43**, 2334–2375 (2004). <https://doi.org/10.1002/anie.200300610>
50. Y. Shen, T. Pan, L. Wang, Z. Ren, W. Zhang et al., Programmable logic in metal–organic frameworks for catalysis. *Adv. Mater.* **33**, 2007442 (2021). <https://doi.org/10.1002/adma.202007442>
51. J. Dong, V. Wee, D. Zhao, Stimuli-responsive metal–organic frameworks enabled by intrinsic molecular motion. *Nat. Mater.* **21**, 1334–1340 (2022). <https://doi.org/10.1038/s41563-022-01317-y>
52. M. Kalaj, K.C. Bentz, S. Ayala Jr., J.M. Palomba, K.S. Barcus et al., MOF-polymer hybrid materials: from simple composites to tailored architectures. *Chem. Rev.* **120**, 8267–8302 (2020). <https://doi.org/10.1021/acs.chemrev.9b00575>
53. A.J. Howarth, A.W. Peters, N.A. Vermeulen, T.C. Wang, J.T. Hupp et al., Best practices for the synthesis, activation, and characterization of metal–organic frameworks. *Chem. Mater.* **29**, 26–39 (2017). <https://doi.org/10.1021/acs.chemmater.6b02626>
54. Z.-J. Lin, J. Lü, M. Hong, R. Cao, Metal–organic frameworks based on flexible ligands (FL-MOFs): structures and applications. *Chem. Soc. Rev.* **43**, 5867–5895 (2014). <https://doi.org/10.1039/C3CS60483G>
55. L. Wang, H. Huang, X. Zhang, H. Zhao, F. Li et al., Designed metal-organic frameworks with potential for multi-component hydrocarbon separation. *Coord. Chem. Rev.* **484**, 215111 (2023). <https://doi.org/10.1016/j.ccr.2023.215111>
56. B. Zheng, G. Maurin, Mechanical control of the kinetic propylene/propane separation by zeolitic imidazolate framework-8. *Angew. Chem. Int. Ed.* **58**, 13734–13738 (2019). <https://doi.org/10.1002/anie.201906245>
57. J. Wan, H.-L. Zhou, K. Hyeon-Deuk, I.-Y. Chang, Y. Huang et al., Molecular sieving of propyne/propylene by a scalable nanoporous crystal with confined rotational shutters. *Angew. Chem. Int. Ed.* **62**, e202316792 (2023). <https://doi.org/10.1002/anie.202316792>
58. M. Najafi, H. Kulak, H.O. Rubiera Landa, I.F.J. Vankelecom, J.F.M. Denayer, Appraising separation performance of MOF-808-based adsorbents for light olefins and paraffins. *Microporous Mesoporous Mater.* **367**, 112961 (2024). <https://doi.org/10.1016/j.micromeso.2023.112961>
59. F. Xie, L. Chen, E.M. Cedefio Morales, S. Ullah, Y. Fu et al., Complete separation of benzene-cyclohexene-cyclohexane mixtures *via* temperature-dependent molecular sieving by a flexible chain-like coordination polymer. *Nat. Commun.* **15**, 2240 (2024). <https://doi.org/10.1038/s41467-024-46556-6>
60. Y. Han, Y. Chen, Y. Ma, J. Bailey, Z. Wang et al., Control of the pore chemistry in metal-organic frameworks for efficient adsorption of benzene and separation of benzene/cyclohexane. *Chem* **9**, 739–754 (2023). <https://doi.org/10.1016/j.chempr.2023.02.002>
61. S. Mukherjee, D. Sensharma, O.T. Qazvini, S. Dutta, L.K. Macreadie et al., Advances in adsorptive separation of benzene and cyclohexane by metal-organic framework adsorbents. *Coord. Chem. Rev.* **437**, 213852 (2021). <https://doi.org/10.1016/j.ccr.2021.213852>
62. M. Wang, Z. Han, K. Wang, B. Zhao, T. Sun et al., Confinement of p-xylene in the pores of a bilanthanide metal-organic framework for highly selective recognition. *Angew. Chem. Int. Ed.* **63**, e202318722 (2024). <https://doi.org/10.1002/anie.202318722>
63. T. Hyun, J. Park, J. So, J. Kim, D.-Y. Koh, Unexpected molecular sieving of xylene isomer using tethered ligand in polymer-metal-organic frameworks (polyMOFs). *Adv. Sci.* **11**, e2402980 (2024). <https://doi.org/10.1002/advs.202402980>
64. Y. Gu, J.-J. Zheng, K.-I. Otake, S. Sakaki, H. Ashitani et al., Soft corrugated channel with synergistic exclusive discrimination gating for CO<sub>2</sub> recognition in gas mixture. *Nat. Commun.* **14**, 4245 (2023). <https://doi.org/10.1038/s41467-023-39470-w>
65. X. Zhang, H. Zhao, Q. Yang, M. Yao, Y.-N. Wu et al., Direct air capture of CO<sub>2</sub> in designed metal-organic frameworks at lab and pilot scale. *Carbon Capture Sci. Technol.* **9**, 100145 (2023). <https://doi.org/10.1016/j.ccst.2023.100145>
66. Z. Sun, Y. Liao, S. Zhao, X. Zhang, Q. Liu et al., Research progress in metal-organic frameworks (MOFs) in CO<sub>2</sub> capture from post-combustion coal-fired flue gas: characteristics, preparation, modification and applications. *J. Mater. Chem. A* **10**, 5174–5211 (2022). <https://doi.org/10.1039/DITA07856A>
67. X.Y.D. Soo, J.J.C. Lee, W.-Y. Wu, L. Tao, C. Wang et al., Advancements in CO<sub>2</sub> capture by absorption and adsorption: a comprehensive review. *J. CO<sub>2</sub> Util.* **81**, 102727 (2024). <https://doi.org/10.1016/j.jcou.2024.102727>
68. P.Z. Moghadam, Y.G. Chung, R.Q. Snurr, Progress toward the computational discovery of new metal–organic framework adsorbents for energy applications. *Nat. Energy* **9**, 121–133 (2024). <https://doi.org/10.1038/s41560-023-01417-2>
69. A. Dong, D. Chen, Q. Li, J. Qian, Metal-organic frameworks for greenhouse gas applications. *Small* **19**, 2201550 (2023). <https://doi.org/10.1002/smll.202201550>
70. H.-R. Liu, S.-C. Liu, L.-P. Zhang, Y.-T. Li, X.-M. Peng et al., Pore chemically modified nickel-based metal-organic frameworks for efficient purification of natural gas. *Sep. Purif. Technol.* **352**, 128267 (2025). <https://doi.org/10.1016/j.sepur.2024.128267>
71. Y. Gu, J.-J. Zheng, K.-I. Otake, M. Shivanna, S. Sakaki et al., Host-guest interaction modulation in porous coordination polymers for inverse selective CO<sub>2</sub>/C<sub>2</sub>H<sub>2</sub> separation. *Angew. Chem. Int. Ed.* **60**, 11688–11694 (2021). <https://doi.org/10.1002/anie.202016673>
72. L. Zhang, K. Jiang, L. Yang, L. Li, E. Hu et al., Benchmark C<sub>2</sub>H<sub>2</sub>/CO<sub>2</sub> separation in an ultra-microporous metal-organic framework *via* copper(I)-alkynyl chemistry. *Angew. Chem. Int. Ed.* **60**, 15995–16002 (2021). <https://doi.org/10.1002/anie.202102810>
73. X. Li, K. Chen, R. Guo, Z. Wei, Ionic liquids functionalized MOFs for adsorption. *Chem. Rev.* **123**, 10432–10467 (2023). <https://doi.org/10.1021/acs.chemrev.3c00248>

74. K.-G. Liu, F. Bigdeli, A. Panjehpour, S. Hwa Jhung, H.A.J. Al Lawati et al., Potential applications of MOF composites as selective membranes for separation of gases. *Coord. Chem. Rev.* **496**, 215413 (2023). <https://doi.org/10.1016/j.ccr.2023.215413>
75. T.-H. Chen, I. Popov, W. Kaveevivitchai, Y.-C. Chuang, Y.-S. Chen et al., Thermally robust and porous noncovalent organic framework with high affinity for fluorocarbons and CFCs. *Nat. Commun.* **5**, 5131 (2014). <https://doi.org/10.1038/ncomms6131>
76. E.J. García, D. Bahamon, L.F. Vega, Systematic search of suitable metal–organic frameworks for thermal energy-storage applications with low global warming potential refrigerants. *ACS Sustain. Chem. Eng.* **9**, 3157–3171 (2021). <https://doi.org/10.1021/acssuschemeng.0c07797>
77. D. Barpaga, V.T. Nguyen, B.K. Medasani, S. Chatterjee, B.P. McGrail et al., Insight into fluorocarbon adsorption in metal-organic frameworks *via* experiments and molecular simulations. *Sci. Rep.* **9**, 10289 (2019). <https://doi.org/10.1038/s41598-019-46269-7>
78. J. Choi, J. Im, K. Noh, J. Kim, T. Vogt et al., Universal gas-uptake behavior of a zeolitic imidazolate framework ZIF-8 at high pressure. *J. Phys. Chem. C* **123**, 25769–25774 (2019). <https://doi.org/10.1021/acs.jpcc.9b08539>
79. H. Chen, Z. Chen, O.K. Farha, R.Q. Snurr, High propane and isobutane adsorption cooling capacities in zirconium-based metal–organic frameworks predicted by molecular simulations. *ACS Sustain. Chem. Eng.* **7**, 18242–18246 (2019). <https://doi.org/10.1021/acssuschemeng.9b05368>
80. F. Yan, Q. Wang, S. Ou, R. Zhang, G. Wang, Molecular simulation study for adsorption and thermal energy storage analysis of refrigerants (R170, R161, R152a, and R143a) mixed with UIO-67 nanoparticles. *Mod. Phys. Lett. B* **34**, 2050334 (2020). <https://doi.org/10.1142/s0217984920503340>
81. D. Barpaga, J. Zheng, B.P. McGrail, R.K. Motkuri, Manipulating pore topology and functionality to promote fluorocarbon-based adsorption cooling. *Acc. Chem. Res.* **55**, 649–659 (2022). <https://doi.org/10.1021/acs.accounts.1c00615>
82. P. Purohit, L. Höglund-Isaksson, Global emissions of fluorinated greenhouse gases 2005–2050 with abatement potentials and costs. *Atmos. Chem. Phys.* **17**, 2795–2816 (2017). <https://doi.org/10.5194/acp-17-2795-2017>
83. Y. Wu, T. Yan, W. Zhang, S. Chen, Y. Fu et al., Adsorption interface-induced H...F charge transfer in ultramicroporous metal–organic frameworks for perfluorinated gas separation. *Ind. Eng. Chem. Res.* **61**, 13603–13611 (2022). <https://doi.org/10.1021/acs.iecr.2c01604>
84. S. Builes, T. Roussel, L.F. Vega, Optimization of the separation of sulfur hexafluoride and nitrogen by selective adsorption using Monte Carlo simulations. *AIChE. J.* **57**, 962–974 (2011). <https://doi.org/10.1002/aic.12312>
85. K. Inami, Y. Maeda, Y. Habuchi, M. Yoshimura, S. Hamano et al., Problems of the application of N<sub>2</sub>/SF<sub>6</sub> mixtures to gas-insulated bus. *Electr. Eng. Jpn.* **137**, 25–31 (2001). <https://doi.org/10.1002/eej.1100>
86. Z. Wan, T. Yan, M. Chang, M. Yang, D. Liu, Nickel-based metal–organic framework for efficient capture of CF<sub>4</sub> with a high CF<sub>4</sub>/N<sub>2</sub> selectivity. *Sep. Purif. Technol.* **306**, 122617 (2023). <https://doi.org/10.1016/j.seppur.2022.122617>
87. Y. Wu, X. Li, Y. Li, C. Tao, Y. Tang et al., Porous aromatic frameworks as HF resistant adsorbents for SF<sub>6</sub> separation at elevated pressure. *Sep. Purif. Technol.* **315**, 123657 (2023). <https://doi.org/10.1016/j.seppur.2023.123657>
88. W. Zhang, Y. Li, S. Wang, Y. Wu, S. Chen et al., Fluorine-induced electric field gradient in 3D porous aromatic frameworks for highly efficient capture of Xe and F-gases. *ACS Appl. Mater. Interfaces* **14**, 35126–35137 (2022). <https://doi.org/10.1021/acsami.2c10050>
89. Y. He, X. Cao, Z. Zhang, Z. Jiang, H. Huang et al., Discovery of high-performing metal–organic frameworks for efficient SF<sub>6</sub>/N<sub>2</sub> separation: a combined computational screening, machine learning, and experimental study. *Ind. Eng. Chem. Res.* **62**, 7642–7649 (2023). <https://doi.org/10.1021/acs.iecr.3c00727>
90. I. Skarmoutsos, M. Eddaoudi, G. Maurin, Highly tunable sulfur hexafluoride separation by interpenetration control in metal organic frameworks. *Microporous Mesoporous Mater.* **281**, 44–49 (2019). <https://doi.org/10.1016/j.micromeso.2019.02.035>
91. C.Y. Chuah, K. Goh, T.-H. Bae, Hierarchically structured HKUST-1 nanocrystals for enhanced SF<sub>6</sub> capture and recovery. *J. Phys. Chem. C* **121**, 6748–6755 (2017). <https://doi.org/10.1021/acs.jpcc.7b00291>
92. S.-M. Wang, X.-T. Mu, H.-R. Liu, S.-T. Zheng, Q.-Y. Yang, Pore-structure control in metal-organic frameworks (MOFs) for capture of the greenhouse gas SF<sub>6</sub> with record separation. *Angew. Chem. Int. Ed.* **61**, e202207066 (2022). <https://doi.org/10.1002/anie.202207066>
93. I. Senkovska, E. Barea, J.A.R. Navarro, S. Kaskel, Adsorptive capturing and storing greenhouse gases such as sulfur hexafluoride and carbon tetrafluoride using metal–organic frameworks. *Microporous Mesoporous Mater.* **156**, 115–120 (2012). <https://doi.org/10.1016/j.micromeso.2012.02.021>
94. W. Zhang, Y. Li, Y. Wu, W. Huang, S. Wang et al., Polypyrene porous organic framework for efficiently capturing electron specialty gases. *ACS Appl. Mater. Interfaces* **15**, 29468–29477 (2023). <https://doi.org/10.1021/acsami.3c05398>
95. J. Wada, G. Ueta, S. Okabe, M. Hikita, Dielectric properties of gas mixtures with per-fluorocarbon gas and gas with low liquefaction temperature. *IEEE Trans. Dielectr. Electr. Insul.* **23**, 838–847 (2016). <https://doi.org/10.1109/TDEI.2015.005373>
96. D. Sun, Y. Zhou, T. Nian, L. Li, Research on the insulation performance of new environmentally friendly insulation gas hexafluoropropylene and carbon dioxide mixed gas. *IOP Conf. Ser. Earth Environ. Sci.* **781**, 052019 (2021). <https://doi.org/10.1088/1755-1315/781/5/052019>
97. W. Wang, Y. Wu, M. Rong, L. Éhn, I. Černušák, Theoretical computation of thermophysical properties of high-temperature F<sub>2</sub>, CF<sub>4</sub>, C<sub>2</sub>F<sub>2</sub>, C<sub>2</sub>F<sub>4</sub>, C<sub>2</sub>F<sub>6</sub>, C<sub>3</sub>F<sub>6</sub>, and C<sub>3</sub>F<sub>8</sub> plasmas. *J.*

- Phys. D Appl. Phys. **45**, 285201 (2012). <https://doi.org/10.1088/0022-3727/45/28/285201>
98. W.-T. Tsai, H.-P. Chen, W.-Y. Hsien, A review of uses, environmental hazards and recovery/recycle technologies of perfluorocarbons (PFCs) emissions from the semiconductor manufacturing processes. *J. Loss Prev. Process Ind.* **15**, 65–75 (2002). [https://doi.org/10.1016/S0950-4230\(01\)00067-5](https://doi.org/10.1016/S0950-4230(01)00067-5)
99. Y. Deng, B. Li, D. Xiao, Analysis of the insulation characteristics of  $C_3F_8$  gas mixtures with  $N_2$  and  $CO_2$  using Boltzmann equation method. *IEEE Trans. Dielectr. Electr. Insul.* **22**, 3253–3259 (2015). <https://doi.org/10.1109/TDEI.2015.005191>
100. X. Li, C. Yang, S. Du, Y. Wu, B. Huang et al., Dynamic adsorption separation of  $c-C_4F_8/C_3F_8$  for effective purification of perfluoropropane electronic gas. *Chem. Eng. Sci.* **273**, 118656 (2023). <https://doi.org/10.1016/j.ces.2023.118656>
101. Y. Hu, L. Wang, R. Nan, N. Xu, Y. Jiang et al., Pore engineering in cost-effective and stable Al-MOFs for efficient capture of the greenhouse gas  $SF_6$ . *Chem. Eng. J.* **471**, 144851 (2023). <https://doi.org/10.1016/j.cej.2023.144851>
102. M.-B. Kim, T.-U. Yoon, D.-Y. Hong, S.-Y. Kim, S.-J. Lee et al., High  $SF_6/N_2$  selectivity in a hydrothermally stable zirconium-based metal–organic framework. *Chem. Eng. J.* **276**, 315–321 (2015). <https://doi.org/10.1016/j.cej.2015.04.087>
103. J.L.C. Rowsell, O.M. Yaghi, Metal–organic frameworks: a new class of porous materials. *Microporous Mesoporous Mater.* **73**, 3–14 (2004). <https://doi.org/10.1016/j.micromeso.2004.03.034>
104. H. Murase, T. Imai, T. Inohara, M. Toyoda, Use of zeolite filter in portable equipment for recovering  $SF_6$  in  $SF_6/N_2$  mixtures. *IEEE Trans. Dielectr. Electr. Insul.* **11**, 166–173 (2004). <https://doi.org/10.1109/TDEI.2004.1266332>
105. M.-B. Kim, T.-H. Kim, T.-U. Yoon, J.H. Kang, J.-H. Kim et al., Efficient  $SF_6/N_2$  separation at high pressures using a zirconium-based mesoporous metal–organic framework. *J. Ind. Eng. Chem.* **84**, 179–184 (2020). <https://doi.org/10.1016/j.jiec.2019.12.032>
106. T. Wang, M. Chang, T. Yan, Y. Ying, Q. Yang et al., Calcium-based metal–organic framework for efficient capture of sulfur hexafluoride at low concentrations. *Ind. Eng. Chem. Res.* **60**, 5976–5983 (2021). <https://doi.org/10.1021/acs.iecr.1c00662>
107. Y. Wu, S. Wang, W. Zhang, S. Chen, Z. Zhang et al., Enhancing perfluorinated electron specialty gases separation selectivity in ultra-microporous metal organic framework. *Sep. Purif. Technol.* **289**, 120739 (2022). <https://doi.org/10.1016/j.seppur.2022.120739>
108. N. Metropolis, A.W. Rosenbluth, M.N. Rosenbluth, A.H. Teller, E. Teller, Equation of state calculations by fast computing machines. *J. Chem. Phys.* **21**, 1087–1092 (1953). <https://doi.org/10.1063/1.1699114>
109. P. Chowdhury, C. Bikkina, D. Meister, F. Dreisbach, S. Gumma, Comparison of adsorption isotherms on Cu-BTC metal organic frameworks synthesized from different routes. *Microporous Mesoporous Mater.* **117**, 406–413 (2009). <https://doi.org/10.1016/j.micromeso.2008.07.029>
110. M. Åhlén, E. Kapaca, D. Hedbom, T. Willhammar, M. Strømme et al., Gas sorption properties and kinetics of porous bismuth-based metal–organic frameworks and the selective  $CO_2$  and  $SF_6$  sorption on a new bismuth trimesate-based structure UU-200. *Microporous Mesoporous Mater.* **329**, 111548 (2022). <https://doi.org/10.1016/j.micromeso.2021.111548>
111. T.-H. Chen, I. Popov, W. Kaveevivitchai, Y.-C. Chuang, Y.-S. Chen et al., Mesoporous fluorinated metal–organic frameworks with exceptional adsorption of fluorocarbons and CFCs. *Angew. Chem. Int. Ed.* **54**, 13902–13906 (2015). <https://doi.org/10.1002/anie.201505149>
112. M. Chang, T. Yan, Y. Wei, J.-X. Wang, D. Liu et al., Metal–organic framework-based single-molecule  $SF_6$  trap for record  $SF_6$  capture. *Chem. Mater.* **34**, 9134–9143 (2022). <https://doi.org/10.1021/acs.chemmater.2c02004>
113. B.S. Whitehead, W.W. Brennessel, S.S. Michtavy, H.A. Silva, J. Kim et al., Selective adsorption of fluorinated super greenhouse gases within a metal–organic framework with dynamic corrugated ultramicropores. *Chem. Sci.* **15**, 5964–5972 (2024). <https://doi.org/10.1039/d3sc07007g>
114. A. Yadav, S. Kumari, P. Yadav, A. Hazra, A. Chakraborty et al., Open metal site (OMS)-inspired investigation of adsorption and catalytic functions in a porous metal–organic framework (MOF). *Dalton Trans.* **51**, 15496–15506 (2022). <https://doi.org/10.1039/d2dt02098j>
115. Ü. Kökçam-Demir, A. Goldman, L. Esrafil, M. Gharib, A. Morsali et al., Coordinatively unsaturated metal sites (open metal sites) in metal–organic frameworks: design and applications. *Chem. Soc. Rev.* **49**, 2751–2798 (2020). <https://doi.org/10.1039/c9cs00609e>
116. J.-W. Yan, S.-Q. Gang, Z.-Y. Liu, H.-Y. Xu, R. Wang et al., An In(III)-MOF based on pore engineering for efficient capture  $SF_6$  from  $SF_6/N_2$  mixture. *Sep. Purif. Technol.* **327**, 124929 (2023). <https://doi.org/10.1016/j.seppur.2023.124929>
117. Y.-S. Bae, O.K. Farha, A.M. Spokoyny, C.A. Mirkin, J.T. Hupp et al., Carborane-based metal–organic frameworks as highly selective sorbents for  $CO_2$  over methane. *Chem. Commun.* **35**, 4135–4137 (2008). <https://doi.org/10.1039/B805785K>
118. M.-B. Kim, S.-J. Lee, C.Y. Lee, Y.-S., Bae High  $SF_6$  selectivities and capacities in isostructural metal–organic frameworks with proper pore sizes and highly dense unsaturated metal sites. *Microporous Mesoporous Mater.* **190**, 356–361 (2014). <https://doi.org/10.1016/j.micromeso.2014.02.028>
119. Z. Ye, J. Yao, W. Zheng, W. Yuan, J. Guan et al., The preparation and adsorption performance of Co-doped MIL-101(Cr) for low-concentration  $C_3F_8$ . *Chem. Eng. Sci.* **282**, 119302 (2023). <https://doi.org/10.1016/j.ces.2023.119302>
120. N. Al-Janabi, P. Hill, L. Torrente-Murciano, A. Garforth, P. Gorgojo et al., Mapping the Cu-BTC metal–organic framework (HKUST-1) stability envelope in the presence of water vapour for  $CO_2$  adsorption from flue gases. *Chem. Eng. J.* **281**, 669–677 (2015). <https://doi.org/10.1016/j.cej.2015.07.020>
121. P. Liu, T. Zhao, K. Cai, P. Chen, F. Liu et al., Rapid mechanochemical construction of HKUST-1 with enhancing water

- stability by hybrid ligands assembly strategy for efficient adsorption of SF<sub>6</sub>. *Chem. Eng. J.* **437**, 135364 (2022). <https://doi.org/10.1016/j.cej.2022.135364>
122. H. Li, Z. Lin, X. Zhou, X. Wang, Y. Li et al., Ultrafast room temperature synthesis of novel composites Imi@Cu-BTC with improved stability against moisture. *Chem. Eng. J.* **307**, 537–543 (2017). <https://doi.org/10.1016/j.cej.2016.08.128>
123. J. Ren, M. Chang, W. Zeng, Y. Xia, D. Liu et al., Computer-aided discovery of MOFs with calixarene-analogous micro-environment for exceptional SF<sub>6</sub> capture. *Chem. Mater.* **33**, 5108–5114 (2021). <https://doi.org/10.1021/acs.chemmater.1c01139>
124. X. Zhang, Y.-L. Zhao, X.-Y. Li, X. Bai, Q. Chen et al., Recovery of high-purity SF<sub>6</sub> from humid SF<sub>6</sub>/N<sub>2</sub> mixture within a Co(II)-pyrazolate framework. *J. Am. Chem. Soc.* **146**, 19303–19309 (2024). <https://doi.org/10.1021/jacs.4c05075>
125. S.-M. Li, Q. Zhang, H.-C. Jiang, Q.-L. Ni, L.-C. Gui et al., Constructing local nanomolecular trap in a scalable, low-cost, and ultramicroporous metal–organic framework for efficient capture of greenhouse gases SF<sub>6</sub> and CO<sub>2</sub>. *Chem. Eng. J.* **496**, 154026 (2024). <https://doi.org/10.1016/j.cej.2024.154026>
126. S.-T. Zheng, R.-Y. Jiang, Y. Jiang, S. Ni, G.-W. Guan et al., Methyl-functionalized microporous metal–organic framework for efficient SF<sub>6</sub>/N<sub>2</sub> separation. *Sep. Purif. Technol.* **318**, 123957 (2023). <https://doi.org/10.1016/j.seppur.2023.123957>
127. M.-B. Kim, K.-M. Kim, T.-H. Kim, T.-U. Yoon, E.-J. Kim et al., Highly selective adsorption of SF<sub>6</sub> over N<sub>2</sub> in a bromine-functionalized zirconium-based metal–organic framework. *Chem. Eng. J.* **339**, 223–229 (2018). <https://doi.org/10.1016/j.cej.2018.01.129>
128. H. Wang, L. Yu, Y. Lin, J. Peng, S.J. Teat et al., Adsorption of fluorocarbons and chlorocarbons by highly porous and robust fluorinated zirconium metal–organic frameworks. *Inorg. Chem.* **59**, 4167–4171 (2020). <https://doi.org/10.1021/acs.inorgchem.0c00018>
129. A. Cholach, D. Yakovin, Removal of CF<sub>4</sub> from NF<sub>3</sub> at the phase interface. *J. Taiwan Inst. Chem. Eng.* **131**, 104178 (2022). <https://doi.org/10.1016/j.jtice.2021.104178>
130. N.J. Ianno, K.E. Greenberg, J.T. Verheyen, Comparison of the etching and plasma characteristics of discharges in CF<sub>4</sub> and NF<sub>3</sub>. *J. Electrochem. Soc.* **128**, 2174–2179 (1981). <https://doi.org/10.1149/1.2127212>
131. X.-Y. Yang, L.-H. Chen, Y. Li, J.C. Rooke, C. Sanchez et al., Hierarchically porous materials: synthesis strategies and structure design. *Chem. Soc. Rev.* **46**, 481–558 (2017). <https://doi.org/10.1039/C6CS00829A>
132. Y.G. Chung, E. Haldoupis, B.J. Bucior, M. Haranczyk, S. Lee et al., Advances, updates, and analytics for the computation-ready, experimental metal–organic framework database: core MOF 2019. *J. Chem. Eng. Data* **64**, 5985–5998 (2019). <https://doi.org/10.1021/acs.jced.9b00835>
133. Y.G. Chung, J. Camp, M. Haranczyk, B.J. Sikora, W. Bury et al., Computation-ready, experimental metal–organic frameworks: a tool to enable high-throughput screening of nanoporous crystals. *Chem. Mater.* **26**, 6185–6192 (2014). <https://doi.org/10.1021/cm502594j>
134. A.K. Rappe, C.J. Casewit, K.S. Colwell, W.A.I.I.I. Goddard, W.M. Skiff, UFF, a full periodic table force field for molecular mechanics and molecular dynamics simulations. *J. Am. Chem. Soc.* **114**, 10024–10035 (1992). <https://doi.org/10.1021/ja00051a040>
135. S.L. Mayo, B.D. Olafson, W.A. Goddard, DREIDING: a generic force field for molecular simulations. *J. Phys. Chem.* **94**, 8897–8909 (1990). <https://doi.org/10.1021/j100389a010>
136. A.I. Skouidas, D.S. Sholl, Molecular dynamics simulations of self-diffusivities, corrected diffusivities, and transport diffusivities of light gases in four silica zeolites to assess influences of pore shape and connectivity. *J. Phys. Chem. A* **107**, 10132–10141 (2003). <https://doi.org/10.1021/jp0354301>
137. J.J. Hurly, Viscosity and speed of sound of gaseous nitrous oxide and nitrogen trifluoride measured with a Greenspan viscometer. *Int. J. Thermophys.* **25**, 625–641 (2004). <https://doi.org/10.1023/B:IJOT.0000034229.03525.aa>
138. H. Demir, S. Keskin, Zr-MOFs for CF<sub>4</sub>/CH<sub>4</sub>, CH<sub>4</sub>/H<sub>2</sub>, and CH<sub>4</sub>/N<sub>2</sub> separation: towards the goal of discovering stable and effective adsorbents. *Mol. Syst. Des. Eng.* **6**, 627–642 (2021). <https://doi.org/10.1039/d1me00060h>
139. Z. Zheng, Z. Rong, N. Rampal, C. Borgs, J.T. Chayes et al., A GPT-4 reticular chemist for guiding MOF discovery. *Angew. Chem. Int. Ed.* **62**, e202311983 (2023). <https://doi.org/10.1002/anie.202311983>
140. K. Lan, D. Zhao, Functional ordered mesoporous materials: present and future. *Nano Lett.* **22**, 3177–3179 (2022). <https://doi.org/10.1021/acs.nanolett.2c00902>
141. Y. Zhu, Y. Zhou, Z. Ji, W. Zhang, M. Wu, A microporous framework with aromatic pores for one-step purification of C<sub>2</sub>F<sub>6</sub> from CF<sub>3</sub>CH<sub>2</sub>F/CF<sub>3</sub>CHF<sub>2</sub>/C<sub>2</sub>F<sub>6</sub> mixture. *Sep. Purif. Technol.* **353**, 128373 (2025). <https://doi.org/10.1016/j.seppur.2024.128373>
142. W. Xia, Y. Yang, L. Sheng, Z. Zhou, L. Chen et al., Temperature-dependent molecular sieving of fluorinated propane/propylene mixtures by a flexible-robust metal–organic framework. *Sci. Adv.* **10**, eadj6473 (2024). <https://doi.org/10.1126/sciadv.adj6473>
143. A.J. Sicard, R.T. Baker, Fluorocarbon refrigerants and their syntheses: past to present. *Chem. Rev.* **120**, 9164–9303 (2020). <https://doi.org/10.1021/acs.chemrev.9b00719>
144. D. O'Hagan, Understanding organofluorine chemistry. An introduction to the C–F bond. *Chem. Soc. Rev.* **37**, 308–319 (2008). <https://doi.org/10.1039/b711844a>
145. H. Li, L. Li, R.-B. Lin, G. Ramirez, W. Zhou et al., Microporous metal–organic framework with dual functionalities for efficient separation of acetylene from light hydrocarbon mixtures. *ACS Sustain. Chem. Eng.* **7**, 4897–4902 (2019). <https://doi.org/10.1021/acssuschemeng.8b05480>
146. B. Li, X. Cui, D. O’Nolan, H.-M. Wen, M. Jiang et al., An ideal molecular sieve for acetylene removal from ethylene with record selectivity and productivity. *Adv. Mater.* **29**, 1704210 (2017). <https://doi.org/10.1002/adma.201704210>
147. Z. Bao, J. Wang, Z. Zhang, H. Xing, Q. Yang et al., Molecular sieving of ethane from ethylene through the molecular cross-section size differentiation in gallate-based metal–organic

- frameworks. *Angew. Chem. Int. Ed.* **57**, 16020–16025 (2018). <https://doi.org/10.1002/anie.201808716>
148. D. Tanaka, K. Nakagawa, M. Higuchi, S. Horike, Y. Kubota et al., Kinetic gate-opening process in a flexible porous coordination polymer. *Angew. Chem. Int. Ed.* **47**, 3914–3918 (2008). <https://doi.org/10.1002/anie.200705822>
149. W. Wang, X.-H. Xiong, N.-X. Zhu, Z. Zeng, Z.-W. Wei et al., A rare flexible metal-organic framework based on a tailororable Mn<sub>8</sub>-cluster showing smart responsiveness to aromatic guests and capacity for gas separation. *Angew. Chem. Int. Ed.* **61**, e202201766 (2022). <https://doi.org/10.1002/anie.202201766>
150. X.-W. Zhang, D.-D. Zhou, J.-P. Zhang, Tuning the gating energy barrier of metal-organic framework for molecular sieving. *Chem* **7**, 1006–1019 (2021). <https://doi.org/10.1016/j.chempr.2020.12.025>
151. L. Bondorf, J.L. Fiorio, V. Bon, L. Zhang, M. Maliuta et al., Isotope-selective pore opening in a flexible metal-organic framework. *Sci. Adv.* **8**, eabn7035 (2022). <https://doi.org/10.1126/sciadv.abn7035>
152. D.-D. Zhou, J.-P. Zhang, On the role of flexibility for adsorptive separation. *Acc. Chem. Res.* **55**, 2966–2977 (2022). <https://doi.org/10.1021/acs.accounts.2c00418>
153. A. Ebadi Amooghin, H. Sanaeepur, M. Ghomi, R. Luque, H. Garcia et al., Flexible–robust MOFs/HOFs for challenging gas separations. *Coord. Chem. Rev.* **505**, 215660 (2024). <https://doi.org/10.1016/j.ccr.2024.215660>
154. C. Jiang, J.-X. Wang, D. Liu, E. Wu, X.-W. Gu et al., Supramolecular entanglement in a hydrogen-bonded organic framework enables flexible-robust porosity for highly efficient purification of natural gas. *Angew. Chem. Int. Ed.* **63**, e202404734 (2024). <https://doi.org/10.1002/anie.202404734>
155. S.-M. Wang, Q.-Y. Yang, A copper-based metal-organic framework for upgrading natural gas through the recovery of C<sub>2</sub>H<sub>6</sub> and C<sub>3</sub>H<sub>8</sub>. *Green Chem. Eng.* **4**, 81–87 (2023). <https://doi.org/10.1016/j.gce.2022.04.006>
156. G. Mehlana, S.A. Bourne, G. Ramon, A new class of thermo- and solvatochromic metal-organic frameworks based on 4-(pyridin-4-yl)benzoic acid. *Dalton Trans.* **41**, 4224–4231 (2012). <https://doi.org/10.1039/C2DT12016J>
157. S. Nandi, S. Collins, D. Chakraborty, D. Banerjee, P.K. Thalapally et al., Ultralow parasitic energy for postcombustion CO<sub>2</sub> capture realized in a nickel isonicotinate metal-organic framework with excellent moisture stability. *J. Am. Chem. Soc.* **139**, 1734–1737 (2017). <https://doi.org/10.1021/jacs.6b10455>
158. F.M. Amombo Noa, O. Cheung, M. Åhlén, E. Ahlberg, P. Nehla et al., A hexagon based Mn(II) rod metal-organic framework–structure, SF<sub>6</sub> gas sorption, magnetism and electrochemistry. *Chem. Commun.* **59**, 2106–2109 (2023). <https://doi.org/10.1039/D2CC06916D>
159. X. Zheng, Y. Shen, S. Wang, K. Huang, D. Cao, Selective adsorption of SF<sub>6</sub> in covalent- and metal-organic frameworks. *Chin. J. Chem. Eng.* **39**, 88–95 (2021). <https://doi.org/10.1016/j.cjche.2021.03.010>
160. P. Horcajada, S. Surblé, C. Serre, D.-Y. Hong, Y.-K. Seo et al. Synthesis and catalytic properties of MIL-100(Fe), an iron(III) carboxylate with large pores. *Chem. Commun.* **27**, 2820–2822 (2007). <https://doi.org/10.1039/B704325B>
161. P.-J. Kim, Y.-W. You, H. Park, J.-S. Chang, Y.-S. Bae et al., Separation of SF<sub>6</sub> from SF<sub>6</sub>/N<sub>2</sub> mixture using metal–organic framework MIL-100(Fe) granule. *Chem. Eng. J.* **262**, 683–690 (2015). <https://doi.org/10.1016/j.cej.2014.09.123>
162. P. Chowdhury, C. Bikkina, S. Gumma, Gas adsorption properties of the chromium-based metal organic framework MIL-101. *J. Phys. Chem. C* **113**, 6616–6621 (2009). <https://doi.org/10.1021/jp811418r>
163. H. Wang, J. Getzschmann, I. Senkovska, S. Kaskel, Structural transformation and high pressure methane adsorption of Co<sub>2</sub>(1, 4-bdc)<sub>2</sub>dabco. *Microporous Mesoporous Mater.* **116**, 653–657 (2008). <https://doi.org/10.1016/j.micromeso.2008.05.037>
164. M. Åhlén, F.M. Amombo Noa, L. Öhrström, D. Hedbom, M. Strømme et al., Pore size effect of 1, 3, 6, 8-tetrakis(4-carboxyphenyl)Pyrene-based metal-organic frameworks for enhanced SF<sub>6</sub> adsorption with high selectivity. *Microporous Mesoporous Mater.* **343**, 112161 (2022). <https://doi.org/10.1016/j.micromeso.2022.112161>
165. J.M. Calm, The next generation of refrigerants—Historical review, considerations, and outlook. *Int. J. Refrig.* **31**, 1123–1133 (2008). <https://doi.org/10.1016/j.ijrefrig.2008.01.013>
166. B.J. Gareau, A critical review of the successful CFC phase-out versus the delayed methyl bromide phase-out in the Montreal protocol. *Int. Environ. Agreem. Polit. Law Econ.* **10**, 209–231 (2010). <https://doi.org/10.1007/s10784-010-9120-z>
167. R.J. Cicerone, R.S. Stolarski, S. Walters, Stratospheric ozone destruction by man-made chlorofluoromethanes. *Science* **185**, 1165–1167 (1974). <https://doi.org/10.1126/science.185.4157.1165>
168. R.K. Motkuri, H.V.R. Annapureddy, M. Vijaykumar, H.T. Schaeff, P.F. Martin et al., Fluorocarbon adsorption in hierarchical porous frameworks. *Nat. Commun.* **5**, 4368 (2014). <https://doi.org/10.1038/ncomms5368>
169. X.-H. Xiong, L. Song, W. Wang, H.-T. Zheng, L. Zhang et al., Capture fluorocarbon and chlorofluorocarbon from air using DUT-67 for safety and semi-quantitative analysis. *Adv. Sci.* **11**, e2308123 (2024). <https://doi.org/10.1002/advs.202308123>
170. Y.-Y. Xiong, R. Krishna, T. Pham, K.A. Forrest, C.-X. Chen et al., Pore-nanospace engineering of mixed-ligand metal-organic frameworks for high adsorption of hydrofluorocarbons and hydrochlorofluorocarbons. *Chem. Mater.* **34**, 5116–5124 (2022). <https://doi.org/10.1021/acs.chemmater.2c00601>
171. C.-X. Chen, S.-P. Zheng, Z.-W. Wei, C.-C. Cao, H.-P. Wang et al., A robust metal-organic framework combining open metal sites and polar groups for methane purification and CO<sub>2</sub>/fluorocarbon capture. *Chemistry* **23**, 4060–4064 (2017). <https://doi.org/10.1002/chem.201606038>
172. D.K.J.A. Wanigarathna, J. Gao, B. Liu, Fluorocarbon separation in a thermally robust zirconium carboxylate metal-organic framework. *Chem. Asian J.* **13**, 977–981 (2018). <https://doi.org/10.1002/asia.201800337>

173. C.-X. Chen, Q.-F. Qiu, C.-C. Cao, M. Pan, H.-P. Wang et al., Stepwise engineering of pore environments and enhancement of CO<sub>2</sub>/R22 adsorption capacity through dynamic spacer installation and functionality modification. *Chem. Commun.* **53**, 11403–11406 (2017). <https://doi.org/10.1039/C7CC06352K>
174. J.E. Sosa, C. Malheiro, P.J. Castro, R.P.P.L. Ribeiro, M.M. Piñeiro et al., Exploring the potential of metal-organic frameworks for the separation of blends of fluorinated gases with high global warming potential. *Glob. Chall.* **7**, 2200107 (2022). <https://doi.org/10.1002/gch2.202200107>
175. S. Cai, S. Tian, Y. Lu, G. Wang, Y. Pu et al., Molecular simulations of adsorption and energy storage of R1234yf, R1234ze(z), R134a, R32, and their mixtures in M-MOF-74 (M = Mg, Ni) nanoparticles. *Sci. Rep.* **10**, 7265 (2020). <https://doi.org/10.1038/s41598-020-64187-x>
176. J.M. Vicent-Luna, A Luna-Triguero adsorption characteristics of refrigerants for thermochemical energy storage in metal-organic frameworks. *ACS Appl. Eng. Mater.* **2**, 542–552 (2024). <https://doi.org/10.1021/acsaenm.3c00474>
177. Q. Wang, S. Tang, Energy storage analysis of R125 in UIO-66 and MOF-5 nanoparticles: a molecular simulation study. *Open Chem.* **17**, 229–234 (2019). <https://doi.org/10.1515/chem-2019-0026>
178. J. Zheng, D. Barpaga, B.A. Trump, M. Shetty, Y. Fan et al., Molecular insight into fluorocarbon adsorption in pore expanded metal-organic framework analogs. *J. Am. Chem. Soc.* **142**, 3002–3012 (2020). <https://doi.org/10.1021/jacs.9b11963>
179. J. Zheng, D. Barpaga, O.Y. Gutiérrez, N.D. Browning, B.L. Mehdi et al., Exceptional fluorocarbon uptake with mesoporous metal-organic frameworks for adsorption-based cooling systems. *ACS Appl. Energy Mater.* **1**, 5853–5858 (2018). <https://doi.org/10.1021/acsaem.8b01282>
180. Z.-W. Mo, H.-L. Zhou, D.-D. Zhou, R.-B. Lin, P.-Q. Liao et al., Mesoporous metal-organic frameworks with exceptionally high working capacities for adsorption heat transformation. *Adv. Mater.* **30**, 1704350 (2018). <https://doi.org/10.1002/adma.201704350>
181. R.-B. Lin, T.-Y. Li, H.-L. Zhou, C.-T. He, J.-P. Zhang et al., Tuning fluorocarbon adsorption in new isoreticular porous coordination frameworks for heat transformation applications. *Chem. Sci.* **6**, 2516–2521 (2015). <https://doi.org/10.1039/c4sc03985h>
182. J. Zheng, R.S. Vemuri, L. Estevez, P.K. Koech, T. Varga et al., Pore-engineered metal-organic frameworks with excellent adsorption of water and fluorocarbon refrigerant for cooling applications. *J. Am. Chem. Soc.* **139**, 10601–10604 (2017). <https://doi.org/10.1021/jacs.7b04872>
183. W. Xiang, Y. Zhang, Y. Chen, C.-J. Liu, X. Tu, Synthesis, characterization and application of defective metal-organic frameworks: current status and perspectives. *J. Mater. Chem. A* **8**, 21526–21546 (2020). <https://doi.org/10.1039/d0ta08009h>
184. Y. Fu, Y. Yao, A.C. Forse, J. Li, K. Mochizuki et al., Solvent-derived defects suppress adsorption in MOF-74. *Nat. Commun.* **14**, 2386 (2023). <https://doi.org/10.1038/s41467-023-38155-8>
185. J.J. Jenks, R.K. Motkuri, W. TeGrotenhuis, B.K. Paul, B.P. McGrail, Simulation and experimental study of metal organic frameworks used in adsorption cooling. *Heat Transf. Eng.* **38**, 1305–1315 (2017). <https://doi.org/10.1080/01457632.2016.1242965>
186. J. Xie, F. Sun, C. Wang, Q. Pan, Stability and hydrocarbon/fluorocarbon sorption of a metal-organic framework with fluorinated channels. *Mater. (Basel)* **9**, 327 (2016). <https://doi.org/10.3390/ma9050327>
187. K.S. Walton, R.Q. Snurr, Applicability of the BET method for determining surface areas of microporous metal-organic frameworks. *J. Am. Chem. Soc.* **129**, 8552–8556 (2007). <https://doi.org/10.1021/ja071174k>
188. J. Hu, C. Liu, L. Liu, Q. Li, Thermal energy storage of R1234yf, R1234ze, R134a and R32/MOF-74 nanofluids: a molecular simulation study. *Mater. (Basel)* **11**, 1164 (2018). <https://doi.org/10.3390/ma11071164>
189. M. Fischer, F. Hoffmann, M. Fröba, New microporous materials for acetylene storage and C<sub>2</sub>H<sub>2</sub>/CO<sub>2</sub> separation: insights from molecular simulations. *ChemPhysChem* **11**, 2220–2229 (2010). <https://doi.org/10.1002/cphc.201000126>
190. Y. Chen, Z. Qiao, D. Lv, C. Duan, X. Sun et al., Efficient adsorptive separation of C<sub>3</sub>H<sub>6</sub> over C<sub>3</sub>H<sub>8</sub> on flexible and thermoresponsive CPL-1. *Chem. Eng. J.* **328**, 360–367 (2017). <https://doi.org/10.1016/j.cej.2017.07.044>
191. W. Fan, S.B. Peh, Z. Zhang, H. Yuan, Z. Yang et al., Tetrazole-functionalized zirconium metal-organic cages for efficient C<sub>2</sub>H<sub>2</sub>/C<sub>2</sub>H<sub>4</sub> and C<sub>2</sub>H<sub>2</sub>/CO<sub>2</sub> separations. *Angew. Chem. Int. Ed.* **60**, 17338–17343 (2021). <https://doi.org/10.1002/anie.202102585>
192. C.-X. Chen, Z. Wei, J.-J. Jiang, Y.-Z. Fan, S.-P. Zheng et al., Precise modulation of the breathing behavior and pore surface in Zr-MOFs by reversible post-synthetic variable-spacer installation to fine-tune the expansion magnitude and sorption properties. *Angew. Chem. Int. Ed.* **55**, 9932–9936 (2016). <https://doi.org/10.1002/anie.201604023>
193. E.D. Bloch, W.L. Queen, R. Krishna, J.M. Zadrozny, C.M. Brown et al., Hydrocarbon separations in a metal-organic framework with open iron(II) coordination sites. *Science* **335**, 1606–1610 (2012). <https://doi.org/10.1126/science.1217544>
194. Q.-F. Qiu, C.-X. Chen, Z. Zeng, Z.-W. Wei, N.-X. Zhu et al., A flexible-robust copper(II) metal-organic framework constructed from a fluorinated ligand for CO<sub>2</sub>/R22 capture. *Inorg. Chem.* **59**, 14856–14860 (2020). <https://doi.org/10.1021/acs.inorgchem.0c02123>
195. D. Morelli Venturi, F. Costantino, Recent advances in the chemistry and applications of fluorinated metal-organic frameworks (F-MOFs). *RSC Adv.* **13**, 29215–29230 (2023). <https://doi.org/10.1039/d3ra04940j>
196. P.D.C. Dietzel, B. Panella, M. Hirscher, R. Blom, H. Fjellvåg, Hydrogen adsorption in a nickel based coordination polymer with open metal sites in the cylindrical cavities of the desolvated framework. *Chem. Commun.* **9**, 1164 (2006). <https://doi.org/10.1039/B515434K>

197. L. Ge, W. Zhou, V. Rudolph, Z. Zhu, Mixed matrix membranes incorporated with size-reduced Cu-BTC for improved gas separation. *J. Mater. Chem. A* **1**, 6350–6358 (2013). <https://doi.org/10.1039/C3TA11131H>
198. A. Alowasheer, N.L. Torad, T. Asahi, S.M. Alshehri, T. Ahamad et al., Synthesis of millimeter-scale ZIF-8 single crystals and their reversible crystal structure changes. *Sci. Technol. Adv. Mater.* **25**, 2292485 (2024). <https://doi.org/10.1080/14686996.2023.2292485>
199. R.P. Ojha, P.-A. Lemieux, P.K. Dixon, A.J. Liu, D.J. Durian, Statistical mechanics of a gas-fluidized particle. *Nature* **427**, 521–523 (2004). <https://doi.org/10.1038/nature02294>
200. C. Serre, F. Millange, C. Thouvenot, M. Noguès, G. Marsolier et al., Very large breathing effect in the first nanoporous chromium(III)-based solids: MIL-53 or Cr<sup>III</sup>(OH)<sub>x</sub>{O<sub>2</sub>C-C<sub>6</sub>H<sub>4</sub>-CO<sub>2</sub>}·{HO<sub>2</sub>C-C<sub>6</sub>H<sub>4</sub>-CO<sub>2</sub>H}<sub>x</sub>·H<sub>2</sub>O<sub>y</sub>. *J. Am. Chem. Soc.* **124**, 13519–13526 (2002). <https://doi.org/10.1021/ja0276974>
201. X.-H. Xiong, Z.-W. Wei, W. Wang, L.-L. Meng, C.-Y. Su, Scalable and depurative zirconium metal-organic framework for deep flue-gas desulfurization and SO<sub>2</sub> recovery. *J. Am. Chem. Soc.* **145**, 14354–14364 (2023). <https://doi.org/10.1021/jacs.3c03309>
202. S. Yuan, W. Lu, Y.-P. Chen, Q. Zhang, T.-F. Liu et al., Sequential linker installation: precise placement of functional groups in multivariate metal-organic frameworks. *J. Am. Chem. Soc.* **137**, 3177–3180 (2015). <https://doi.org/10.1021/ja512762r>
203. J.E. Mondloch, W. Bury, D. Fairen-Jimenez, S. Kwon, E.J. DeMarco et al., Vapor-phase metalation by atomic layer deposition in a metal-organic framework. *J. Am. Chem. Soc.* **135**, 10294–10297 (2013). <https://doi.org/10.1021/ja4050828>
204. H.-Q. Xu, J. Hu, D. Wang, Z. Li, Q. Zhang et al., Visible-light photoreduction of CO<sub>2</sub> in a metal-organic framework: boosting electron-hole separation via electron trap states. *J. Am. Chem. Soc.* **137**, 13440–13443 (2015). <https://doi.org/10.1021/jacs.5b08773>
205. G. Férey, C. Mellot-Draznieks, C. Serre, F. Millange, J. Dutour et al., A chromium terephthalate-based solid with unusually large pore volumes and surface area. *Science* **309**, 2040–2042 (2005). <https://doi.org/10.1126/science.1116275>
206. T.N. Ang, S. Baroutian, B.R. Young, M.M. Hyland, M. Taylor et al., Adsorptive separation of volatile anaesthetics: a review of current developments. *Sep. Purif. Technol.* **211**, 491–503 (2019). <https://doi.org/10.1016/j.seppur.2018.10.012>
207. A. Jerath, N.D. Ferguson, B. Cuthbertson, Inhalational volatile-based sedation for COVID-19 pneumonia and ARDS. *Intensive Care Med.* **46**, 1563–1566 (2020). <https://doi.org/10.1007/s00134-020-06154-8>
208. D. Bucher, C. Pasel, M. Luckas, J. Bentgens, D. Bathen, Adsorption of inhalation anaesthetics (fluranes and ethers) on activated carbons and zeolites at trace level concentrations. *J. Chem. Eng. Data* **62**, 1832–1841 (2017). <https://doi.org/10.1021/acs.jced.7b00079>
209. R. Ortmann, C. Pasel, M. Luckas, R. Heimböckel, S. Kraas et al., Adsorption and desorption of isoflurane on carbonaceous adsorbents and zeolites at low concentrations in gas phase. *J. Chem. Eng. Data* **61**, 686–692 (2016). <https://doi.org/10.1021/acs.jced.5b00844>
210. M. Mehrata, C. Moralejo, W.A. Anderson, Adsorbent comparisons for anesthetic gas capture in hospital air emissions. *J. Environ. Sci. Health A Tox Hazard. Subst. Environ. Eng.* **51**, 805–809 (2016). <https://doi.org/10.1080/10934529.2016.1181438>
211. Francis Duval Smith MSN, Management of exposure to waste anesthetic gases. *AORN J.* **91**, 482–494 (2010). <https://doi.org/10.1016/j.aorn.2009.10.022>
212. M.P. Sulbaek Andersen, S.P. Sander, O.J. Nielsen, D.S. Wagner, T.J. Sanford Jr. et al., Inhalation anaesthetics and climate change. *Br. J. Anaesth.* **105**, 760–766 (2010). <https://doi.org/10.1093/bja/aeq259>
213. M.K. Vollmer, T.S. Rhee, M. Rigby, D. Hofstetter, M. Hill et al., Modern inhalation anaesthetics: potent greenhouse gases in the global atmosphere. *Geophys. Res. Lett.* **42**, 1606–1611 (2015). <https://doi.org/10.1002/2014GL062785>
214. T. Langbein, H. Sonntag, D. Trapp, A. Hoffmann, W. Malms et al., Volatile anaesthetics and the atmosphere: atmospheric lifetimes and atmospheric effects of halothane, enflurane, isoflurane, desflurane and sevoflurane. *Br. J. Anaesth.* **82**, 66–73 (1999). <https://doi.org/10.1093/bja/82.1.66>
215. M. Charlesworth, F. Swinton, Anaesthetic gases, climate change, and sustainable practice. *Lancet Planet. Health* **1**, e216–e217 (2017). [https://doi.org/10.1016/S2542-5196\(17\)30040-2](https://doi.org/10.1016/S2542-5196(17)30040-2)
216. A.A. Lindley, A. McCulloch, Regulating to reduce emissions of fluorinated greenhouse gases. *J. Fluor. Chem.* **126**, 1457–1462 (2005). <https://doi.org/10.1016/j.jfluchem.2005.09.011>
217. B.F. Abrahams, A.D. Dhama, P.S. Donnelly, T.A. Hudson, C.J. Kepert et al., Tunable porous coordination polymers for the capture, recovery and storage of inhalation anaesthetics. *Chemistry* **23**, 7871–7875 (2017). <https://doi.org/10.1002/chem.201700389>
218. T.-H. Chen, W. Kaveevivitchai, A.J. Jacobson, O.Š Miljanic, Adsorption of fluorinated anaesthetics within the pores of a molecular crystal. *Chem. Commun.* **51**, 14096–14098 (2015). <https://doi.org/10.1039/c5cc04885k>
219. C. Janiak, J.K. Vieth, MOFs, MILs and more: concepts, properties and applications for porous coordination networks (PCNs). *New J. Chem.* **34**, 2366–2388 (2010). <https://doi.org/10.1039/C0NJ00275E>
220. Y. Hua, N. Gargiulo, A. Peluso, P. Aprea, M. Eić et al., Adsorption behavior of halogenated anaesthetic and water vapor on Cr-based MOF (MIL-101) adsorbent. Part I. equilibrium and breakthrough characterizations. *Chem. Ing. Tech.* **88**, 1730–1738 (2016). <https://doi.org/10.1002/cite.201600051>
221. N. Gargiulo, A. Peluso, P. Aprea, Y. Hua, D. Filipović et al., A chromium-based metal organic framework as a potential high performance adsorbent for anaesthetic vapours. *RSC Adv.* **4**, 49478–49484 (2014). <https://doi.org/10.1039/C4RA05905K>
222. R. Szpera, D.F.J. Moseley, L.B. Smith, A.J. Sterling, V. Gouverneur, The fluorination of C–H bonds: developments

- and perspectives. *Angew. Chem. Int. Ed.* **58**, 14824–14848 (2019). <https://doi.org/10.1002/anie.201814457>
223. T. Liang, C.N. Neumann, T. Ritter, Introduction of fluorine and fluorine-containing functional groups. *Angew. Chem. Int. Ed.* **52**, 8214–8264 (2013). <https://doi.org/10.1002/anie.201206566>
224. M. Bobek, I. Kavai, E. De Clercq, Synthesis and biological activity of 5-(2, 2-difluorovinyl)-2'-deoxyuridine. *J. Med. Chem.* **30**, 1494–1497 (1987). <https://doi.org/10.1021/jm00391a036>
225. G.J.M. Velders, D.W. Fahey, J.S. Daniel, M. McFarland, S.O. Andersen, The large contribution of projected HFC emissions to future climate forcing. *Proc. Natl. Acad. Sci. U.S.A.* **106**, 10949–10954 (2009). <https://doi.org/10.1073/pnas.0902817106>
226. H. Furukawa, K.E. Cordova, M. O'Keeffe, O.M. Yaghi, The chemistry and applications of metal-organic frameworks. *Science* **341**, e1230444 (2013). <https://doi.org/10.1126/science.1230444>
227. P. Kittikhunnatham, G.A. Leith, A. Mathur, J.K. Naglic, C.R. Martin et al., A metal-organic framework (MOF)-based multifunctional cargo vehicle for reactive-gas delivery and catalysis. *Angew. Chem. Int. Ed.* **61**, e202113909 (2022). <https://doi.org/10.1002/anie.202113909>
228. M.E. Zick, J.-H. Lee, M.I. Gonzalez, E.O. Velasquez, A.A. Uliana et al., Fluoroarene separations in metal-organic frameworks with two proximal Mg<sup>2+</sup> coordination sites. *J. Am. Chem. Soc.* **143**, 1948–1958 (2021). <https://doi.org/10.1021/jacs.0c11530>
229. K.T. Keasler, M.E. Zick, E.E. Stacy, J. Kim, J.-H. Lee et al., Handling fluorinated gases as solid reagents using metal-organic frameworks. *Science* **381**, 1455–1461 (2023). <https://doi.org/10.1126/science.adg8835>
230. S. Choi, T. Kim, H. Ji, H.J. Lee, M. Oh, Isotropic and anisotropic growth of metal-organic framework (MOF) on MOF: logical inference on MOF structure based on growth behavior and morphological feature. *J. Am. Chem. Soc.* **138**, 14434–14440 (2016). <https://doi.org/10.1021/jacs.6b08821>
231. P. Falcaro, K. Okada, T. Hara, K. Ikigaki, Y. Tokudome et al., Centimetre-scale micropore alignment in oriented polycrystalline metal-organic framework films via heteroepitaxial growth. *Nat. Mater.* **16**, 342–348 (2017). <https://doi.org/10.1038/nmat4815>
232. Y. Gu, Y.-N. Wu, L. Li, W. Chen, F. Li et al., Controllable modular growth of hierarchical MOF-on-MOF architectures. *Angew. Chem. Int. Ed.* **56**, 15658–15662 (2017). <https://doi.org/10.1002/anie.201709738>
233. M.-S. Yao, K.-I. Otake, T. Koganezawa, M. Ogasawara, H. Asakawa et al., Growth mechanisms and anisotropic softness-dependent conductivity of orientation-controllable metal-organic framework nanofilms. *Proc. Natl. Acad. Sci. U.S.A.* **120**, e2305125120 (2023). <https://doi.org/10.1073/pnas.2305125120>
234. A.M. Wright, M.T. Kapelewski, S. Marx, O.K. Farha, W. Morris, Transitioning metal-organic frameworks from the laboratory to market through applied research. *Nat. Mater.* (2024). <https://doi.org/10.1038/s41563-024-01947-4>
235. D. Liu, J. Pei, X. Zhang, X.-W. Gu, H.-M. Wen et al., Scalable green synthesis of robust ultra-microporous Hofmann clathrate material with record C<sub>3</sub>H<sub>6</sub> storage density for efficient C<sub>3</sub>H<sub>6</sub>/C<sub>3</sub>H<sub>8</sub> separation. *Angew. Chem. Int. Ed.* **62**, e202218590 (2023). <https://doi.org/10.1002/anie.202218590>
236. H.-M. Wen, C. Yu, M. Liu, C. Lin, B. Zhao et al., Construction of negative electrostatic pore environments in a scalable, stable and low-cost metal-organic framework for one-step ethylene purification from ternary mixtures. *Angew. Chem. Int. Ed.* **62**, e202309108 (2023). <https://doi.org/10.1002/anie.202309108>
237. E. Wu, X.-W. Gu, D. Liu, X. Zhang, H. Wu et al., Incorporation of multiple supramolecular binding sites into a robust MOF for benchmark one-step ethylene purification. *Nat. Commun.* **14**, 6146 (2023). <https://doi.org/10.1038/s41467-023-41692-x>
238. A. Bétard, R.A. Fischer, Metal-organic framework thin films: from fundamentals to applications. *Chem. Rev.* **112**, 1055–1083 (2012). <https://doi.org/10.1021/cr200167v>
239. S. Yang, L. Peng, O.A. Syzgantseva, O. Trukhina, I. Kochetygov et al., Preparation of highly porous metal-organic framework beads for metal extraction from liquid streams. *J. Am. Chem. Soc.* **142**, 13415–13425 (2020). <https://doi.org/10.1021/jacs.0c02371>
240. S. Qiu, M. Xue, G. Zhu, Metal-organic framework membranes: from synthesis to separation application. *Chem. Soc. Rev.* **43**, 6116–6140 (2014). <https://doi.org/10.1039/C4CS00159A>
241. Q. Ma, T. Zhang, B. Wang, Shaping of metal-organic frameworks, a critical step toward industrial applications. *Matter* **5**, 1070–1091 (2022). <https://doi.org/10.1016/j.matt.2022.02.014>
242. Y. Xuan, Q. Li, Heat transfer enhancement of nanofluids. *Int. J. Heat Fluid Flow* **21**, 58–64 (2000). [https://doi.org/10.1016/S0142-727X\(99\)00067-3](https://doi.org/10.1016/S0142-727X(99)00067-3)

**Publisher's Note** Springer Nature remains neutral with regard to jurisdictional claims in published maps and institutional affiliations.